PB84-236611

St. Louis Ozone Modeling Project

(U.S.) Environmental Protection Agency
Research Triangle Park, NC

Aug 83

U.S. Department of Commerce
National Technical Information Service
NTIS

PB84-236611

United States
Environmental Protection
Agency

Office of Air Quality
Planning and Standards
Research Triangle Park NC 27711

EPA-450/4-83-019
August 1983

Air

EPA

The St. Louis Ozone Modeling Project

REPRODUCED BY
NATIONAL TECHNICAL
INFORMATION SERVICE
U.S. DEPARTMENT OF COMMERCE
SPRINGFIELD, VA. 22161

TECHNICAL REPORT DATA
(Please read Instructions on the reverse before completing)

1. REPORT NO EPA 450/4-83-019	2.	3. RECIPIENT'S ACCESSION NO. PB8 4 236611
4. TITLE AND SUBTITLE The St. Louis Ozone Modeling Project		5. REPORT DATE August 1983
		6. PERFORMING ORGANIZATION CODE
7. AUTHOR(S) Henry S. Cole, David E. Layland, Gerald K. Moss, Conrad F. Newberry		8. PERFORMING ORGANIZATION REPORT NO.
9. PERFORMING ORGANIZATION NAME AND ADDRESS U.S. Environmental Protection Agency Office of Air Quality Planning and Standards Monitoring and Data Analysis Division (MD-14) Research Triangle Park, North Carolina 27711		10. PROGRAM ELEMENT NO. A13A2A
		11. CONTRACT/GRANT NO.
12. SPONSORING AGENCY NAME AND ADDRESS SAME AS BOX 9		13. TYPE OF REPORT AND PERIOD COVERED
		14. SPONSORING AGENCY CODE
15. SUPPLEMENTARY NOTES		

16. ABSTRACT

The results of applying a refined photochemical model to the St. Louis area are described. The model is a three-dimensional grid model which incorporates a generalized chemical kinetics mechanism. The report describes the performance of the model using a variety of statistical and graphical techniques. Model simulations for a set of 20 days during 1975 and 1976 are utilized in the analysis. The report also examines the effect of changes in emissions on predicted ozone concentrations for a smaller subset of days.

17. KEY WORDS AND DOCUMENT ANALYSIS

a. DESCRIPTORS	b. IDENTIFIERS/OPEN ENDED TERMS	c. COSATI Field/Group
Air pollution Atmospheric models Photochemical reactions Smog Ozone Nitrogen Oxides Hydrocarbons	Urban Airshed Model SAI Airshed Model Carbon-Bond Mechanism St. Louis	
18. DISTRIBUTION STATEMENT Unlimited	19. SECURITY CLASS *(This Report)* Unclassified	21. NO. OF PAGES 207
	20. SECURITY CLASS *(This page)* Unclassified	22. PRICE

EPA Form 2220-1 (Rev. 4-77) PREVIOUS EDITION IS OBSOLETE

EPA-450/4-83-019

The St. Louis Ozone Modeling Project

by

Henry S. Cole, David E. Layland,
Gerald K. Moss, Conrad F. Newberry

U.S. ENVIRONMENTAL PROTECTION AGENCY
Office of Air Quality Planning and Standards
Monitoring and Data Analysis Division (MD-14)
Research Triangle Park, NC 27711

August 1983

DISCLAIMER

This report has been reviewed by the Office of Air Quality Planning and Standards, EPA, and approved for publication. Mention of trade names or commercial products is not intended to constitute endorsement or recommendation for use.

Contents Page

1.0 Introduction 1

1.1 Organization of the Report 4

1.2 Background 4

2.0 The Urban Airshed Model 7

2.1 Mass Transfer (Advection and Dispersion) 9

2.2 Emissions 11

2.3 Chemistry 12

2.4 Surface Removal Processes 15

2.5 Assumptions and Limitations 16

3.0 Methods and Data Bases 17

3.1 General Approach 17

3.2 The RAPS Data Bases 18

3.2.1 Emissions 18

3.2.2 Air Quality 20

3.2.3 Meteorological Data 21

3.2.4 Selection of Test Days 22

3.3 Preparation of Airshed Inputs 22

3.3.1 The Modeling Domain 22

3.3.2 Input Files 23

4.0 Model Performance Evaluation 27

4.1 Methods 28

4.1.1 Accuracy of Peak/Near-Peak Predictions 28

4.1.2 Overall Accuracy and Precision 31

4.1.3 Replication of Patterns 34

4.2 Results of Model Evaluation Analysis 35

4.2.1 Results: Peak/Near-Peak Accuracy Analyses. 35

4.2.2 Overall Accuracy/Precision. 39

4.2.3 Replication of Spatial and Temporal Patterns. . . . 43

4.3 Potential Sources of Error 50

4.4 Summary of Model Performance 56

5.0 Model Sensitivity 58

5.1 Introduction 58

5.2 Test Days. 61

5.3 Uniform Changes in Hydrocarbon Emissions 63

5.4 Uniform Changes in Oxides of Nitrogen Emissions. 69

5.5 Uniform Changes in Hydrocarbon Reactivity. 74

5.6 Other Sensitivity Tests. 79

5.6.1 Spatial Distribution 80

5.6.2 Temporal Distribution 81

5.6.3 Mixing Height 82

5.6.4 Photolytic Rates. 84

5.7 Discussion 85

6.0 Estimating Control Requirements 89

6.1 Response to Uniform Changes in Emissions 90

6.2 Control Strategy Simulations/Methods 91

6.2.1 RACT. 91

6.2.2 FMVPC 92

6.2.3 I/M 94

6.3 Control Strategy Results 95

6.4 Uncertainties. 101

Page

7.0 Conclusions 104

  7.1 Conclusions on Model Performance 104

  7.2 Model Sensitivity 105

    7.2.1 Findings 105

    7.2.2 Recommendations for Further Sensitivity Analyses 107

  7.3 Conclusions with Regard to Control Requirements 108

  7.4 Errors and Uncertainties. 109

  7.5 Feasibility of the Airshed Approach 111

8.0 References 113

1.0 Introduction

Refined photochemical grid models have a number of distinct advantages over the simple techniques currently being used to develop control strategies for most urban regions. They treat physical and chemical processes more realistically and completely and allow for a more precise spatial and temporal resolution of model inputs and outputs. The problem is that photochemical grid models require more intensive emissions and aerometric data bases than do simple models such as EKMA. The collection and preparation of data and the model are demanding and require considerable expertise and resources. Moreover, the typical photochemical grid model analysis will require 3 years or more.

It is therefore essential for EPA to conduct studies to determine whether the accuracy and resolution of photochemical grid models warrant the extensive efforts and resources required for their application. Such studies will also enable the Agency to identify and resolve problems and to provide guidance on photochemical modeling. To meet these objectives, the EPA is conducting modeling studies in St. Louis, Tulsa, Philadelphia, and Denver. The purpose of this report is to present the findings of the St. Louis Ozone Modeling Study.

The model tested is a three-dimensional photochemical grid model developed by Systems Applications, Incorporated, known as the Urban Airshed Model (Airshed).[1] This model numerically simulates the effects of emissions, interurban transport of ozone and precursors, advection, diffusion, chemistry and surface removal processes on pollutant concentrations in a large number of grid cells.

While several photochemical grid models are available, the Urban Airshed Model has been tested most extensively. An alternative model, LIRAQ,[2] was also tested for St. Louis; however, preliminary results indicated that LIRAQ contained technical and logistics problems and was unable to produce significant ozone levels for St. Louis.[3]

St. Louis was selected for an extensive test program for several reasons: (1) it is a moderate-sized city with periodic occurrence of high ozone; (2) its terrain is relatively simple; (3) it does not lie immediately downwind of other major urban areas in that ozone influx is not a major complication and (4) the Regional Air Pollution Study (RAPS) provided extensive air quality, meteorological and emissions data bases for Airshed modeling.

It is emphasized that the project is not aimed at prescribing control requirements for the St. Louis Air Quality Control Region (AQCR); its purpose is to serve strictly as a demonstration project designed to increase the Agency's understanding of Airshed modeling and to provide guidance to potential users of this model. The specific objectives of the St. Louis Study are as follows:

1. to evaluate the ability of the Airshed Model to reproduce observed concentrations and patterns of concentration;

2. to determine the model's sensitivity to important input parameters;

3. to use the model to estimate the degree of control required to attain the ozone standard and to test the effectiveness of specific control programs;

4. to determine sources of uncertainty and error in the analyses;

5. to assess time and resource requirements of Airshed applications;

6. to gain first-hand experience with extensive data preparation and with problems likely to be encountered by users;

7. to compare Airshed performance and control estimates to that obtained using simpler methods such as EKMA and Rollback.

While most of the objectives are self evident, several require amplification. Evaluation of the model's performance (objective 1), required the authors to identify a set of performance measures. We basically used the procedures recommended by the American Meteorological Society.[4] In some cases we found that some of the recommended measures were particularly useful while others were difficult to interpret or not applicable to the case of grid models. Thus, an ancillary objective for the St. Louis Study is to make recommendations on procedures for model performance evaluation.

The sensitivity analyses (objective 2) were conducted to establish the model's response (in terms of ozone concentration) to changes in various input parameters. These tests are useful for identifying those variables which result in the most significant change in model output. Those parameters shown to be critical deserve the greatest attention in data collection and preparation activities. Conversely, approximations which save time and resources are warranted for those parameters to which the model results are insensitive. Secondly, efforts to identify sources of error should focus on the critical parameters. Similarly, sensitivity analyses can contribute to an understanding of uncertainty associated with the value used and (2) the model's sensitivity to the input. The greatest uncertainty is introduced by those inputs which are difficult to specify accurately and which induce a strong response in model output. While quantification is beyond the scope of this study, the report does attempt to identify major sources of uncertainty in the analysis.

1.1 Organization of the Report

The report is ordered as follows. Chapter 2 is a description of the Airshed Model, its basic approach, its treatment of physical and chemical processes, and its underlying assumptions and limitations. Chapter 3 outlines the basic approach used in the modeling analysis and summarizes procedures used to obtain model input data from the emissions and aerometric data bases. The results of base-case simulations and the results of the statistical evaluation of model performance are given in Chapter 4. Chapter 5 presents the results of sensitivity analyses and Chapter 6 describes the control strategy analysis. Chapter 7 summarizes the main conclusions of the study and makes recommendations on modeling procedures and inputs, the need for additional work and when it is appropriate, to use advanced photochemical grid models as opposed to simpler techniques.

1.2 Background

Two organizations within EPA have contributed to the Agency's Airshed Model Application for St. Louis. The Environmental Sciences Research Laboratory (ESRL) of the Office of Research and Development (ORD) has had the lead role in the development and refinement of photochemical models and has used the St. Louis data base for base-case simulations and comparisons of computed and observed concentrations. The Monitoring and Data Analysis Division (MDAD) of the Office of Air Quality Planning and Standards (OAQPS) has used the ESRL simulations to perform a statistical evaluation of model performance, has conducted sensitivity analyses and control strategy simulations using a subset of the ESRL test days. While ESRL's analysis focuses on the scientific validity of model components (numerical diffusion, chemistry, windfields, etc.), the MDAD analysis focuses on the evaluation and application of the model from a a regulatory standpoint.

Initial simulations conducted in 1978-1979 resulted in a strong tendency toward underestimation of afternoon ozone concentrations. As a result, EPA carried out an extensive program to determine the causes of poor model performance. Detailed examinations of model components, the emission inventory and data preparation methods led to substantial modifications in these areas. The most significant changes are (1) the replacement of the Carbon-Bond I chemical mechanism with the Carbon-Bond II mechanism, (2) correction of the emissions inventory with the result that the quantity and reactivity of emissions were increased, (3) layer-averaged photolytic rate constants used in place of surface-based rate constants and (4) replacement of the numerical advection routine to eliminate artificial numerical diffusion. A substantial improvement in model performance resulted from these modifications.

The methodologies and results for the ESRL base-case simulations are detailed in the "Final Evaluation of Urban-Scale Photochemical

Air Quality Simulation Models" by Schere and Shreffler.[3] While the current report summarizes the ESRL work, its primary emphasis is on the performance evaluation, sensitivity studies and control strategy analysis conducted by MDAD.

2.0 The Urban Airshed Model

As previously stated, the Airshed Model is a three-dimensional photochemical grid model which numerically simulates ozone and precursor concentrations for a large number of grid cells which collectively represent the urban domain. The purpose of this chapter is to describe the technical basis for the Airshed Model, its theoretical foundation, its treatment of important physical and chemical processes and its assumptions and limitations.*

Overview

The Airshed Model is Eulerian, meaning that computations simulate the time changes in precursor and secondary pollutant concentrations which take place at given locations, i.e., within grid cells. For each simulation, the user designates the horizontal extent of modeling grid and a uniform dimension for the grid squares; both remain constant during the course of simulation. The user also designates the depth of the modeling region and the width of the vertical layers used; these dimensions, however, are allowed to vary diurnally to account for changes in mixing. In typical simulations, the modeling region encompasses the entire metropolitan area including the downwind region which often experiences high ozone concentrations and the region immediately upwind of urban areas. The choice of grid square size reflects a balance between the need for resolution and the increase in cost encountered as the number of grid cells grow. For the St. Louis application, a 4 km square length was found to represent a reasonable compromise. In most applications, the first several thousand meters of the atmosphere are modeled and the regions above and within the mixed layer are each represented by several layers. Figure 1 illustrates the three-dimensional grid approach used by the model.

---

*More detailed discussions of the Airshed Model are presented in several reports.[1,5]

The mathematical basis for simulating concentrations of ozone and precursors is the conservation of mass. The major processes which cause changes in the amount of mass in a given air parcel (cells) are emissions, transfer of mass into and out of the cell associated with advection and dispersion and chemical changes in the composition of the cell. The Airshed Model solves the following equation (stated in terms of concentrations rather than as time differentials). For each cell,

$$\text{Concentration } (t_i) = [\text{Concentration } (t_{i-1})] + \left[\frac{\text{rate of mass transfer}}{\text{cell volume}}\right] \Delta t$$

$$\left[\frac{\text{mass emission rate}}{\text{cell volume}}\right] \Delta t + \left[\text{chemical transformation rate}\right] \Delta t$$

This equation is iterated through many time steps. In a typical simulation each time step may represent several minutes. In the above equation each time step is represented by Δt where $\Delta t = t_i - t_{i-1}$. The left hand term in the equation represents the concentration of a specific species at the end of a time step. This concentration equals the concentration at the beginning of the time step plus the changes in concentration due to transfer, emissions and chemistry (right-hand terms) that occur during the time step. At the beginning of the simulation ($t = t_0$) an initial concentration based on measured or assumed ambient concentration must be designated. A typical time for starting simulations is 5 a.m.; this is prior to the morning rush hour when concentrations are still fairly low. This practice makes the model estimates less sensitive to initial concentrations.

While the primary concern may be ozone, simultaneous solution for precursors and intermediate species as well as ozone is necessary. Precursors include NO, NO_2 and organic compounds split into five different classes corresponding roughly to paraffins, olefins, ethylene, aromatics and aldehydes. The intermediate species include various types of organic and inorganic free radicals.

The right-hand terms of the equation are discussed in greater detail in the following sections. Detailed mathematical expressions are available elsewhere.[5]

2.1 Mass Transfer (Advection and Dispersion)

The Airshed Model simulates the transfer of pollutants in the atmosphere which result from atmospheric motions. Advection refers to a transfer by the mean wind flow and dispersion to a transfer by atmospheric turbulence. The effect of both processes is dilution or from the standpoint of fixed cells a net transfer of mass from cells with higher concentrations to those with lower concentrations. Advection in the model is a function of the gradient in concentration (differences in concentration between cells) and the speed of the flow component along the direction of the gradient. (Flow perpendicular to the gradient results in no advection.)

The rate of transfer due to dispersion is a function of the concentration gradient and the intensity of random or turbulent motions (departures from mean flow). In the model, the intensities are represented by horizontal and vertical proportionality constants known as eddy diffusivity coefficients (K_h and K_v respectively). Because they are difficult to measure and specify precisely, the approach used in the model is one of approximation.

With regard to horizontal pollutant transport, advection tends to be significantly more important than turbulent diffusion. This dominance is strengthened because local concentration gradients near point and line sources cannot be represented in the Airshed Model owing to the use of a grid with relatively coarse resolution. Given the insensitivity of the model to horizontal diffusion, K_h is set to a constant value of 50 m^2/sec. In contrast to horizontal transport, turbulent diffusion is frequently the dominating vertical transfer process. Thus, the model uses an individual value of K_v values as a function of stability class, ground-level wind speed, surface roughness and the height of the grid cell, all parameters which affect the intensity of vertical mixing. (Reference 5, Appendix, for detailed discussion).

The Airshed Model also simulates vertical advective transfer. Vertical transfer arises primarily from two sources: (1) balancing the effect of convergence and/or divergence of horizontal winds in order to achieve a proper mass balance of air, and (2) accounting for changes in cell height as the mixing height changes. The first source of vertical transfer must be considered in preparing the wind data for use in the model. For example, if the horizontal winds are converging in a cell, the wind field used in the model must have a sufficient vertical component to prevent an artificial accumulation of pollutants in the cell. The second source of vertical transfer is an artificial one arising from the mechanics of the simulation program. As the cell height increases, material located at a given height may be transferred from one cell to another without actually changing its relative vertical position.

Thus far we have discussed the transfer of mass between cells. The model also estimates the mass which is advected and diffused into the modeling region from the surrounding region. Thus, an input requirement of the Airshed Model is a set of concentrations at the margins of the modeling region. More specifically, the model requires concentration estimates for all key species for each hour simulated along the sides and at the top of the modeling region. Transfer into the region is particularly important where interurban transport of ozone (and precursors) occurs. However, even the naturally occurring ozone background (on the order of 0.04 ppm) can have a significant effect on urban photochemistry.

2.2 Emissions

The treatment of emissions is straightforward conceptually: the emissions into a cell are added uniformly throughout the cell. Thus, the change in concentration due to emissions simply equals the mass added divided by the volume of the cell. Ground-level emissions are added into the lowest level cell. Elevated emissions are added into upper level cells. This requires that certain stack parameters be input for the major point sources. The stack parameters are used along with the wind speed to estimate an effective plume height for each major point source according to the methods of Briggs.[6] The emissions are then added uniformly throughout the (upper level) cell which is calculated to receive the plume.

The Airshed Model is designed to treat emissions of eight pollutants: NO, NO_2 five classes of organics and CO. NO_x emissions must therefore be divided into emissions of NO and NO_2 and organics must be divided into emissions of five organics classes. These classes are discussed in Section 2.3.

A point of comparison between the Airshed Model and Gaussian dispersion models is the treatment of plume rise. Like most inert pollutant dispersion models, the Airshed Model uses the Briggs[6] formulae to estimate plume rise. However, unlike most Gaussian models, the Airshed Model is capable of simulating emissions that rise above the mixed layer. Although the Airshed Model also disregards any emissions in plumes that rise above top of the modeling region, the modeling region in the Airshed Model can extend above the mixing height. It is thus possible to simulate plumes that rise into an inversion layer between the mixing height and the top of the modeling region. With diurnal growth in mixing height, such pollutants may enter the mixed region and affect surface concentrations at a later time.

2.3 Chemistry

The chemical mechanism is one of the most complex components of the Airshed Model. The chemistry of ozone production has been the subject of intensive study for well over a decade, and yet there is surprisingly little agreement on the list of reactions to use in simulating ozone photochemistry. Thus, this discussion will only provide a general outline of the photochemistry of ozone production. The discussion will then outline the major distinguishing features of the chemical mechanism used in the Airshed Model.

The general process by which tropospheric ozone is formed is illustrated in Figure 2a shows the NO_2-NO-O_3 cycle. These reactions may be written as chemical equations:

a. NO_2 + sunlight → NO + O

b. $O + O_2 \rightarrow O_3$

c. $O_3 + NO \rightarrow NO_2 + 2$

Ozone is not emitted in any measurable quantity, and, in fact, reactions (a) and (b) represent the only significant sources of tropospheric ozone. However, these reactions are fully reversed by reaction (c). Thus, NO_x by itself will not cause significant concentrations of ozone. The only way significant concentrations of ozone will occur is for some other species to oxidize NO to NO_2 without destroying ozone. This is exactly what is shown in Figure 2. This may be written as:

d. Organic radicals + $NO \rightarrow NO_2$ + miscellaneous products

The net result of reactions (a), (b), and (d), then, is a recycling of NO_2/NO, a modification of the organic species, and the generation of an excess O_3 molecule. That is, organic species permit the ozone formation step while bypassing the ozone destruction step of the NO_2 - NO - O_3 cycle. The result is a buildup of the ozone concentration. Reactions (a), (b), and (c) are fast enough that a balance or equilibrium is still maintained between the concentrations of NO_2, NO, and O_3, but this balance involves a much higher ozone concentration than would occur without organics.

The above four reactions provide an overview of the chemical processes of ozone formation. However, the number of reactions which affect this process is far larger and the chemical reactions simulated in these models are a simplified representation of the innumerable reactions that actually occur.

It is more difficult to represent the various reactions or organics than it is to represent the reactions of NO_x. There is substantial agreement on about 10 to 15 NO_x reactions as being the most significant reactions for describing the fate of NO_x. However, there is relatively little agreement as to how best to represent organic reactions. This is primarily due to the almost infinite number of species and reactions that occur. Moreover, urban emissions include a wide variety of organic species. Therefore, a simplified representation of all these reactions is needed.

The typical means of representing significant organic reactions is to utilize a small number of reactions for about three to five categories of organics. In contrast to other photochemical models, the categories used in the Airshed Model represent total numbers of bonds of specific bond types rather than total numbers of molecules of specific molecular types. In other words, the Airshed Model treats individual compounds not as molecular units but rather as carbon-bond units. Several different carbon-bond types are recognized: single bonds, double bonds, aromatic bonds, and carbonyl bonds. (These can be recognized as the identifying bond types for paraffins, olefins, aromatics and aldehydes.) The double bonds (olefins) are further broken down into highly reactive and moderately reactive double bonds. Carbonyl bonds include not only those associated with aldehydes, but also those associated with ketones and esters. The single bonds are the least reactive while the highly reactive double bonds are, as their description implies, the most reactive; the others are of intermediate reactivity.

Another species which can be considered in the Airshed Model is CO. Carbon monoxide plays only a minor role in ozone photochemistry and most photochemical models consider it insignificant enough to ignore. Carbon monoxide has more significance as a relatively inert gas which may be used as a tracer. By comparing the CO concentrations estimated by the model to measurements of CO concentrations, it is possible to obtain a direct assessment of the accuracy of the treatments of emissions, advection, and dispersion without the complicating influence of chemistry. This can be quite useful for assessing model performance.

Another feature of the chemical mechanism is the option to consider temperature effects. Temperature has a significant effect on the rates at which many reactions occur, although it is unclear what effect it has on overall ozone production. Unfortunately, there is little known about the temperature dependence of the rates of many important photochemical reactions. Nevertheless, the Airshed Model does provide the option to utilize current knowledge about the temperature variation of the rate constants used in the chemical mechanism.

2.4 Surface Removal Processes

Ozone, NO_2 and other pollutants treated in the Airshed Model are removed from the atmosphere by adsorption, absorption, or chemical processes at the different surfaces in the region being modeled. The rate of removal is dependent on the species, the type of surface and the rate of turbulent transfer in the lowest portion of the atmosphere. In the Airshed Model, surface removal is treated using the concept of deposition velocity; that is, the uptake of a given pollutant at the surface is proportional to the concentration in the lowest cell and the proportionality constant is the deposition velocity. The deposition velocity is estimated by defining a resistance to mass transport and a resistance to surface removal. The transport resistance is calculated for each surface cell (for each hour) as a function of surface roughness, stability and windspeed, while the resistance to surface removal is a function of pollutant and land use category.[7]

2.5 Assumptions and Limitations

It is important for the reader to understand the major assumptions and limitations inherent in the Airshed Model since these assumptions limit the accuracy of the model in replicating observed concentrations and in estimating control requirements. The model assumes that:

1. The chemical processes affecting ozone in real urban atmospheres can be accounted for accurately with the simplified chemical mechanism.

2. Subgrid processes are not considered in the current version of the Airshed Model; since the model assumes instantaneous mixing of emissions into an entire grid cell, it tends to overestimate the dispersion rate for line and point sources.

3. Similarly, the degree of vertical mixing is artificially enhanced by limiting the number of vertical layers (for economic reasons), four layers were used in the current analysis.

The limitations in 2 and 3 appear to have the effect of suppressing estimated ozone levels downwind of major NO_x sources; this problem is discussed in Chapter 4.

Additional limitations are associated with the collection and preparation of data required by the model. For example, the user must construct a three-dimensional windfield for the modeling region--usually from a limited set of observations. Assumptions are made regarding the speciation of hydrocarbon emissions from various sources and boundary concentration profiles are often assembled from sparse data. These problems are discussed in subsequent chapters.

3.0 Methods and Data Bases

The purposes of this chapter are: (1) to outline the general approach used in the St. Louis Ozone Modeling Study; (2) to describe the RAPS (Regional Air Pollution Study) emissions, meteorological, and air quality data bases used in the analysis; and (3) to describe in brief the data preparation required to create model input files.

3.1 General Approach

The general approach used in the St. Louis Study is outlined as follows:

1. Twenty test days from the 1975-1976 RAPS period were selected for base-case simulations.

2. Necessary input files were prepared from the RAPS data bases. Meteorological and air quality inputs were derived for the 20 days. Emissions files represent typical summer weekdays for the 1975-1976 period.

3. The Airshed Model was used to simulate air quality for the 20 test days. (Base case simulations)

4. The AMS recommended procedures[4] were used to compare the computed values for the base-case concentrations with observed values. Most of the comparisons made are day specific. (Chapter 4)

5. Sensitivity analyses were carried out for a 3-day subset of the 20-day data base. (Chapter 5)

6. Control strategy simulations were conducted using modified emission inventories for the 3-day subset. Emission inventories used were adjusted to represent the effects of stationary and/or mobile source control; meteorology was held constant. (Chapter 6)

As previously stated, several rounds of testing were required to improve the initially poor model performance. The results used in this study are based on the fully revised emissions inventory and the 1982 version of the Airshed Model.[3] One other point needs clarification. Given the large uncertainties associated with population and economic trends in the St. Louis area, we assumed that the levels of activity for stationary and mobile sources remain constant at 1976 levels for the control strategy cases. For stationary sources, changes in emissions reflect federally mandated controls. For motor vehicles, the distribution and age mix are estimated for 1987. No changes in automobile numbers, traffic volumes or traffic patterns were considered in estimating emissions.

3.2 The RAPS Data Bases

The following sections give brief descriptions of the emissions, air quality and meteorological data bases used in the study. The discussion focuses on the data bases used for base-case simulations; descriptions of input modifications for sensitivity and control strategy simulations are presented in Chapters 5 and 6 respectively.

3.2.1 Emissions

The Airshed Model requires two different emissions files: one for area sources and a second for major point sources. The area-source file includes small stationary sources, minor point sources and mobile sources. Emissions from the area sources are all treated as ground-level sources and are added to the lowest layer of the modeling region. Major point sources include large industrial sources of hydrocarbons and NO_x. (There are about 100 of each in the RAPS inventory). The model requires parameters for major point sources which allow the calculation of plume rise. The plume-height calculations are used to determine the layer in which major point-source emissions are introduced.

The emissions for both area and point sources are designated for each hour of the model simulation and allocated into the appropriate species (NO, NO_2 and five classes of organics). The area-source emissions are allocated spatially into nearly 2000 grid cells varying in size from 1 km in areas of dense emissions to 10 km in outlying areas. Prior to modeling, the emissions from the RAPS inventory were reallocated into a new grid array consisting of 374 grid squares 4 km on a side. Locations of the major point sources are retained in both the RAPS and Airshed Model grids.

A complete description of the information sources and methods used for the point and area-source emissions is beyond the scope of this report. (Interested readers may refer to an extensive report by Littman[8] for documentation). Nevertheless, some additional information is useful. In general, emissions for larger point sources are based on houly records of process flows or fuel combustion for the specific sources. However, smaller stationary sources are treated as area sources and emissions from the different categories are obtained using various indirect methds. For example, NO_x emissions from commercial and residential heating are derived from county-wide sales using allocation factors based on population and land-use distribution. Mobile-source emissions are estimated using transportation models of traffic flow and emission factors estimated by Mobile I. Roadways are represented primarily as straight lines or links whose emissions are determined as a function of average daily traffic, hourly distribution of traffic and speed. Link emissions are then allocated into the RAPS grid cells.

The RAPS emission inventory has been set up as an automated archive system by ESRL. This system tracks point emissions not only by source, but also by industrial or process category. This feature was utilized in the development of emission inventories for stationary source control.

Tables 1 and 2 show the distribution of HC and NO_x emissions by source type for the St. Louis AQCR. Area sources are summarized in Table 1 and point sources in Table 2. Note that for hydrocarbons, stationary and mobile (highway plus off-highway) sources each contribute about half of the emissions. Stationary source HC emissions are associated primarily with evaporative source (e.g., miscellaneous solvent use, surface coating, painting, degreasing). In contrast, nearly two-thirds of the NO_x emissions stem from a single source-type electric power generation. About 25 percent of the NO_x emissions are from mobile sources. That a large portion of NO_x is emitted from a relatively small number of power plants with elevated stacks is extremely significant from the standpoint of photochemistry. During the morning hours much of the NO_x emssions will be emitted above the urban mixed layer; on the other hand, a majority of HC emissions are emitted within the mixed layer and the HC/NO_x concentration ratio tends to be higher than indicated by the total emissions.

3.2.2 Air Quality

Measured pollutant concentrations were used (1) to estimate boundary and initial concentrations used in the model simulations, and (2) for purposes of comparison with predicted concentrations. Air quality measurements were obtained largely from the RAPS network of 25 surface stations which operated on a continuous basis during 1975 and 1976. The location of these monitors is shown on Figure 3. Each station was equipped with gaseous pollutant analyzers to measure ozone, NO, NO_x (NO_2 by difference), hydrocarbons (gas chromotography), total suspended particulates SO_2, and CO. As Figure 4 shows, the monitoring stations are clustered in the urbanized portion of the modeling region and large portions of the nonurban modeling region have no monitors. Four sites (122, 123, 125 and 125) are located just outside of the modeling region and were used to obtain boundary concentrations. An aerial monitoring system consisting of three helicopters complimented the surface network. The airborne data (total NO_x, O_3, SO_2, total hydrocarbons, methane and particulate measurements) were used to depict three-dimensional pollutant distributions in the urban region, and estimate the flow of ozone and precursors into the modeling region (vertical boundary concentration profiles). Documentation of the surface land airborne measurement program is found in an EPA report by Strothmann and Shiermeier.[9]

3.2.3 Meteorological Data

The 25 monitoring stations discussed in the preceding section were also used to obtain meteorological measurements including wind speed and direction (at 10 or 30 m), temperature, dew point, barometric pressure and solar radiation. Vertical profiles of winds and temperature were obtained from slow ascent rawinsondes released at 6-hour intervals with pibals released hourly between radiosonde observations at urban site 141 and at outlying sites 142, 143 and 144. The meteorological data were used to generate three-dimensional wind fields, to estimate diffusivity and to estimate mixing heights for each hour of the simulations. (See Section 3.3 for discussion of data preparation methods. Additional information on the meteorological network is available in the EPA report).[9]

Analyses of the RAPS aerometric data and on the relationship between observed concentration and meteorological factors are presented in a series of reports by ESRL.[10,11,12,13,14]

3.2.4 Selection of Test Days

The evaluation of model performance contained in this paper is based on Airshed simulations for 20 days (11 days from 1975 and 9 from 1976). There were three criteria for selection: data availability, high measured ozone, and representation of different meteorological regimes. For all 20 days the maximum hourly ozone concentration for at least one site exceeded 0.16 ppm (160 ppb). Table 3 lists the basic meteorological conditions and peak ozone concentrations for the 20 days. Most of the days were characterized by sunshine and low to moderate wind speeds reflecting the presence of high pressure systems which are conducive to photochemical oxidant formation.

Three of the 20 days (Days 159, 195 and 275) were used for extensive sensitivity testing and control strategy applications. All 3 days experienced high ozone; 2 of the 3 had moderate wind speed and a third (275) was characterized by very low wind speeds and mixing heights (stagnation).

3.3 Preparation of Airshed Inputs

3.3.1 The Modeling Domain

The horizontal extent of the modeling region used for St. Louis is shown in Figure 4. The grid is composed of 374 squares 4 km on a side. The outermost rows and columns are boundary cells and are used only to account for the transfer of mass between the modeling region and the surrounding area. Vertically, four layers of cells were used; two bottom layers for the mixed layer and the two top layers for the stable air above the mixed layer.

3.3.2 Input Files

Extensive manipulation of the aerometric and emissions data bases is performed using a set of preprocessors to obtain the input files required for the Airshed Model. The content of these files is summarized in Table 4. Several of the files warrant additional comment.

The diffusion break and region-top files describe variations in the mixing heights and modeling region depths respectively over the domain during the course of the simulation. In the St. Louis Study, the region top was designated to be higher than the mixing height for all hours; this ensures that all of the urban emissions introduced into the mixed layer will be treated. The diffusion break file requires hourly values of the mixing height for representative locations within the modeling region. As previously stated, rawinsondes were released at single urban site and several rural sites at 6-hour intervals. The resulting temperature profiles were used to estimate mixing heights at these locations and linear interpolation was used to generate hourly values. Spatial interpolations are made within the Airshed Model.

In order to construct the windfield file, ESRL used a preprocessor developed by Systems Applications, Inc.[15] The preprocessor assimilates all available surface and upper air winds and produces a gridded field of U and V wind components for each of the four vertical levels used in the model. The preprocesor utilizes an objective analysis which: (1) derives an average surface wind vector for the entire network; (2) simulates mesoscale urban circulation patterns using the surface temperature patterns and basic dynamic equations; and (3) uses measured upper air winds to define wind profiles. Vertical velocities are calculated internally by Airshed from the equation of mass continuity. The spatial averaging of surface winds is done in order to eliminate unrealistically large horizontal divergence, divergence that will result in excessively large vertical motions within the model.*

The metscalers file describes the temporal variation of vertical temperature gradients, stability class, atmospheric pressure, water vapor concentration, and the NO_2 photolysis rate constant. Values for these parameters do not vary spatially in the model. The top concentration file specifies the concentrations of principal species at the top of the modeled region throughout the simulation. In most cases these concentrations will be close to the clear air background values for these species, although substantial concentrations of O_3 can be advected over the region. Its value is determined from the O_3 measurements at the far upwind surface monitoring sites after the nocturnal inversion has eroded and the air aloft mixes through the atmosphere to the surface. The range of inflow ozone concentrations experienced can be seen in the final column of Table 3.

---

*A report by Schere[16] examines the use of alternative wind routines for the St. Louis Application of Airshed.

The air quality, temperature and wind speed files all require data from the surface monitoring network. Hour averages of observed species concentrations are objectively interpolated across the model grid to produce a field of initial concentrations for the Airshed Model. Typically, this initial field is applied at a near-sunrise time. The temperature file produces gridded fields of surface temperature at each hour of model simulation. These are required for both the wind and emissions point source files (for plume rise).

The emissions file for the current study was prepared by reallocating the hourly area-source emissions from the RAPS inventory (see Section 3.2.1) into a new grid array (the Airshed Grid) consisting of 374 grid squares, 4 km on a side. Similarly, the point-source file required a reallocation from the RAPS to the Airshed Grid. Figures 5 and 6 show the emissions distributions from all sources of THC and NO_x, respectively, allocated into the Airshed Grid. The particular emissions shown are for the 1-hour period 0800-0900 CST on July 13, 1976, but also characterize the typical summer, weekday rush hour in St. Louis. Downtown and industrial areas are evident in the central area from the higher emission rates. The stacks from several large power plants are seen in high cell NO_x emissions in the north central and south central portions of the regime.

Finally, the terrain file describes the spatially varying types of surfaces in the modeling region. Both surface roughness and deposition velocities are calculated within the model as a function of the land-use categories in the terrain file.[17] (For detailed discussion of methods used to develop this file, see reference 17). The land-use distribution is shown in Figure 7.

4.0 Model Performance Evaluation

The purpose of performance evaluation is to assess how well a model can reproduce observed concentrations using emissions data and meteorological conditions for the same period as the observed concentrations. In actuality, it is not only the model that is being tested, but the application of the model including the appropriate use of the model and the validity of the inputs. The objectives of this chapter are to report on the St. Louis evaluation of the Airshed Model--its methods and its results. Several concerns are foremost: (1) the accuracy of the model applications, especially in simulating the peak and near-peak concentrations; (2) the precision of the estimates; and (3) the ability to replicate observed spatial and temporal patterns. The authors view accuracy as the most critical of the attributes; however, the precision measures are used to establish the level of confidence that we have in our estimates of accuracy. An additional objective is to identify sources of error. The primary focus of the study is ozone; the full complement of statistical tests described below were performed for ozone; however, a smaller number of tests were conducted for CO and NO_2.

The specific procedures used in this study are those recommended by the AMS Workshop on Model Evaluation[4] as supplemented by Cox.[18] Before discussing these procedures in detail, it is necessary to make several statements about the data sets used in the analysis and their treatment prior to statistical analysis. The starting point for the calculation of performace measures is a table of observed and predicted concentrations for each day arranged by hour and by monitoring station. An example for one day (Day 226) is shown in Table 5. The predicted concentrations shown are not the grid square concentrations obtained directly from the model but are estimates of discrete concentrations for the locations of the monitoring sites. These estimates were derived by averaging the values from the grid cells in close proximity to the monitor. The grid values were weighted according to the inverse of the distance between cell and monitor. Secondly, it is important to note that the performance measures were calculated separately for each day due to the large variation of meteorological conditions from day to day. However, several techniques are used to examine the behavior of the performance measures over the whole 20-day data set.

The methods used to evaluate model performance are discussed in Section 4.1, results in Sections 4.2 through 4.6. Section 4.7 reports on a partial analysis made for pollutants other than ozone and 4.8 is a summary of the main conclusions on model evaluation.

4.1 Methods

4.1.1 Accuracy of Peak/Near-Peak Predictions

From the standpoint of regulation, the most important aspect of the evaluation is determining how accurately the model reproduced peak and near-peak observed concentrations. The methods used in the current study are outlined in Table 6; these include the recommendations of the AMS Model Evaluation Workshop[4] and the refinements of Cox.[18]

Table 6a summarizes the calculations made for each of the 20 test days separately. Peaks are compared for four different residuals using observed and predicted maximum hourly concentrations. Residuals are for observed and predicted values which are paired in time and location (F1), paired in time but not space (F2), paired in space but not time (F3), and unpaired in time and space (F4). F1 is clearly the most stringent measure; a zero residual (no bias) requires that the computed value for the time and location of the observed peak be identical to that of the observed peak. In the least strigent measure F4, the model peak is compared to the observed peak without regard to location or hour. F2 and F3 have intermediate stringencies; for example in F2, the maximum observed concentration is compared to the highest value predicted for the same hour but without regard to location.

Several authors have pointed out that the F1, F2 and F3 measures have an inherent tendency to show underprediction even when the model has no actual overall bias.[18,19] This tendency is illustrated in the following simple example. Suppose the observed peak is 200 ppb and occcurs at 3:00 p.m. at Station A. The model on the other hand predicts that the peak for the day will occur at Station A and will also be 200 ppb; however, the time is 4:00 p.m. rather than 3:00 p.m. The predicted value for station A at 3:00 p.m. is 160 ppb. One can see that residuals F1 and F2 are both equal to (200-160 = 40 ppb), i.e., the model is interpreted as underpredicting the overall and temporal peak. However, in actuality the calculated bias is the product of temporal displacement, rather than a failure of the model to generate sufficient ozone. Similarly, a displacement in the location of the peak will result in a positive bias (underprediction) for F3. Only the totally unpaired residual F4, is free from this characteristic. A second problem is that these measures are based on a single residual and thus are not robust.

To overcome the problems associated with the residuals, more robust alternative procedures for evaluating near-peak accuracy of models are also considered. For the A1 statistic (see Table 6a), the peak residuals paired by hour are calculated for all hours and not merely for the hour of the highest observed value. Similarly, for A2, residuals of peak values paired by site are calculated for all sites. Thus, as Table 6a shows, the availability of multiple residuals allows an A1 and A2 bias ($\overline{d}$) to be calculated for each day. We are also able to track the residuals (d) over time or by location and to calculate the standard deviation of A1 and A2 residuals. The standard deviations (S_d) are then used to construct confidence intervals about the daily bias values. As the table shows, these procedures are not possible using the peak residuals.

One problem with the A1 and A2 measures is that they include hours and stations which are likely to experience low ozone values (i.e., early morning hours, upwind stations). The A4 measure, on the other hand, uses only the 25 highest observed and predicted concentrations. The bias ($\overline{d}$) is obtained in a totally unpaired fashion by subtracting the average value of the 25 highest predicted concentrations from the average of the 25 highest observed concentrations. Confidence intervals are constructed using the standard deviations of observed and predicted values.*

As evident from Table 5, the F measures are actually a subset of the A measures. In Section 4.2.1, a numerical comparison of the two measures is presented.

Table 6b shows the measures obtained to show the behavior of residuals over the full 20-day test set. For the F residuals, a 20-day bias ($\bar{d}$ for F1, F2, F3 and F4) is obtained by averaging the residuals for the 20 days. For the A residuals, the 20-day bias is the average of the 20 daily bias values. Calculation of precision values (standard deviation) for the 20-day data base is shown in Table 6b. In addition to the bias and precision measures, a number of scatter diagrams of observed versus predicted values were constructed using the different F and A residuals; respective correlation coefficients of observed and predicted values were also obtained. The results of the analysis on peak and near-peak accuracy are reported in Section 4.2.1.

4.1.2 Overall Accuracy and Precision

The measures used to assess overall accuracy and precision across the full range of concentrations are essentially those recommended by the AMS Workshop.[4] These measures are outlined in Table 7.

---

*The reader should keep in mind, however, that both the "F" and the "A" statistics are tied to predictions made at specific stations. Thus, neither is completely free of the effects of spatial displacement if such displacement is associated with predicted peaks which were not precisely at the monitoring sites. The A statistics are freer from this effect than the F statistics.

As this table shows, measures of bias and scatter were obtained using paired and unpaired analyses. In the paired analysis residuals are calculated by subtracting the predicted concentration for a given hour and site from the observed value for the same hour and site. For the unpaired analysis, individual residuals are not calculated; instead the characteristics of the sample of observed values are compared to the characteristics of the sample of predicted values. For example, the cumulative frequency distributions of observed and predicted concentrations are plotted separately and compared.

For both the paired and unpaired analyses, the study uses a simple graphical approach to combine information on accuracy and precision. In this approach, the bias values for each day are bracketed by day-specific 95 percent confidence intervals; this arrangement enables one to weigh the relative importance of bias and scatter. For example, when the confidence intervals do not overlap zero we may assume that the bias is statistically significant and indicates systematic rather than random error. The methods of constructing the confidence intervals are given on Table 7. For the paired analysis, the intervals are based on standard deviation of the residuals; for the unpaired analysis a pooled standard deviation (from S_o and S_p) is used. It should be noted that the confidence intervals were computed assuming independence of the data. This assumption however, is not true. We know that spatial and temporal autocorrelation exists in the observed and predicted data sets and also among the residuals. The confidence intervals should therefore be viewed as first approximations which tend to underestimate the true extent of scatter about the bias.

In addition, to determine how well the model does in an overall sense, it is important to find out whether the errors fall into any discernible patterns. For example, is the model more accurate (or precise) at high concentrations versus low concentrations? Is there a relationship between bias and time of day or between bias and receptor location (upwind versus downwind of the urban core)? Is the model more accurate for transport days versus stagnation days?

Several analyses were conducted to study how bias and scatter vary with concentration level. The bias/confidence interval graphs were constructed separately for three subsets of paired residuals: (1) all values; (2) those for which either the observed or predicted values exceeded 80 ppb; and (3) those for which either observed or predicted values exceeded 120 ppb. Secondly, scatter diagrams showing predicted vs. observed concentrations were plotted to further establish day-specific relationships between bias and concentration level. For unpaired analysis, day-specific frequency distributions of observed and predicted concentrations are compared.

To test for diurnal and spatial patterns of error, a series of diagrams was prepared showing the errors as a function of hour and site for each of the 20 days. In addition, an analysis was made to determine whether the ability of the model to predict daily peak observed concentration varies with meteorological conditions such as wind speed and mixing height.

4.1.3 Replication of Patterns

As stated in Chapter 1, grid models are designed not only to predict maximum concentrations, but also to predict spatial and temporal distributions. For example, we would like to use the Airshed Model to forecast how the aerial extent of exceedances (e.g., number of cell/hours with ozone concentration >0.12 ppm) changes with given control programs. Prior to using the model in this way, it is necessary to demonstrate that the model can in fact reproduce spatial and temporal patterns of variation with a reasonable degree of accuracy. As Table 8 indicates, the techniques used to examine these attributes include (1) visual comparison of time series and spatial plots of observed and predicted concentration, and (2) computation of spatial and temporal correlation coefficients between observed and predicted concentrations. Both of these techniques were used for each of the 20 test days. One fact to bear in mind is that the correlation coefficients reflect only the degree of covariation between observation and prediction; thus, a high correlation coefficient may be computed when the predicted values contain a large systematic error or bias. Thus, the visual comparisons are more useful in determining how well the model does in estimating the distribution of areas exceeding the NAAQS or other levels. Formulae for correlation coefficents are found in Table 8. While no attempt was made to establish confidence intervals about the correlation coefficients (as suggested in the AMS report), temporal correlation coefficients were calculated for all monitoring sites and spatial correlation coefficients were calculated for all hours. Thus, the average values and the range of temporal and spatial correlation coefficients are established for each day.

4.2 Results of Model Evaluation Analysis

The basis for all of the model evaluation analyses are matrices of observed and predicted values for each day; the matrices are arranged by hour and by station. An example (for Day 226) is presented in Table 5.

For convenience, the results are presented and discussed in three sections corresponding to the three Protocol Tables 6, 7, and 8. Results of the peak/near-peak accuracy analysis are presented in Section 4.2.1; those of the overall acuracy and precision analysis are given in 4.2.2 and 4.2.3 provides an assessment of the model's ability to replicate spatial and temporal patterns.

4.2.1 Results: Peak/Near-Peak Accuracy Analyses

The computed values of the performance measures for peak accuracy are presented in Table 9. The values for each day are given in Table 9a and the 20-day average residuals and 20-day confidence intervals are given in Table 9b. All calculations have been made according to the formulae given in Table 6.

The analysis of the results focuses on a number of questions: (1) is there an overall tendency towards negative or positive bias in the peak and near-peak predictions? (2) does this bias vary from day to day? (3) how large is the random component or scatter of the errors? (i.e., what uncertainty is associated with our estimates of bias), and (4) what differences and relationships can we discern in the behavior of the different residual measures (F4, A1, A2, etc.)? A number of graphs have been prepared to facilitate interpretation of the results and to answer the above questions.

Figure 8 is a graphical presentation of the 20-day average residuals and confidence intervals presented in Table 9. The average residuals shown are all positive, and most may be interpreted as being significantly different from zero; only A4 confidence intervals (based on S^2_o, S^2_p)* overlap the zero bias line to a small extent. Thus, we can state with considerable confidence that the model has a systematic tendency to underpredict peak and near-peak ozone concentration over the 20-day data set, irrespective of the particular measure used.

Figure 8 demonstrates that the choice of measure used will have a pronounced effect on one's perception of the degree of bias. The differences between the values of the different measures are consistent with conclusions drawn in Section 4.1.1. Estimates of underprediction are largest for the F residuals because they are based on the time and/or location of the observed peak; temporal and spatial displacements of the predicted peaks are constrained to introduce positive bias (underprediction). Only F4 is free from this effect and is shown to have a smaller positive bias.

---

*Confidence intervals for the unpaired measures F4 and A4 were calculated using two methods. The inner confidence intervals measure the variability of the $\bar{d}$ values over the 20-day period and are based on the standard deviations of the differences (S^2_d). The outer intervals are used to determine whether $\bar{d}$ is significantly different from zero and are based on $S = \sqrt{S^2_o + S^2_p}$.

The A residual measures for temporal and spatial pairing have values of 12 and 14 ppb compared to a value of 48 ppb for both of the corresponding F2 and F3 measures. As expected, the F1 measure which is paired in both time and space to the observed peak has the largest value (61 ppb).

The solid bars represent 95 percent confidence intervals about the mean residuals based on the variance of the residuals over the 20-day data set. The intervals on A measures are considerably smaller than those of the F measures, indicating that the former are more stable indicators of bias. This is to be expected since the F measures are based on single residuals for each day, while A measures are more robust averages (A1: based on 15 hours; A2: based on 21 sites; A4: 25 highest observed, 25 highest predicted values).

Figures 9 and 10 show how the measures vary from day to day. Figure 9 presents the spatially paired measures. Confidence intervals based on within-day variation are constructed about the A2 mean residuals.

The A2 measures demonstrate statistically significant underprediction for 13 of the 20 days, significant overprediction for 3 days and near zero bias (confidence intervals substantially overlap zero line) for 4 days. These measures allow us to assess how well the model matches the observed maxima (regardless of time) for the ensemble of sites. They demonstrate that for the ensemble of sites, underprediction occurs on most but not all days and suggest that the extent of underprediction is less serious than indicated by the F3 measure.*

---

*The F3 measures are positive (underestimates) for all days. This finding suggests that the constraints inherent in this statistic mask its ability to distinguish true model bias. From the F3 measure we can conclude only that at the location of the observed peak, the maximum model concentration is underpredicted for all days.

Figure 10 shows the values of A4 and F4 measures for each of the 20 test days. Although both are unpaired, the F4 is based on the single residual (O_{max} - P_{max}) while A4 is based on a comparison of the average of the highest 25 observed values and the average of the highest 25 predicted values.

The behavior of the unpaired measures over the 20-day data set is similar to that for the spatially paired measures (Fig. 9). However, two of the F4 measures show negative bias (overprediction) and several are close to the zero line. However, F4 is a less stable indicator and undergoes more day-to-day variation than does the A4 indicator. Note also that the F4 values tend to be greater than the A4 values in an absolute sense (i.e., where both positive and negative bias appear to be magnified by the F4 estimator). The smaller magnitudes of bias for A4 probably result from averaging the predicted and the observed values to obtain the A4 values.

Model evaluation exercises often include scatter diagrams of observed and predicted concentrations. It is possible to construct such diagrams using the observed and predicted concentrations which correspond to the different measures used to estimate the bias of peak and near-peak values. Figure 11a gives scatter diagrams for the spatially paired measures A2 and F3 for the 20 test days. Figure 11b gives similar diagrams for the unpaired measures A4 and F4. Correlation coefficients (obs. vs. pred.) and centroid position ($\bar{O}$, $\bar{P}$) are also given for each of the four measures. The diagrams reaffirm the findings discussed previously with regard to the bias estimates: all of the estimators indicate positive bias (underprediction) for the data set as a whole; the F measures show a greater apparent positive bias than do the A measures. In addition, the A measures result in a much higher correlation between observed and predicted concentrations; this result probably stems from the fact that the A measures are averages and eliminate irregularities associated with individual values. Note also that while the F4 (unpaired) measure shows less positive bias than the F3 (spatial) measure, the scatter of the F4 measure is greater and its correlation coefficient smaller than those for F3.

4.2.2 Overall Accuracy/Precision

Table 10a gives the bias and confidence intervals for the unpaired analysis for each of the 20 test days. The first set of columns gives the results for the entire set of pairs; the second set gives the results for those pairs in which either the observed or predicted value is 80 ppb.* In the third set, the cut-off level is 120 ppb. In Figure 12, the bias values and confidence intervals for the three data sets are portrayed graphically. Figure 13 is identical except that the bias and confidence intervals are based on normalized data.**

Several conclusions can be drawn from Figures 12 and 13. The normalized and unnormalized analyses show nearly identical results. For all pairs (a), 15 of the 20 days have bias values which fall within

---

*Stratification in this manner ensures that the analysis is not biased. Had the cut-off been based on observed value, the results would have tended artificially toward underprediction.

**The bias and confidence intervals in Figure 13 are based on normalized data obtained by dividing residuals by the term $(\overline{P} + \overline{O})/2$.

±15 ppm (about 20 percent of the zero line; of these, 3 days have no significant bias. Of the 5 days with strong bias, 2 showed negative bias (overprediction) and 3 showed positive bias (underprediction). On the whole, the number of days having negative and positive bias is nearly equal.

There is, however, a marked shift toward underprediction for the analyses based on the higher ozone concentrations, especially for (c) based on the 120 ppb cut-off. Note that the degree of imprecision also tends to grow as one restricts the analysis to data pairs with higher cut-offs. A similar result can be seen in Fig. 14, scatter diagram of predicted vs. observed ozone concentration for Day 195. For values lower than 80 ppb, the points tend to cluster about the line of perfect prediction. At higher concentrations, the tendency is towards underprediction and the spread of the points tends to increase.

What explains the change in bias and confidence intervals with the magnitude of ozone concentration? Several factors may be involved. The all-inclusive data set contains a greater proportion of low concentrations, many of which are from early in the day. The early-day ozone calculations are dependent to a large extent on observed concentrations which are used to initialize the model. In a sense, the model is forced to come up with the right answer. Higher predictions on the other hand are much more dependent on the mathematical simulations of physical and chemical processes and it is possible that problems with model algorithms contribute toward the larger bias. There is a greater chance for error and both the size of the bias and the scatter tends to increase.

Unpaired analysis. Table 10b presents bias values and confidence intervals for the unpaired analysis. Results were obtained only from the all-inclusive data set. The bias values are identical to those of the paired (all-inclusive) analysis.* However, the confidence limits tend to be from two to three times larger than those obtained from the paired analysis. This ocurs because the unpaired analysis uses a pooled standard deviation based on the standard deviations of observed and predicted values rather than on the standard deviation of residuals. Both the observed and predicted values show considerably more spread than do the residuals.

---

* $\bar{d}$ unpaired $= \bar{O} - \bar{P} = \frac{1}{N}\left(\Sigma O_i - \Sigma P_i\right) = \frac{1}{N}\Sigma(O_i - P_i)$

$\bar{d}$ paired $= \frac{1}{N}\Sigma(O_i - P_i)$ by definition.

In order to determine whether the unpaired bias varies with concentrations, cumulative frequency distributions (CFD's) of observed and predicted concentration were plotted for the 20 days. Two examples (those for Days 159 and 195) are given in Figure 15. These graphs are used by comparing the observed and predicted concentrations at the same percentile. Figure 15a gives the CFD's for Day 195. For this day the model-predicted values are substantially lower than observed values at higher percentiles. At lower percentiles, predictions and observations are simiar in magnitude. Most of the days fall into this pattern which is consistent with the result of the paired analysis. However, there are a number of exceptions, one of which is shown in Figure 15b (Day 159).

For this day, predicted values exceed observed values for percentiles less than 40 and greater than 90. In the intermediate range, observed and predicted values are about equal. A similar relationship is indicated in the scatter diagram of observed and predicted pairs for Day 159 (Fig. 16). In this paired analysis, overprediction is found at lower concentrations and higher concentrations, while the pairs in the mid-range exhibit both under- and overprediction.

In summary, both the paired and unpaired analyses tend to show similar results, results which are also consistent with those of the peak and near-peak accuracy (Section 4.2.1). The Airshed Model for St. Louis has a systematic tendency to underestimate for areas and periods of high observed ozone. This pattern occurred on about 75 percent of the days. Possible causes for this underprediction are discussed in Section 4.3 which focuses on interpreting the errors.

Several additional comments on model precision are in order. Table 10a includes the variances of observed and predicted values for the all-inclusive data sets for each of the 20 days (S^2_o and S^2_p). Also given is the ratio S^2_o/S^2_p (F_{calc}) for each day. For a perfect model application we could expect $S^2_o = S^2_p$ and $F_{calc} = 1$. However, as is shown, S^2_o is significantly greater than S^2_p for all but 4 days. This indicates that the model is not reproducing the full extent of variation exhibited by the observed data, a result that is consistent with the finding that the model tends to underpredict at high concentrations and on many of the days to overpredict at low concentrations. This result is evident in the time series diagrams presented in Section 4.2.3.

4.2.3 Replication of Spatial and Temporal Patterns

The ability of the Airshed Model to replicate spatial and temporal patterns is measured by using Pearson correlation coefficients of paired predicted and observed values. Secondly, time series and isopleth diagrams of predicted concentrations are compared to their observed counterparts.

Table 11 gives spatial, temporal and overall correlation coefficients for each day. Examination of the coefficients reveals that the temporal correlation coefficients are very high. Similarly, time series of predicted and observed ozone concentration shown in Figure 17 demonstrate that the model is accurately able to simulate the diurnal pattern found in observed data: low values in the morning, a build-up toward afternoon and decreasing values toward evening.* (The reader should recall that the correlation coefficients reflect only covariance between the observed and predicted values; thus, high values can result even when substantial bias exists). As discussed in the previous section S^2_o/S^2_p is significantly greater than one for nearly all of the days; this finding indicates that the model tends to underestimate the full extent of temporal variation. The overall correlation coefficients reflect the temporal covariance and are moderately high in value.

---

*Figure 17 gives the diurnal pattern of observed and predicted ozone averaged over all stations and the corresponding residual $O-\overline{P}$ for the 20 test days.

Figure 18 presents an overview of the daily time series shown in Figure 17. This figure is the 20-day, all station average time series of observed and predicted concentrations and residuals ($\overline{O}-\overline{P}$). This diagram illustrates the strong covariance between observed and predicted values, but also highlights a distinct diurnal pattern of errors. Over the 20 days the model has a tendency to overpredict in the early morning and evening hours and to underpredict from the mid-morning to late afternoon. This pattern is clearly discernible on 12 of the 20 days (See Fig. 17). Several days, for example 275, were notable exceptions. On 275, the model bias was near-zero for the early morning to mid-afternoon; however, the predicted ozone values decreased more slowly than the observed values and overpredicted ozone for the late afternoon and evening hours. On Day 142, the usual pattern was reversed, underprediction occurred early and late in the day and overprediction characterized the afternoon.

Another issue regarding the model's ability to reproduce temporal patterns is its accuracy in predicting the time of the observed peak. Figure 18 suggests that for the overall 20-day data set, the model does quite well; the curve for the observed maxima shows highest and equal values at hours 1300 and 1400. The model predicted maximum value is for the 1400 hour. To examine this issue in greater detail, the time of the observed and predicted maximum concentrations were compared for each day and a histogram of the daily Δt values (time of observed max minus time of predicted max) is shown in Figure 19. The histogram demonstrates that the model estimate of the peak hour is early on some days and late on others. For the 20 days as a whole, there is no consistent pattern of error in the time of the peak and the differences cluster about zero Δt. (The sample size is too small to verify the bimodal distribution suggested by the histogram.)

Examination of the spatial correlation coefficients (Table 11) suggests that model's ability to reproduce geographical patterns varies considerably from day to day. While most of the spatial r values are statistically significant (0.05 level) they are generally lower than the temporal values and vary from high positive to negative for peak hours. In interpreting the spatial correlation coefficients, we would emphasize that the values are based only on those locations having monitoring sites. There is a sparsity of sites in the outlying regions and the correlation coefficients tend to weight the central portion of the modeling region. Thus, the analysis is not representative of the outlying regions which often experience the highest ozone concentrations. A similar limitation affects our interpretation of the spatial displays of observed and predicted values discussed below.

Figure 20 presents isopleths of observed and predicted concentrations for the hour of the observed peak for test Days 159, 195, 225, 231 and 275. Accompanying the isopleth diagrams are estimates of wind trajectories which pass through the hour and location of the maximum observed ozone concentration. These can be used to get a rough idea as to how urban precursor emissions and the developing ozone cloud will move throughout the day. In examining these figures, an attempt was made to answer several questions for each day. Are the areas of maximum predicted concentration coincident with the areas of highest observed concentration and consistent with the trajectories? Are the patterns and gradients of the predicted values similar to those of observed values? Are the areas of exceedance indicated by the predicted values similar to those indicated by the observed values?*

Our ability to answer these questions is constrained by the sparsity of sites in outlying regions. Thus, while it is possible to draw the isopleths of predicted ozone with confidence (using all grid cells in the modeling region), less certainty can be ascribed to the isopleths of observed concentration particularly in the downwind regions of high ozone.

1. Highest predicted values are generally found in the area downwind of the urban area.

2. For those cases where sufficient monitors are available, there appears to be a general correspondence between predicted and observed areas of high ozone (this was not the case on several days).

---

*Exceedance areas are those for which the ozone concentration is greater than 120 ppb, i.e., the NAAQS level. Observed and predicted exceedance zones are indicated on the isopleth diagrams in Figure 20.

3. For most of the test days, there was a general correspondence in the spatial patterns indicated by the isopleths; however, the fit varied from day to day (subjective comparisons were often difficult).

4. The model tends to underestimate the size of the exceedance zone on most days.

These results are generally consistent with those of previously discussed analyses. The apparent underestimation of the area exceeding the NAAQS level is consistent with the bias analysis shown on Figure 12c (for ozone > 120 ppb). Secondly, isopleth comparisons indicate day-to-day variation in the model's ability to reproduce spatial patterns as did the correlation coefficients. However, it is difficult to establish a relationship between the spatial daily correlation coefficients and subjective judgment based on the isopleth comparisons. In certain cases (mainly stagnation days) the visual patterns suggest a much stronger agreement than indicated by the spatial r values. Day 275 is an excellent example. Both the observed and predicted displays show similar patterns of concentric isopleths of ozone with highest values in and near the urban core. However, the spatial correlation coefficient for this hour was 0.12 (barely significant at the 95 percent level). This apparent discrepancy stems from the effects of slight spatial displacements where gradients are extremely sharp. In such cases, the visual comparisons probably give a better measure of the model's ability to simulate spatial patterns than the correlation coefficients. (For stagnation days, high concentrations are found in the inner portion of the modeling region where the monitoring network is dense; thus, isopleths of observed values can be drawn with confidence.)

An additional finding is that the Airshed Model on certain test days creates zones in which the predicted ozone levels are well below background (upwind) levels. These areas are located downwind of major point sources of NO_x (power plants). An example is seen in the isopleths of predicted ozone for 1400-1500 Day 231 (Fig. 20d). Below background ozone values extend in a plume-line pattern downwind of a cell containing a large power plant which is the largest single source of NO_x in the modeling region (4386 kg/hr). Unfortunately, the monitoring network is not sufficiently dense to determine whether the "deficit zones" associated with NO titration (scavenging) are as pronounced as those simulated by the model. The model may overestimate the size of these zones and underestimate O_3 because of the way it instantaneously mixes point source NO_x emissions into a 4 x 4 km grid cell.

Day 225 (Fig. 20c) is also worthy of detailed examination. The bias measures indicated that the extent of model underprediction for this day far exceeded that shown on the other test days. As Fig. 20 indicates, the highest observed ozone (<160 ppb) for this day occurred during the midafternoon in the southeast quadrant of the modeling region. Yet the model concentrations barely reached 70 ppb, nor are any well-organized zones of high ozone discernible. The trajectory information (shown below the isopleths) suggest an explanation for the problem. It is probable that most of the morning emissions were advected out of the modeling region (i.e., to the north and east). Once mass is transported to the boundaries, it is lost to the model. On the other hand, in "the real world," it is quite possible for a pollutant-laden mass to be advected back into the region later in the day. A test of this hypothesis would be to simulate this day using a larger modeling region, one that is extended to the east. An alternate and equally plausible explanation is that windfield errors resulted in a much exaggerated transport of precursor mass out of the modeling region. It is obvious that Day 225 is clearly an outlier and should not be used for estimating control requirements unless substantial improvement is obtained through refinement of the inputs or expansion of the modeling region.

Day 159 (Fig. 20a) illustrates the case where the network of monitoring sites is insufficient to evaluate the model's ability to replicate spatial patterns. The model predicts a broad region of ozone concentrations in excess of 200 ppb in the northwestern corner of the grid (the predicted peak is 312 ppb). Unfortunately, there are no monitors in this region to verify the predictions.

The pattern of errors for the area covered by monitors is interesting. As Figure 21 shows, the afternoon hours show a persistent tendency for overprediction (+ bias) to the west and underprediction (- bias) to the east. One might speculate that this pattern may be associated with errors in the windfield.

For Day 195, the model does fairly well at replicating the overall spatial pattern. However, substantial underprediction is evident in the size of the exceedance zone and in the concentrations near the urban zone; the model also shows "deficit zones" downwind of major NO_x point sources in the north central and south central portions of the region.

4.3 Potential Sources of Error

To a certain extent, constraints of the monitoring network may contribute to the underprediction that is evident for most test days. Evidence suggests that the ozone measurements themselves may be biased. Gas-phase titration with excess NO was used during the RAPS field studies as the ozone calibration technique.[20] Comparison studies have since shown that gas-phase titration may on average give ozone concentrations as much as 7.5 percent higher than does uv photometry, the latter being the EPA designated calibration method for ozone analyzers. In controlled laboratory experiments, uv photometry on average yielded values 3.6 percent lower than did gas-phase titration.[21] Thus, the ozone observations used for model evaluation may be slightly on the high side.

Secondly, the paucity of monitoring sites in outlying regions may affect the model performance measures of bias. It is emphasized that all of the bias measures presented are restricted to those grid cells which lie in the immediate vicinity of monitors. Thus, to a certain extent, even the unpaired measures are restrictive. For example, if the model peak occurs in a region void of monitors, this peak will not be included in the F or A residuals discussed previously. When one plots the highest peak ozone computed for any grid cell in the modeling region against the highest observed ozone (Figure 22), the perception of model performance is different and the bias appears to disappear. The problem, however with this approach is that the predicted values are drawn from a much larger sample than the observed values and thus, the results are biased towards overprediction. It does appear, however, that for several days, a displacement in the model's area of highest ozone may have contributed to the finding of underprediction. Days 230, 207, 231, and 184 (Fig. 23) appear to fall into this category. For these days the model predicts a zone of maximum ozone in areas where no monitors exist.

Constraints in the observational data base, notwithstanding, the conclusion that the model tends to underpredict at higher ozone concentration remains. In order to explore potential sources of this problem, the authors attempted to determine whether the model performance was related to the type of days being modeled. To address this question, regression analysis was used to determine whether peak accuracy is related to any of the critical atmospheric input variables used to simulate the different days. In this analysis the F4 residual (O_{max} - P_{max}, unpaired in location and time for each day) is the dependent variable and mean wind speed,* temperature,* solar radiation,* maximum mixing height and ozone aloft are the independent variables. The correlation coefficients shown in Table 12 demonstrate that only the wind speed parameter is significantly correlated to the F4 residual. In this relationship, days with higher wind speeds tend to exhibit more underprediction. A similar analysis for the A2 (spatially paired average residuals) results in a significant but smaller correlation between near-peak bias and wind speed.

---

*Meteorological parameters are averaged over the period 0700-1400 CST.

Significant correlation does not necessarily imply a causal relationship. Yet, a plausible explanation for this relationship is available. On days with low wind speed, the model results are controlled largely by emissions. On the days with higher wind speeds, two additional factors, advection and boundary concentrations, affect the simulations and model performance. The additional uncertainty is heightened because the wind fields which define advection are perhaps the most uncertain of the inputs used in the Airshed Model. Secondly, boundary concentrations are based on interpolations made using a limited number of measurements.

The relationship between wind field errors and advection is shown conceptually in Figure 24. For the low wind speed case, errors in wind field result in only a small latitudinal displacement of the model "ozone cloud" and the cloud remains over the urban area with its dense network of monitors. For the high wind speed case, the dislocation of the model's urban plume is magnified as it is advected downwind. There is a much higher probability that the model's zone of maximum ozone will be located in an area without monitors, a factor that as stated previously, results in apparent positive bias.

Not only is the location in error, but the emissions encountered along the trajectory will be different from those encompassed by the actual urban plume. Thus, the error in wind direction manifests itself as errors in the location of and magntude of peak ozone.

To further understand the model's performance with regard to ozone, the authors examined the model's abilty to estimate average concentrations of NMHC and NO_x precursors and CO. Figure 25 shows scatter diagrams of daily average observed and predicted concentrations of these pollutants. The use of values averaged over all simulation hours for all sites can be used to make a preliminary assessment as to the accurcy of the precursor emission inventories.* Furthermore, the results give some insights into the model's ability to simulate dispersive conditions that affect ground-level concentration.

From the diagrams in Figure 25, it is evident that the model simulates average NMHC and NO_x concentrations with a high degree of accuracy (near zero bias), correlation, and precision. Since the emissions remain essentially constant from day to day, substantial errors in emissions should show up as a systematic bias in the results. The decided absence of bias suggests that in the aggregate, the NMHC and NO_x emission inventories are accurate. The day-to-day discrepancies between the observed and predicted average precursor concentrations may be related to errors in the simulation of advection, dispersion, and in specifying the diurnal changes in mixing layer height.

Carbon monoxide, on the other hand, appears to be underpredicted by the model. However, this finding may be related to the fact that a number of CO monitors may be located near "hot spots." Model predictions, on the other hand, are grid values averaged over 4 x 4 km squares. There is also the possibility that the emissions inventory underrepresents the full extent of CO emitted in the region; however, CO unlike NMHC and NO_x has almost no effect on ozone levels.

---

*Predicted values were obtained in a similar manner to predicted ozone concentrations; estimates were derived by averaging values from cells adjacent to the monitoring site. Both predicted and observed concentrations were obtained from the ESRL Report.[3]

While the precursor emission inventories appear to be accurate in the aggregate, we can draw no conclusions about the accuracy of temporal or spatial distributions of emissions. Similarly, our analysis says nothing about the accuracy of the NMHC species distribution. Peak ozone is more dependent on precursor concentrations associated with the morning urban rush-hour emissions than it is on region-wide daily averages. Nevertheless, it is reassuring that available evidence suggests that the overall NMHC and NO_x inventories are accurate.

Aside from the concentration of NMHC in the atmosphere, the NMHC/NO ratio is an important determinant of ozone level. Figure 26 is a scatter diagram of mean observed and predicted NMHC/NO_x ratios (averaged over all sites for all hours). This diagram indicates that the model has an overall tendency to overpredict NMHC/NO_x; however, there is considerable day-to-day variation in the accuracy of the predicted ratios. This variation is reflected in a relatively low correlation coefficient of 0.44. The tendency toward overprediction is associated with a slight tendency towards underprediction of NO_x and the variation is associated with errors in both NO_x and NMHC.

Given the sensitivity of model peak ozone to the NMHC/NO_x ratio of emissions (demonstrated in Chapter 5), one might ask whether the model's accuracy with regard to peak ozone is related to errors in the NMHC/NO_x ratios. To address this question, the A2 residuals (measure of near-peak accuracy were plotted against residuals of NMHC/NO$_x$. This diagram (Fig. 27) shows a significant relationship (correlation coefficient of .52) between the residuals of peak ozone and the average NMHC/NO$_x$. Note that with increasingly large underprediction (+ bias) in NMHC/NO$_x$, peak ozone levels are underpredicted to a larger extent. The diagram shows that the model is less likely to underpredict on those days for which the predicted NMHC/NO$_x$ ratios are higher than observed.

This finding leads to the hypothesis that the model needs an artificially high NMHC/NO$_x$ ratio to compensate for deficiencies in the model and/or inputs, deficiencies which restrict the model's ability to generate ozone. While this hypothesis is tentative, it is consistent with several concerns that have been raised regarding the treatment of NMHC emissions and boundary concentrations. First, vegetative emissions have been ignored and secondly, it appears that the carbonyl (aldehydes and ketones) fraction used in the NMHC emissions and boundary concentrations may be on the low side.

Several studies [22,23] have shown that vegetative emissions particularly in rural areas are substantial and that the reactivity of species emitted is at least comparable to that of urban NMHC mixtures.[24] The fact that the monoterpenes and isoprenes associated with natural emissions have not been measured in appreciable quantities possibly is related to their rapid conversion to intermediate species. Thus, vegetative emissions may have a substantial impact on ozone levels without contributing to the levels of NMHC measured at urban sites. Thus, the neglect of vegetative factors cannot be ruled out as a contributor to the underprediction of ozone, not only by St. Louis, but for a number of other applications including Los Angeles,[25] and Denver.[26]

The second factor, carbonyl fraction, is of particular concern for St. Louis. As Table 13 indicates, the fraction of emissions for this reactive group used for St. Louis is considerably less than that used for other cities and is lower than the fraction that has been measured in several cities. Whereas the fraction used for St. Louis is about 1.5 percent, SAI, in a recent report, recommends an urban value ranging from 5-10 percent.[27] This faction is particularly significant not only because carbonyls are highly reactive species, but also because the fraction of aldehydes and ketones add to the total organic emissions rather than merely redistributing it. This is because most HC emission factors do not include these compounds.

4.4 Summary of Model Perfomance

In summary, the assessment of model performance indicates that the Airshed Model tends to underestimate ozone concentrations for areas and times of high ozone. The model was found to have a systematic tendency to underestimate peak and near-peak ozone concentrations. The assessment is, however, limited by the sparse number of monitors in outlying areas for which predicted values are high on many of the days.

Several factors contribute to the underprediction of peak ozone and the aerial extent of exceedance zones. These include: (1) the current model's inappropriate mixing of point and possibly line) source NO_x into entire grid cells; (2) neglect of vegetative emissions; (3) the use of a carbonyl fraction which appears to be low; and (4) errors in advective transfer associated with windfield errors on transport days; and (5) problems with the chemical mechanism. The evidence indicates that the overall NMHC (sum) and the total NO_x inventories are accurate and there is no cause to search for additional anthropogenic sources that may have been neglected from the inventory.

Correlation coefficients indicate that the model replicates temporal variations accurately. However, while the model is generally in phase with the observed temporal pattern, it tends to underestimate the full degree of variation found in the observations. The "flatter" than observed predicted diurnal curves is explained largely by an underprediction of peak ozone. Paucity of sites in outlying areas restricts assessment of the model's ability to replicate spatial patterns. However, comparison of observed and predicted fields appear to indicate that the model is able to locate the general area of high ozone, but it tends to underestimate the size of the NAAQS exceedance zone.

5.0 Model Sensitivity

5.1 Introduction

Model sensitivity refers to the response of model outputs to changes in model inputs. The purpose of sensitivity analysis is to determine the percent change (y) in a given output variable which results from a percent change (x) in a given input parameter, holding other factors constant. In this chapter, the results of applying this simple technique to Urban Airshed Model simulations in St. Louis are discussed.

While the technique is staightforward, the interpretation and significance of the results are made difficult by two separate but related factors. First, is the question of model performance; base-case simulations must compare favorably with observations before much confidence can be placed in the model as a predictive tool. A broader question is that of model validity; changes in base-case simulations should agree with changes in observations, given concurrent and equivalent changes in model inputs on the one hand, and changes in physical and chemical features of the atmosphere on the other. However, assessing model validity in this sense is rendered nearly impossible by confounding factors which vary from one day of observations to the next. Second, is the factor of input interaction. Urban Airshed is a multi-variate nonlinear model. The response of such a model to changes in a single output parameter is modulated by the values taken on by other input parameters as well. For example, a change in mixing height may increase or decrease the mass of pollutants entrained into the surface layer from aloft as well as affect pollutant concentrations resulting from low level emissions. Thus, the sensitivity of a photochemical model to emission changes depends on meteorological parameters, on the concentrations of chemical species at the boundaries of the modeling region, and on the concentrations used to initialize the model. Such interactions can modify both the magnitude and direction of the model response.

Notwithstanding their limitations, model sensitivity analyses are quite useful for a variety of objectives. These include: (1) identification of input parameters exhibiting significant influence on model results, (2) assessment of the types of quantity and basic data from which model inputs are derived and are needed for successful model applications, and (3) diagnosis of possible causes contributing to unsatisfactory model performance. In this study, primary emphasis is placed on the first objective. Furthermore, much of the study focuses on the response of the model to changes in emissions in order to assess effects on both area-wide and peak ozone concentrations. Inferences regarding possible outcomes associated with regulatory actions necessarily assume a high level of model validity over a wide range of input values. Regulatory aspects related to emission changes are discussed in Chapter 6.

Consistent with the model performance results discussed earlier, the sensitivity results reported here reflect the most recent version of the Airshed Model and associated base-case preprocessor files. As discussed earlier, changes were made to the emissions inventory, to various air quality parameters along the borders of the modeling region and aloft, to initial conditions, and to the photolytic rate constants input to the model. The model itself was also revised in two respects: (1) the Carbon-Bond

Mechanism was replaced with Carbon-BondII[27,28,29] and (2) the SHASTA numerical technique originally employed for advection calculations was replaced with the FCT algorithm developed by Zalesak.[30] Extensive sensitivity testing was conducted using previous versions of the Airshed Model and St. Louis data base.[31,32] These tests included uniform changes in hydrocarbon and oxides of nitrogen emissions, in the spatial and temporal distribution of emissions, in the mix of hydrocarbon reactivity classes, in hydrocarbon and ozone concentrations aloft and at the borders of the modeling region, and in the maximum afternoon mixing height. However, the earlier test results cannot be compared to those reported here since the revisions to the model and preprocessor files led to significant changes in the base-case simulations.

Some 48 sensitivity tests were conducted using the most recent version. These may be conveniently grouped and discussed as follows: (1) uniform changes in hydrocarbon emissions, (2) uniform changes in emissions of nitrogen oxides, (3) uniform changes in the mix of hydrocarbon chemical classes (referred to hereafter as hydrocarbon reactivity), and (4) miscellaneous changes in the spatial and temporal distribution of emissions and in meteorological parameters. To date, only effects on ozone concentrations have been analyzed.

Two concepts employed in this chapter are those of "peak" prediction and "trajectory." The peak prediction is the highest one-hour average ozone concentration simulated by the model from among all hours and all surface layer grid cells. The peak prediction is therefore not constrained to grid cells in which ozone monitoring stations are located. However, the peak prediction is constrained to the first (surface) layer of grid cells. The concept of trajectory is employed in interpreting model results although the Airshed Model is not a trajectory, or lagrangian, model. The path of a trajectory is determined by the mean wind and may be constructed using the three-dimensional wind field input to the model. The actual path taken by transported pollutants is modified by wind shear and by horizontal and vertical diffusion. Nevertheless, surface trajectories such as the hypothetical one depicted in Figure 28, do indicate the emissions burden assumed by a particular air parcel and do suggest the source areas that contribute to high ozone concentrations predicted by the model for a given location, particularly in the absence of extreme stagnation.

Sensitivity results vary markedly from day to day. Therefore, before the tests themselves are discussed, the simulation days will be described.

5.2 Test Days

All sensitivity tests were performed on one or more of 3 separate test days. These are Monday, June 7, 1976 (Day 159); Tuesday, July 13, 1976 (Day 195); and Friday, October 1, 1976 (Day 275).

Day 159 (June 7, 1976). A large high pressure system associated with weak pressure gradients dominated the eastern half of the nation. As the trajectory for this day shows (Fig. 20a), flow during early morning hours was light and northeasterly. The flow shifted to southeasterly by mid-morning and transport toward the northwest persisted throughout the day. As

Fig. 20a demonstrates, predicted ozone concentrations exceed 200 ppb over a large area of grid cells in the northwestern portion of the modeling grid. The location of max predicted ozone is consistent with the urban trajectory shown in the figure. The very high predicted maximum concentrations may be plausible, given the slow passage of the trajectory over regions of dense NMHC; however, the bias measures restricted to the monitoring sites indicate a tendency toward overprediction especially at high concentrations. Unfortunately, there were no monitors in the region of peak predicted ozone.

Day 195 (July 13, 1976). Winds were moderate and ranged from southeasterly in the morning to SW during the afternoon. As Fig. 20b illustrates, the area of maximum predicted and observed ozone concentrations in the north central portion of the region are consistent with wind trajectories. However, as bias statistics for this day show, there was a tendency toward underprediction at high concentrations. Note, for example, that the observed ozone distribution for 1500-1600 hours suggests a larger exceedance zone than that of the predicted values.

Day 275 (Oct. 1, 1976). Of the 20 test days modeled, Day 275 recorded the highest observed ozone concentration (244 ppb). This day is somewhat unusual in that it occurred beyond the usual ozone season; it was characterized by extreme stagnation conditions, light winds and very low mixing depths. (The maximum mixing depth for this day is estimated to be about 500 m). As Fig. 20e shows, observed and predicted concentrations were maximal near the central urban core. While there are some discrepancies, the overall patterns of observed and predicted concentrations are closely matched. The bias statistics for this day suggest a moderate overprediction; however, this result is associated with the post-peak late afternoon and evening hours. The model shows a much slower decrease in ozone level than was observed at the monitors.

Subsequent to evaluating model performance on these 3 days, a reexamination of the ambient nonmethane hydrocarbon (NMHC) measurements used for specifying boundary and initial concentrations was undertaken. Representing the difference between two relatively large numbers, total hydrocarbon and methane, considerable uncertainty exists in the reported data. In obtaining an hourly average NMHC value, spurious negative 1-minute readings were eliminated. Also, a background value of 0.050 ppm C was assumed so that the hourly average NMHC was never allowed to fall below this. In addition, on Day 275, NMHC along the southern boundary was reset to a constant 0.050 ppm. These changes in hydrocarbon concentrations along the borders of the modeling region did not affect peak ozone concentrations on Days 159 and 195. However, on Day 275 the peak was reduced from 246 ppb to 232 ppb. The revised simulation is used as the base case for all sensitivity analyses.

5.3 Uniform Changes in Hydrocarbon Emissions

In these tests, uniform reductions of 5, 17, 42, and 75 percent and increases of 1 and 6 percent were made to the hydrocarbon emissions. All five carbon-bonds (PAR, ARO, OLE, ETH, CARB) were reduced or increased by the same percentage even though, strictly speaking, CARB represents aldehydes rather than hydrocarbons. This was done for each grid cell each hour and for all sources. In addition, concentrations of the five carbon-bonds used for initialization were also reduced or increased by a like amount, but only after subtracting out an assumed background value. The background values were as follws:

PAR	33 ppbC
CARB	4 ppbC
OLE	4 ppbC
ARO	7 ppbC
ETH	2 ppbC

The adjustment to initial conditions was intended to represent the expected effect of emission reductions on early morning ambient hydrocarbon concentrations. The background values could represent uncontrolled anthropogenic sources or biogenic sources of emissions; no distinction is intended. Hydrocarbons at the borders of the modeling region and aloft were left unchanged.

The effect of these changes on peak ozone predicted anywhere in the modeling region during the course of the simulation is tabulated in Table 14 and illustrated in Figure 29. On all 3 days the change in peak ozone concentration is in the same direction as the change in hydrocarbons but is invariably of a smaller magnitude. However, the relative change in ozone concentration for the same change in hydrocarbons varies widely among the 3 days. This is readily apparent from the slopes of the curves shown in Figure 29. Day 159 is particularly insensitive to increases in hydrocarbon emissions. This behavior may be associated with the high levels of ozone aloft and a relatively high afternoon mixing height, the combined effect of which is a large influx of transported ozone into the urban plume. The addition of more hydrocarbon to such a system may be more effective at removing NO_2 (via PAN formation) than in generating additional ozone. Day 195 is the least sensitive to large reductions in hydrocarbon emissions. This day, which experienced relatively higher wind speeds, as well as good vertical mixing, shows the lowest predicted precursor concentrations of the 3 days. Boundary concentrations of NMHC, therefore, may contribute a larger fraction of the predicted NMHC concentrations, a fraction which is not reduced by reductions in hydrocarbon emissions. Among the 3 days, Day 275, having the poorest overall ventilation and the lowest ozone aloft, exhibits the greatest sensitivity to both increases and decreases in hydrocarbon emissions.

The results for these simulations may also be presented in terms of changes in the hydrocarbon to oxides of nitrogen emissions ratio. Figure 30 illustrates the relationship between the peak ozone prediction and the HC/NO_x ratio. The ratio is defined as the total moles of the five carbon-bonds, expressed as carbon, divided by the total moles of NO and NO_2. The totals are across all grid cells and all hours of the day.* With NO_x held constant (open symbols), peak ozone predictions invariably increase with increasing HC/NO_x ratio, but to varying degrees. A suggestion of asymptotic behavior at large ratios is apparent on Day 195. However, on Day 159, this behavior is strikingly evident. In these tests, increases in hydrocarbon emissions were limited to 67 percent. Whether and to what extent further increases might actually suppress ozone formation is indeterminant. Furthermore, whether the curve seen on Day 159 is due to peculiarly high HC/NO_x ratio along the particular trajectory to the peak prediction, to a high influx of ozone from aloft, mollifying the effect of further hydrocarbon increases as suggested earlier, or to possibly both cannot be determined without further analysis.

---

*The emissions ratio so defined is much lower than ambient ratios observed at the ground, due to the inclusion of a large mass of elevated NO_x emissions which are not instantaneously mixed to the surface.

Uniform changes in hydrocarbon emissions affect the time and location of the peak ozone prediction as well as the value itself. In general, decreases in hydrocarbon emissions tend to move the ozone peak further downwind and shift it to later in the day. This is likely associated with a delay in the conversion of NO to NO_2. Conversely, increases in hydrocarbon emissions move the ozone peak closer to the urban center and shift it to earlier in the day. Changes in the timing of the buildup of ozone would directly affect both the location and the time of the ozone peak; a delay in the buildup would move the peak further downwind and shift it to later in the day. On Day 159, the ozone peak moves approximately 25 kilometers to the northwest, away from the city, and is delayed 5 hours as emissions are changed from +67 percent to -42 percent. However, a reduction of -75 percent has little effect on the peak locations but the time of the peak is accelerated 3 hours, relative to the -42 percent case. A closer examination shows that the peak for the -42 percent case occurs the last hour of the simulation (1800-1900, CST) nearly at the boundary of the modeling region. Along this particular trajectory, a further delay in ozone buildup could move the peak beyond the modeling region or past the end of the simulation or, on the other hand, it might have no effect on the timing and location of the peak if the rate of NO_2 photolysis drops rapidly, effectively halting the ozone buildup. That the peak prediction occurs 3 hours sooner when hydrocarbon emissions are reduced further to -75 percent is strong evidence however, that an entirely different trajectory, carrying a different burden of hydrocarbon and oxides of nitrogen emissions, in fact leads to the peak ozone prediction.

A subset of this group of sensitivity tests was further analyzed to examine the effect of hydrocarbon emission changes on area-wide ozone predictions. The entire set of model predictions for a given sensitivity test was contrasted with the base case using several statistics. These included the mean absolute normalized residual and the mean normalized residual, the latter computed as the base-case prediction minus the sensitivity case prediction. Since the modeling region is 15 by 20 cells and the simulation is run for 14 hours, these residuals are taken over 4200 data pairs. Only predictions in the surface layer are considered. In addition, a correlation coefficient which measures the similarity of the spatial alignment of the two sets of predictions was computed in two steps. First, a 1-hour Pearson product-moment correlation coeffcient was computed for all grid cells. Second, because the hourly correlation coefficients are not normally distributed, a change of variable was made.[53] This procedure led to computation of the average population spatial correlation coefficient.

These statistics are given in Table 15 for Days 159 and 195 for three sensitivity tests: +67 percent, -42 percent, and -75 percent.

The mean normalized error, as used here, represents the average relative change in predicted ozone concentrations, when the sign is reversed. Changing the sign in Table 15 and converting to percentages, it is readily apparent that average ozone concentrations are, in most cases, changed much less than are peak ozone concentrations, as given in Table 14. This is illustrated better in Figure 31 where the average percentage change, the percentage change of the peak, and a reference 1:1 line are plotted for Days 159 and 195. It is noteworthy, however, that on Day 159, average ozone concentrations are increased more than is the peak ozone concentration when hydrocarbon emissions are increased by 67 percent. This behavior would tend to suggest that the insensitivity of the peak ozone prediction to increases in hydrocarbon emissions is associated more with the particular HC/NO_x ratio along the trajectory to the peak than with ozone aloft. Tables 14 and 15 demonstrate that day-to-day differences in model sensitivity tend to be much less for average ozone concentrations than for peak concentrations.

The effect of uniform changes in hydrocarbon emissions on computed correlation coefficients between the base case and sensitivity case is illustrated in Figure 32. The average sample spatial correlation coefficient is reduced as hydrocarbon emissions are either decreased or increased. Had all ozone predictions for a given sensitivity case been reduced or increased by the same amount, the correlation coefficient would be 1.0. The drop in the correlation coefficient, therefore, reflects changes in the spatial patterns of predicted ozone concentrations.

Further analysis of this subset of sensitivity runs was made to evaluate the effect on are a-wide exceedances of the ozone National Ambient Air Quality Standard (NAAQS) of 0.12 pm. For this purpose, the overall normalized areal exceedance (ONAE) statistic was derived. The ONAE is defined as the difference between the base case and sensitivity case number of grid cells that equal or exceed 0.12 ppm during any hour of the simulation, normalized by the base case number of grid cells which exceed 0.12 ppm during any hour of the simulation. The values taken on by this statistic, converted to percentages, are given in Table 16. An ONAE of -100 percent indicates a doubling in the numnber of grid cells exceeding the NAAQS while an ONAE of +100 percent indicates that no cells in the sensitivity case exceed the NAAQS. A plot of these data in Figure 33 emphasizes again the relatively large day-to-day differences. As expected, the ONAE shows a highly nonlinear behavior. On Day 195, the ONAE approaches the +100 percent value ("attainment") asymptotically. On this day, a 75 percent reduction in hydrocarbon emissions has the effect of reducing all model predictions below the NAAQS. On Day 159, the data points are too widely separated to define the model's behavior as the ONAE approaches +100 percent; two possible curves are illustrated. If the model behaves asymptotically, as on Day 195, it appears that no amount of emissions reduction would reduce all model predictions below the NAAQS. Given the level of ozone aloft (0.114 ppm), such a result would not be surprising.

5.4 Uniform Changes in Oxides of Nitrogen Emissions

In these tests, reductions of 20 percent and increases of 20 percent were made to the oxides of nitrogen emissions on Days 159, 195, and 275. In addition, a reduction of 40 percent and an increase of 40 percent were made on Day 275. Each of these reductions was combined with a 42 percent decrease in hydrocarbon emissions. In implementing these changes, both nitric oxide and nitrogen dioxide were reduced or increased by the same percentage for each grid cell each hour and for all sources. Besides emissions, concentrations of NO and NO_2 used for initialization were also reduced or increased by a like percentage, but only after subtracting out an assumed bckground value. The background values were as follows:

NO	3.0 ppb
NO_2	2.0 ppb

The adjustment to initial conditions was intended to represent the expected effect of emission changes on early morning ambient oxides of nitrogen concentrations. These background values could represent "uncontrolled" anthropogenic emission sources or other sources; no distinction is intended. Oxides of nitrogen at the borders of the modeling region and aloft were left unchanged.

Because NO_x changes were combined with HC reductions, the base case for this set of tests was changed from the original base case listed in Table 14. Instead the sensitivity test in which hydrocarbon emissions were reduced by 42 percent, as discussed previously, was used. Noteworthy is the greatly reduced HC/NO_x emission ratio of the new base case relative to the original. The ratio dropped from 4.6 to 2.7 on Day 159, 4.2 to 2.5 on Day 195, and 5.4 to 3.1 on Day 275. At these reduced ratios, oxides of nitrogen emissions are in excess relative to the available hydrocarbons. What effect this might have on the sensitivity of the model predictions of ozone to changes in oxides of nitrogen emissions has not been examined. Model predictions may be more sensitive to changes in NO_x at higher hydrocarbon levels when NO_x is more limiting. Ideally, uniform changes in oxides of nitrogen should be made at various hydrocarbon levels.

The effect of these tests on peak ozone predicted anywhere in the modeling region during the course of the simulation is tabulated in Table 17 and illustrated in Figure 34. On all 3 days, the change in peak ozone concentration is in the opposite direction as the change in oxides of nitrogen emissions. Decreases in oxides of nitrogen emissions lead to higher peak ozone predictions. Furthermore, the magnitude of the change in peak ozone is in all cases less than the magnitude of the change in emissions. However, there is again considerable variability from day to day. Day 195 shows the least sensitivity to oxides of nitrogen emissions which may be related to the relatively greater importance of estimated boundary conditions on a day characterized by advective transport. Day 159 shows the greatest sensitivity to increases in oxides of nitrogen emissions, while Day 275 shows the greatest sensitivity to decreases.

This behavior is consistent for the 3 days with the relationship established previously between the HC/NO_x emissions ratio and the peak predicted ozone concentration for constant oxides of nitrogen emissions, as illustrated in Figure 30. The relationship between HC/NO_x ratio and peak ozone at constant hydrocarbon emissions is also shown in Figure 30. (On each curve connecting the solid symbols, "B" indicates the base case.) On Day 159, it can be seen that a decrease in the HC/NO_x

ratio (increase in NO_x) gives the steepest slope, one which is nearly identical to the HC/NO_x curve established by changing HC at constant NO_x. However, a decrease of 20 percent in oxides of nitrogen emissions (increase in HC/NO_x ratio) on Day 275 produces the highest slope of the 3 days, but a further decrease of 40 percent leads to a greatly diminished slope, and therefore sensitivity. In general, for the limited range of hydrocarbon and oxides of nitrogen levels examined here, changes in HC/NO_x ratios at constant HC have less effect on peak ozone concentrations than do those at constant NO_x. This is particularly evident as oxides of nitrogen are decreased. For the case in which decreases of 40 percent in oxides of nitrogen emissions on Day 275 are accompanied by decreases in hydrocarbon emissions of 42 percent, the HC/NO_x ratio remains essentially constant, yet a reduction of 24.1 percent from the base case in Table 14 is seen in the peak ozone prediction. Thus, while the behaviors at constant HC and constant NO_x are consistent, the HC/NO_x emission ratio alone does not convey a complete picture; the absolute level of hydrocarbon and oxides of nitrogen emissions are primary determinants of the peak ozone concentration on any particular day.

Another way of viewing the results of these tests is to examine how changes in oxides of nitrogen emissions modify the effect on peak ozone of changes in hydrocarbon emissions. This is illustrated in Figure 35. Here, decreases in oxides of nitrogen emissions are seen to diminish the effect of a 42 percent reduction in hydrocarbon emissions on all 3 days. Conversely, increases in oxides of nitrogen enhance the effect that hydrocarbon emissions reductions have on reducing peak ozone predictions.

Whether this same effect might occur at other hydrocarbon levels has not been studied.

Of interest also is the effect uniform changes in oxides of nitrogen emissions have on the time and location of the peak ozone prediction. In general, decreases in oxides of nitrogen emissions accelerate the time of the peak predicted ozone concentration and/or translocate the peak closer to the urban center. On Day 275, no well-defined advective transport occurs and no clear pattern is exhibited in the movment of the peak ozone prediction across the modeling grid. For the same reasons that decreases in oxides of nitrogen accelerate the peak, increases are expected to delay the peak. However, this does not occur. Instead, on Days 159 and 195 the peak occurs earlier in the day at about the same location as the base case. This suggests that another trajectory carrying a different burden of hydrocarbon and oxides of nitrogen emissions leads to the peak prediction. Photochemical activity along the trajectory is sufficiently suppressed so that it no longer produces the peak ozone concentration. Although the peak prediction for the base case occurs near the downwind edge of the modeling region, it also occurs during the late afternoon on both Days 159 and 195, making it unlikely that extension of the modeling region would have identified a higher peak further downwind. On Day 275, increases in oxides of nitrogen emissions have no effect on the timing of the peak and only a 40 percent increase in oxides of nitrogen has any effect on the location.

The results of these sensitivity tests suggest that controls on oxides of nitrogen emissions are counterproductive with regard to reducing ozone concentrations and that allowing oxides of nitrogen to increase will enhance the benefits achieved by lowering hydrocarbon emissions. However, results with the Airshed Model in Los Angeles indicate that NO_x controls are necessary to achieve significant ozone reductions in the eastern (downwind) part of the South Coast air basin. Whether such an effect might be seen in St. Louis had the influence of secondary nitrogen compounds carried over from one day to the next or transported long distances downwind been considered, has not been addressed. Except during episodes of extreme stagnation, such a multi-day simulation would require greatly increasing the size of the modeling region. Use of a trajectory model would be the only practical means of evaluation in this event. Moreover, it should be strongly emphasized that possible adverse effects on nitrogen dioxide has not been analyzed.

5.5 Uniform Changes in Hydrocarbon Reactivity

The Carbon-Bond II kinetics mechanism incorporated in the Airshed Model recognizes five cabon-bond categories which serve as surrogates for the wide variety of hyrocarbon compounds emitted into the atmosphere. The five carbon-bonds are distingushed by their markedly different reaction pathways and reaction rates These differences lead directly to differences in their relative potential for contributing to the formation of ozone. The particular mix of carbon-bonds therefore defines the photochemical potential of the hydrocarbon emissions. This mix is what is referred to here as "hydrocarbon reactivty." Typically, the more reactive a particular mix, the more ozone that is predicted by the kinetics mechanism.

Table 18 lists the mix of carbon-bonds, in terms of the carbon fraction of total hydrocarbon emissions, used in these sensitivity tests.

The fractions were developed from different sources of information and in part represent differences in the relative contribution of different source types to the overall carbon-bond mix and in part different methods of treating individual hydrocarbon species for input to the carbon-bond mechanism.* Whether these differences are real or methodological is not of great concern in the context of sensitivity testing; it is the effect of these differences regardless of their origin which is.

In applying these carbon fractions to the hydrocarbon emissions, the base case emissions of each carbon-bond must first be summed and then redistributed. In so doing, the number of carbons associated with each carbon-bond category must be taken into account. The total reactive hydrocarbon emissions (in gram-moles carbon) for each grid cell each hour was obtained as follows:

$$\mathrm{RHC} = \mathrm{PAR} + (2 * \mathrm{OLE}) + (2 * \mathrm{ETH}) + (6 * \mathrm{ARO}) + \mathrm{CARB}$$

The total hydrocarbon was then redistributed to carbon-bonds as follows:

$$\mathrm{PAR} = C_1 * \mathrm{THC}$$

$$\mathrm{OLE} = 1/2 * C_2 * \mathrm{THC}$$

$$\mathrm{ETH} = 1/2 * C_3 * \mathrm{THC}$$

$$\mathrm{ARO} = 1/6 * C_4 * \mathrm{THC}$$

$$\mathrm{CARB} = C_5 * \mathrm{THC}$$

where C_1, C_2, C_3, C_4, and C_5 are the carbon fractions corresponding to PAR, OLE, ETH, ARO, and CARB from Table 18. This procedure resulted in a uniform mix of carbon-bonds for each grid cell each hour. This procedure was also used to redistribute initial concentrations. No modification was made to hydrocarbon concentrations at the borders of the modeling region or aloft.

---

*In the Philadelphia and Tulsa inventories, for example, cycloparaffins and internal olefins were treated as surrogate carbonyls (CARB). In St. Louis, these were simply treated as paraffins or olefins.

The first simulation listed in Table 18 uses the overall St. Louis regional carbon-bond mix, based on the emissions from all sources for all hours combined. This simulation, which serves as the base case for the next three simulations, was conducted to assure a uniform distribution of carbon-bonds and thereby eliminate temporal and spatial differences in the actual distribution of carbon-bonds. The second and third simulations in Table 18 use the overall regional carbon-bond mix derived from emission inventories compiled for Tulsa and Philadelphia. The fourth simulation uses a carbon-bond mix derived from the average composition of automotive exhaust as determined from measurements of individual hydrocarbon species taken by the Bureau of Mines (BOM).

The effect of these uniform changes in hydrocarbon activity on peak ozone predictions on Days 195 and 275 is summarized in Table 19. The hydrocarbon reactivity derived from the Philadelphia inventory produces modestly higher peak ozone predictions on both days. That derived from the Tulsa inventory produces only slightly less ozone than the base case. However, a uniform reactivity corresponding to the BOM automobile exhaust data produces markedly higher peak ozone predictions, particularly on Day 275 where nearly a 30 percent increase is computed. Day 275 also shows significantly greater sensitivity than Day 195 when the Philadelphia hydrocarbon reactivity is used. This behavior is consistent with the relatively greater importance of estimated boundary concentrations on Day 195. However, Day 195 exhibits greater sensitivity when using the Tulsa hydrocarbon reactivity though the difference is small. While these tests are very limited in number, the results suggest that the reactivity of the hydrocarbon emissions, as determined by the carbon-bond mix, does significantly influence peak ozone predictions. Furthermore, significant differences result from differences in reactivity representative of a variety of emissions data bases. These changes in reactivity originate in two ways: (1) the particular combination of source types, and (2) the method by which emissions are classified for inclusion in the carbon-bond kinetics mechanism. Either or both can have a significant impact on ozone predictions.

Another method of exploring the sensitivity of the Airshed Model changes in hydrocarbon reactivity would be to vary the amount of each carbon-bond, one at a time. However, in order not to alter the total carbon emitted, one or more other carbon-bonds would have to be reduced the same amount. While these kinds of sensitivity tests have not been performed utilizing the present version of the Airshed Model and the revised St. Louis preprocessor files, some indication of the relative sensitivity of ozone predictions to the individual carbon-bonds can be gained by further examination of Tables 18 and 19. It is apparent from Table 18 that only small differences in the ethylene (ETH) carbon fraction exist among the four simulations; the range is 4.1 to 5.4 percent. Paraffinic carbon, represented by PAR, is recognized as the least reactive carbon. Therefore, the differences in peak ozone seen in Table 19 must be associated with the relative proportion of OLE, ARO, and CARB. Broadly speaking, these represent the characteristic bonds of olefins, aromatics, and aldehydes, respectively.

The BOM simulation has the highest percent (30.7) of olefins aromatics, and aldehydes combined, and the highest peak ozone concentrations. The Philadelphia simulation, having the next highest percent (21.9) of olefins, aromatics, and aldehydes combined, has the next highest peak ozone concentration on both days. By contrast, the sum of the olefins, aromatics, and aldehydes for Philadelphia (21.9 percent) is about the same as for St. Louis (21.2 percent) but the peak ozone concentrations for the Philadelphia simulations are higher. Aromatics and olefins are somewhat lower in Philadelphia (13.2 and 2.8 percent) than in St. Louis (14.9 and 4.8 percent). The major difference is in the aldehyde fraction, which is almost four times higher in Philadelphia (5.9 percent) than in St. Louis (1.5 percent).

Contrasting the St. Louis and Tulsa simulations, the sum of the olefins, aromatics, and aldehydes is substantially greater in St. Louis (21.2 percent) than in Tulsa (15.8 percent). Moreover, the sum of the olefin and aromatic carbon fractions alone is greater for St. Louis (19.7 percent) than for Tulsa (12.2 percent). Nevertheless, on both days, the simulations for Tulsa and St. Louis produce similar peak ozone concentrations. This result appears then to be associated with the fraction of aldehydes, which is more than twice as great in Tulsa (3.6 percent) as in St. Louis (1.5 percent).

In all four simulations, the CARB fraction is less than six percent. Despite its relatively small contribution to the total mass of hydrocarbon emissions, the weight of the evidence points strongly to the major role played by aldehydes, and other oxygenated compounds which are included in the CARB carbon-bond category, in the formation of ozone in urban areas. These results support the suggestion of Killus and Whitten,[27] developers of the Carbon-Bond Mechanism, that special attention be given to the level of oxygenated compounds in emission inventories. By extension, similar attention should be given to the level of oxygenated compounds in ambient air.

Further sensitivity tests on days 195 and 275 were conducted to examine the effect of hydrocarbon reactivity on the change in peak predicted ozone associated with uniform reductions in hydrocarbon emissions. For this purpose, the most reactive carbon-bond mix, the BOM, was used in combination with a 42 percent reduction in hydrocarbon emissions. As can be seen from Table 20, greater hydrocarbon reactivity leads to only slightly greater sensitivity to decreases in hydrocarbon emissions than is shown by the base case. This small difference could possibly be explained by spatial and temporal differences in the carbon-bond mix of the base case, which have been eliminated in the sensitivity case, rather than the overall change in hydocarbon reactivity. Spatial and temporal effects are discussed further in Section 5.6.

5.6 Other Sensitivity Tests

A variety of other sensitivity tests were also performed as listed in Table 21. These tests were designed to examine the sensitivity of Airshed to the spatial and temporal distribution of emissions, to changes in mixing height, and to changes in photolysis rates.

5.6.1 Spatial Distribution

The first of these tests replaced the grid cell by grid cell variation in emissions implicit in a spatially disaggregated inventory with a uniform distribution. The total hourly ground-level emissions (from highway mobile sources, nonhighway area sources, and minor point sources) from all grid squares combined were divided equally among the 300 grid squares in the modeling region. Major point source emissions were distributed equally among 55 fictitious point sources within each of the four vertical layers to be simulated. These 55 point sources were then randomly distributed among the 300 grid cells during each hour and within each vertical layer. This finely detailed randomization, in combination with vertical wind shear and horizontal diffusion, should produce a nearly uniform distribution of emissions in all vertical layers. All emission species treated by the Airshed Model were redistributed in this way.

Table 21 indicates that a rather large reduction in peak ozone is predicted for both Days 195 and 275. The percentage decrease is nearly the same on each day (18.9 and 18.5 percent). A substantial reduction in the peak ozone levels is expected since the primary effect of the redistribution is to dilute the high-level emissions which occur in the immediate urban environs. As suggested by Figure 29, a decrease in precursor concentrations reduces the peak ozone prediction. This occurs even when the HC/NO_x emissions ratio is held constant, as indicated by the 24.1 percent drop on Day 275 when hydrocarbon emissions were reduced by 4 percent and oxides of nitrogen by 40 percent. The time and location of the peak is also affected by the redistribution. On Day 195, the peak occurs nearly 20 km further downwind and one hour later. On Day 275, the peak occurs an hour earlier but in the northeast corner of the region, outside the immediate influence of the trajectory illustrated in Figure 20c for the base case.

A second test replaced the hourly and spatially varying mix of carbon-bonds with a uniform mix equivalent of the overall regional mix based on the emissions from all sources for all hours combined. (This test was discussed previously in Section 5.5 but was not contrasted with the original base case. Table 21 shows that the peak ozone predicted is modestly reduced on Day 275 (6.9 percent) but only slightly lessened on Day 195 (1.1 percent). The uniform hydrocarbon reactivity has no effect on the time or location of the peak on Day 195. However, on Day 275 the peak is delayed two hours.

5.6.2 Temporal Distribution

A single sensitivity test was conducted on Days 195 and 275 to examine the sensitivity of peak ozone predictions to a temporal redistribution of emissions. In this test, late morning emissions of all pollutants were displaced to midmorning hours; namely, emissions from 9:00 to 10:00 were shifted to 6:00 to 7:00, emissions from 10:00 to 11:00 were shifted to 7:00 to 8:00, and emissions from 11:00 to 12:00 were shifted to 8:00 to 9:00, Central Standard Time. The overall effect of this test was to increase precursor concentrations during the morning rush hours and to eliminate all fresh emissions for the hours immediately following. The results are given in Table 21. As would be expected from an increase in the morning emissions peak, maximum predicted ozone concentrations increase for both days (5.7 and 21.1 percent). The effect is less on Day 195 when winds were higher and precursor concentrations lower than on Day 275. On Day 195 the peak ozone prediction is advanced 1 hour; however, the peak occurs at a location some 20 kilometers further downwind. Entirely different trajectories must therefore be associated with the peak prediction for the base case and sensitivity simulations. On Day 275, two peaks are predicted; the early peak is seen at the same hour as the base-case simulation. The second peak, which is somewhat greater (281 ppb vs. 276), occurs 3 hours later. Although these spatial and temporal effects are difficult to explain, the overall effect of higher morning rush-hour emissions is an increase in the peak ozone prediction.

5.6.3 Mixing Height

Two sensitivity tests examined the effect of uniformly increasing or decreasing the mixing height by 25 percent throughout the day. Because the mixing height is the key to defining the vertical structure of the modeling region in the Airshed simulations, these changes can be expected to have pronounced effects on other model inputs which in turn influence ozone. For example, the region top is defined with respect to the mixing height; the treatment of elevated emissions is influenced by it; and entrainment of pollutants aloft is directly proportional to changes in the height of the mixed layer. The sensitivity test results are tabulated in Table 21 and illustrated in Figure 36. In all cases, a change in the mixing height increases the peak ozone prediction. On Day 195, peak ozone is insensitive to mixing height; both increases and decreases of 25 percent produce very small increases (1.1 and 1.7 percent). A quite large increase in the peak ozone concentration (33.6 percent) is predicted on Day 275 when mixing heights are reduced, but an increase though small (1.7 percent), is also seen when mixing heights are increased. In the absence of entrainment aloft and ignoring elevated point-source plumes, an increase or decrease in the mixing height is equivalent to an increase or decrease in dilution. As suggested by earlier sensitivity tests, the more dilute the mix of precursors, the less ozone is subsequently formed. However, ozone aloft on days 195 and 275 was significant, estimated as 78 and 6 ppb respectively. For both days it appears then that the effect of increased ozone entrainment associated with an increase in mixing height offsets the reduction in morning precursor concentrations. In contrast, a 25 percent decrease shifts the balance in the opposite direction; the loss of ozone aloft appears to be outweighed by the increase in morning precursor concentrations. Further analysis is required to explain why the same relative reduction in vertical mixing produces vastly different effects on peak ozone concentration. A possible clue may, however, lie in the morning (7:00 to 8:00 CDT) inversion height which was estimated as approximately 420 m on Day 195 and 120 m on Day 275, and its relation to the height of elevated point source plumes of oxides of nitrogen. It is conceivable that a 25 percent reduction from 120 meters may have had a much larger impact on surface HC/NO_x ratios than did the same reduction from 420 meters. Regardless, somewhat more predictable effects are seen on the time and location of the peak ozone concentration. A 25 percent increase in mixing height, which has little impact on the magnitude of the peak, delays the timing of the peak 2 hours on Day 275. A 25 percent decrease on Day 195 accelerates the peak by 1 hour, although it occurs over 20 kilometers further downwind. Decreases on Day 275 and increases on Day 195 have no effect on the time and location of the peak prediction.

5.6.4 Photolytic Rates

A final test explored the sensitivity of the Airshed Model to changes in the photolytic rate constants utilized by the Carbon-Bond II Mechanism. While the major such reaction is the photolysis of nitrogen dioxide (NO_2), which leads directly to the production of ozone, other important photolyzable species included in the mechanism are aldehydes (CARB) and glyoxals (GLY) both of which are oxygenated products of primary hydrocarbon species, the former derived from olefins and paraffins and the latter from aromatics. The photolytic rate constants for CARB and GLY are estimated by scaling the NO_2 photolytic rate constant which in turn is estimated from ambient measurements of total solar radiation. In these tests, the NO_2 photolysis rate was increased or decreased by 10 percent; those for CARB and GLY were then automatically raised or lowered by the same percentage. The results are given in Table 21 and are plotted in Figure 37. A 10 percent increase in photolysis produces a similar, but slightly smaller, increase in the peak ozone prediction on both Days 195 and 275 (7.5 and 9.5 percent). A 10 percent decrease has about the same but opposite effect on peak ozone (8.0 and 7.8 percent). These results are expected since the concentration of ozone is directly proportional to the rate of NO_2 photolysis in the absence of removal by reaction with hydrocarbon. The time and location of the peak ozone concentration predicted by the Airshed Model is also affected by changes in photolysis rate. On Day 275, an increase in the photolysis rate advances the peak by 1 hour while a decrease of 10 percent delays it 2 hours. On Day 195, a 10 percent increase has no effect on the time or location of the peak prediction whereas a 10 percent decrease delays it 1 hour and moves it 5 kilometers downwind.

5.7 Discussion

In the foregoing sections, the sensitivity of the Airshed Model to uniform changes in hydrocarbon and oxides of nitrogen emissions, to uniform changes in hydrocarbon reactivity, and to changes in the spatial and temporal distribution of emissions was discussed. Several additional tests were discussed which dealt with two meteorological variables (mixing height and solar insolation, (the latter expressed via photolysis rates). While much information has been obtained, large gaps still exist in understanding the sensitivity of the Airshed Model.

Numerous sensitivity tests were made using previous versions of both the Airshed Model and the preprocessor files which were developed from the St. Louis data base. A major sensitivity study was also conducted on the Airshed Model using a data base for Los Angeles.[25] However, only the study reported here utilizes the most recent version of the Airshed Model, one incorporating both the Carbon-Bond II kinetics mechanism and the FCT algorithm for numerical advection. As was pointed out earlier, these changes had significant effects on ozone predictions for the St. Louis base-case simulations. More significant was the effect these changes had on the sensitivity of the model. The effects on sensitivity were frequently unexpected, sometimes large, and most often unexplained to date. Results of previous sensitivity tests must, therefore, be viewed with a large measure of caution.

Despite the emphasis placed on the sensitivity of the Airshed Model to emissions changes, this area is far from being fully explored. Most notable, perhaps, is the combined effect of both hydrocarbon and oxides of nitrogen changes. Specifically, the response of the Airshed Model to changes in oxides of nitrogen emissions at various levels of hydrocarbon emissions has not been examined. The sensitivity of the Airshed Model to the spatial and temporal resolution of emissions has not been clearly established either. The tests reported here represent radical departures from actual spatial and temporal emissions patterns. These tests do not address the questions of what size grid squares ought to be or for what time intervals emissions ought to be estimated (hourly vs. some longer or shorter interval).

Not investigated with the current version of the Airshed Model is the entire area of air quality data: initial conditions, boundary conditions along the borders of the modeling, and boundary values aloft. Although initial conditions were varied in the tests reported here, they were varied along with emissions. Of particular interest for providing guidance on modeling and establishing rational data requirements are the sensitivity of the Airshed Model to concentrations of hydrocarbons, oxygenated organics (predominantly aldehydes), and ozone aloft. Also of considerable interest are the effect of various levels of hydrocarbons, oxygenated organics, and organic nitrates (primarily PAN) present in urban air in the early morning hours, concentrations which serve as initial conditions for the model.

The area of meteorological inputs is also unchanged. Although the meteorological tests discussed in Section 5.6 do show considerable sensitivity to photolysis rates and great sensitivity to mixing heights under certain circumstances, such across-the-board uniform changes in these parameters provide only very limited insight into the role which differences in the richness of meteorological data or the methods by which it is interpreted, analyzed, and prepared for model input have on model results. For example, a single technique for developing a three-dimensional wind field based on surface wind and temperature data and upper air wind data was used for all Airshed Model simulations in St. Louis.

Basic to a numerical model such as Airshed is the grid cell structure. The horizontal and vertical dimensions of each grid cell are established early in the modeling process. (The horizontal dimension of grid cells for modeling is to be distinguished from the size of emissions grid squares which need not necessarily coincide). What these grid cell dimensions should be has not been systematically investigated. Instead, perceived computational constraints have decided the issue. The extent to which grid cell dimensions should be tailored to the type of meteorological events being modeled has not been considered. Whereas relatively large grid cells may be sufficient for stagnation conditions, more severe requirements may be needed regarding the resolution of grid cells on transport days, a hypothesis which is consistent with the relative performance of the Photochemical Box Model (PBM) on different days in St. Louis.[3] Wind shear may well be another factor which should be considered in establishing the vertical dimensions of grid cells. What effect changes in the in the grid cell structure have on both model sensitivity and model performance could be assessed by further sensitivity analysis.

Resolution of at least two technical issues could also be promoted by additional sensitivity testing. The first of these is biogenic emissions of various hydrocarbon species. Biogenic emissions, components of which have been shown in smog chamber studies to be as reactive as a typical mix of urban anthropogenic emissions[33] and other components of which have been shown to be relatively more reactive in terms of their ozone formation potential,[34] have not been included in any of the Airshed Model simulations in St. Louis. Of compelling interest is the extent to which these compounds modify the sensitivity of the model to changes in anthropogenic emissions of both hydrocarbons and oxides of nitrogen. A second technical issue is the aromatics chemistry of the Carbon-Bond II mechanism which has recently been updated and incorporated in what is now Carbon-Bond III. To what extent this new understanding of the chemistry of aromatics may influence model predictions in the base case or, more importantly, the sensitivity of the Airshed Model to emissions changes or other changes in inputs can only be assessed by further sensitivity tests.

6.0 Estimating Control Requirements

This chapter demonstrates the use of the Airshed Model to assess the types of programs that may be required in order for the St. Louis AQCR to meet the NAAQS for ozone. It is emphasized that this study is not intended to prescribe specific control programs relative to State Implementation Plans (SIP's) but rather to demonstrate the feasibility of the Airshed Model approach.

Two approaches were used to estimate the type of programs that may be required for the St. Louis Air Quality Control Region to meet the NAAQS for ozone. First, a series of simulations were performed in which hydrocarbon emissions were decreased uniformly. For each of the simulations, peak ozone is compared to that of the base case. This approach enables one to estimate the overall degree of control that is likely to be needed but ignores the spatial, temporal and reactivity effects of specific control measures. The second approach used is to test the effect of specific control programs. To do this, the area source and point-source emission files were modified to reflect reductions associated with particular source categories. The control programs tested were: (1) Reasonably Available Control Technology (RACT) for stationary sources; (2) the Federal Motor Vehicle Emissions Control Program (FMVECP); and (3) Inspection and Maintenance (I & M) for motor vehicles.

Simulations were performed using 3 high ozone days from 1976 (159, 195, and 275). These are the same days that were used for sensitivity testing described in Chapter 5. Description of the meteorological conditions, ozone distribution and model performance (relative to observed ozone) for the 3 days is discussed in detail in Section 5.1.

In summary, Days 159 and 195 were days of moderate wind speed and mixing height. Day 275, on the other hand, was characterized by extremely low wind speeds and restricted mixing heights. For Day 275, the model was extremely accurate in estimating observed peak and near-peak ozone in the base-case simulations. Day 159 showed a tendency toward overprediction and Day 195 underprediction.

6.1 Response to Uniform Changes in Emissions

Sensitivity tests were conducted to determine how the Airshed Model predictions of ozone respond to changes in hydrocarbon emissions. To establish the response over a wide range, reductions of 5 percent, 17 percent, 42 percent and 75 percent and increases of 17 percent and 63 percent over the base case were tested. The results for the 3 test days are discussed in Chapter 5 and are summarized in Figure 38, in which percent change in peak ozone concentration is plotted as a function of percent change in hydrocarbon emissions. For all 3 days the response to changes in hydrocarbon concentration is less than 1:1; for example, on Day 195 a 40 percent reduction in hydrocarbon emissions is required to reduce peak ozone by 20 percent. Furthermore, the model's sensitivity to HC emission changes is substantially different for the 3 days. The model's response to reductions (or increases) in HC emissions is strongest for Day 275, the severe stagnation day with the highest observed peak ozone of the 20-day data base. Another finding is that with greater degrees of hydrocarbon control, the location of the predicted peak ozone is displaced downwind and tends to occur later in the day.[35]

Additional sensitivity tests were conducted in order to assess how changing NO_x emissions would affect the model's ozone/hydrocarbon response response curve. Specifically, uniform increases and decreases of NO_x emissions were coupled with a 42 percent reduction in HC emissions for the 3 test days. The results of this analysis are shown in Figure 35 and indicate that decreases in NO_x emissions (by 20 percent from the base case) result in a lessening in the effectiveness of HC emission reduction in decreasing peak ozone concentration. The effect was small on Day 195 (ozone reduction diminished by about 2 percent) and substantial (about 7 percent) for the remaining 2 days. Additional tests are required to assess the effect of $N\,O_x$ emission changes with greater reduction in hydrocarbons.

6.2 Control Strategy Simulations/Methods

The sensitivity tests described above are based on uniform reductions of total emissions. However, actual control programs have varying effects on different sources, different parts of the region and on different classes of hydrocarbons. For this reason, simulations were conducted using emission inventories which were modified to reflect changes in the actual sources to which the control programs are applied. In the following inventories, no adjustments were made for changes in population, production or traffic.

6.2.1 RACT

According to CFR 40, Part 51, "'Reasonable available control technology' means devices, systems, process modifications, or other apparatus or techniques, the application of which will permit attainment of the emission limitations. . . ."[36] Furthermore, RACT requires that attention be given to (1) the necessity of imposing emission limitations to achieve and maintain a national standard, (2) the corresponding social and economic impact and (3) alternative methods for achieving and maintaining the national standard. RACT measures are further defined by available Control Technique Guidelines (CTG's) for specific sources, e.g., EPA-450/3-78-120.[37]

The RACT emission inventories used in the Airshed Model control strategy simulations described herein, were based on a number of studies by Baverman.[38,39,40,41] These studies were performed to determine the reactive hydrocarbon reductions that could be achieved if RACT were applied to major stationary sources within the St. Louis modeling region. Most of the stationary source hydrocarbon emissions are evaporative in character and include industrial point sources (e.g., surface coating, petroleum refining and storage) and area sources (gasoline marketing, dry cleaning and surface coating). The application of RACT to stationary sources results in a daily hydrocarbon emission reduction of approximately 22 percent. The hydrocarbon reduction varies from a low of 21 percent for Day 159 to a high of 24 percent for Day 275.

6.2.2 FMVPC

The Federal Motor Vehicle Pollution Control (FMVPC) program is broadly defined in the Clean Air Act (as amended in 1977). A more detailed discussion is presented in CFR 40, Parts 85 and 86.[42,43] In the present study, FMVPC was considered to affect only the hydrocarbon and oxides of nitrogen components of the mobile source portion of the 1976 (baseline) emissions inventory. In order to prepare the FMVPC, the St. Louis baseline mobile source inventory was modified to reflect projected 1987 hydrocarbon and oxides of nitrogen emission levels mandated by the 1977 Clean Air Act (CAA) amendments. The FMVPC strategy required a change in mobile source hydrocarbon speciation as well as a reduction in mobile source hydrocarbon and oxides of nitrogen emissions.

This study utilized estimates of total HC and NO_x reductions associated with FMVPC which were prepared by Mayer.[44,45] These emission reductions were determined from representative composite mobile source emission factors generated by Mobile 1.[46] Representative vehicle speeds were chosen for each of the road classifications (i.e., freeways and arterials) considered in the Mobile 1 simulations. Traffic volume and driving patterns were held constant. The FMVPC strategy resulted in an approximate 69 percent reduction in mobile source hydrocarbon emissions. This corresponds to a 41 percent reduction in area-source hydrocarbon emissions or a 33 percent reduction in total hydrocarbons. The FMVPC strategy total hydrocarbons (carbon) reduction varies from a low of 33 percent for Julian Day 275 to a high of 34 percent for Julian Day 159. The NO_x reduction represents a 43 percent reduction in NO_x in the mobile source inventory, a 27 percent reduction in area-source emissions and an 8 percent reduction in total NO_x emissions. (NO_2 is assumed to be 10 percent of total NO_x emissions, the remainder to be NO.)

The FMVPC strategy required a change in the distribution of hydrocarbon species as well as a reduction in mobile source hydrocarbon emissions. In addition to the mobile source emission factors, Mobile 1 simulations also yielded the evaporative and exhaust-gas component fractions of the mobile emissions for 1976 and 1987. The 1976 evaporative and exhaust gas species profiles were provided by Novak.[47] For the purpose of this study, it was assumed that all automobiles operating in St. Louis in 1987 would be equipped with catalytic reactors for exhaust gas emission control and with canisters for evaporative emission control. The 1987 gas emission species profile is assumed to be that given by Table 9-06-021A of the EPA VOC Species Data Manual.[48] The corresponding evaporative emission species profile is given by Table 9-06-021C of the same report. Both profiles are based on Black and High (EPA) data.[49,50]

The species data in Table 9-06-021A and C are based on a test fuel composition not necessarily representative of St. Louis gasoline. Therefore, the test fuels exhaust gas and evaporative species profiles require an adjustment to reflect some appropriate St. Louis fuel composition. The assumption that all 1987 automobiles have catalyst control for the exhaust gas implies that the automobiles consume unleaded gasoline. Johnson[51] has reported on the composition of fuels sampled during the DuPont 1978 summer road octane survey. It was assumed that St. Louis would be in the same market area as Detroit, Chicago, and Kansas City. Johnson's unleaded fuel composition data were used to adjust the exhaust gas and evaporative species profiles given in Tables 9-06-021A and 9-06-021C.

6.2.3 I/M

As with RACT and FMVPC, the authority for inspection and maintenance is found in the Clean Air Act as amended in 1977. Additional requirements are presented in the Federal Register.[36,42] It should be noted that the I/M control strategy is considered to be a secondary control strategy. As such, its effectiveness is dependent, in part, upon the effectiveness of the primary control strategy--FMVPC. The present study assumes that I/M affects hydrocarbon emissions but does not affect emissions of the oxides of nitrogen. In addition, it is assumed that all automobiles are included in the inspection and maintenance program; the inspection failure rate is 30 percent and there is mechanics training. These assumptions form the basis of a strong inspection and maintenance program for St. Louis. According to Mayer,[45] this strong I/M program results in a hydrocarbon reduction of approximately 11,700 tons/year. This corresponds to a reduction of some 10 percent in mobile-source hydrocarbon, 6 percent in area-source hydrocarbon and 4.5 percent in total hydrocarbon emissions.

6.3 Control Strategy Results

The 16 control strategy simulations performed in this study are described in Table 22. The table shows that four strategies each were simulated for Days 159 (transport) and 275 (stagnation). Eight control strategies were simulated for Day 195 (transport). RACT and FMVPC were simulated individually and in combination for all 3 days. The combination of RACT and FMVPC control strategies in conjunction with boundary changes in both hydrocarbons and ozone was also investigated for all 3 days. The effects of the I/M strategy as well as the effects of NO_x reductions were evaluated only for Day 195. Additional boundary changes were evaluated only for Day 195. It should be noted that boundary concentration changes in hydrocarbons, the oxides of nitrogen and ozone were limited to changes only in the anthropogenic portion of these pollutant concentrations.

In using the results of uniform reduction and specific control measure simulations, several alternative approaches are possible. First, one can track the changes in ozone concentration that take place at the sites of ozone monitors. The emission control requirement is defined as that needed so that none of the monitor sites have predicted peaks which exceed 120 ppb (the NAAQS level). This approach has the advantage of using only model results from grid cells represented by monitoring sites, i.e., the same portion of the modeling region for which performance measures relative to observed concentrations have been calculated. In addition, this approach meshes with the current practice (being used with EKMA for the 1982 SIP's) of basing control on analyses for specific monitoring sites.

The site-specific method, however, has one drawack. The sensitivity analyses discussed previously have shown that the location of the peak ozone tends to migrate downwind. Thus, the control curve for a particular site will be steeper (greater reduction in ozone with reduction in emissions) than that for the region as a whole. Given the paucity of monitoring sites in outlying regions, there is a strong possibility that relying solely on the behavior of peak predicted ozone at the monitoring sites will underestimate the full extent of control needed to bring the entire AQCR into attainment. In the current study, an alternative approach, tracking the peak predicted ozone concentration regardless of position is used. This method utilizes the entire spatial domain of the model and offers greater assurance that the predicted control requirements will affect the entire region and not merely shift the problem downwind.

A second issue is that of calibration. As stated in Chapter 4, the model has a systematic tendency to underestimate peak and near-peak ozone. For control strategy simulations, we have selected 3 days--one for which peak ozone was overpredicted (159), a second for which peak ozone was underpredicted (195), and a third for which the model predicted peak ozone accurately (275). The question is whether the model results should be calibrated for the 2 days showing bias. In the current study, we have used the model in a relative sense, such that we are concerned with percent reductions in peak ozone.

$$\text{\% ozone control required} = \frac{P_{max} - 120 \text{ ppb}}{P_{max}} \times 100\%$$

This approach contains an implicit form of calibration, one in which the relative percent error remains constant as emissions are reduced in the simulations. This is demonstrated in the following example. Suppose that the predicted peak ozone is 240 ppb. However, we have shown that the model overpredicts by 20 ppb (8.3%) on this day. Using our approach we estimate a control requirement of

$$\left(\frac{240 - 120}{240}\right) \times 100\% = 50\%$$

However, this is exactly the same as adding a constant relative error to the base case and the control case, i.e.,

$$\left(\frac{[240-20] - [120-10]}{[240-20]}\right) \times 100\% = \frac{220-110}{220} = 50\%$$

when the relative error $\left(\frac{20}{240}\right)$ for the base case is equal to the relative error for the control case $\left(\frac{10}{120}\right)$.

The results of control strategy tests for the 3 days are presented in Table 23 and are plotted on Figure 39 along with the HC/O_3 response curves for uniform HC reductions discussed previously.

Except as otherwise indicated in Figure 39, boundary concentrations (i.e., transported ozone and precursors) were held constant. For a number of strategies, the model was run with reduced boundary concentrations to test the effect that parallel control programs for upwind cities would have on St. Louis ozone levels.* For these cases the anthropogenic portion of boundary precursor concentrations was reduced in proportion to the emission reductions. For ozone, the anthropogenic portion (i.e., that in excess of 0.04 ppm) was reduced less than proportionately to HC emissions reductions using the HC/O_3 response curves (discussed in the previous section) as a first approximation.

Examination of Figure 39 reveals that the control strategies tested tend to follow the general patterns indicated by the HC/O_3 response curves based on uniform emission reductions. However, for the two transport days (19 and 195), the combined (RACT + FMVPC) simulations tend to be somewhat more effective than the uniform reduction runs in reducing peak ozone. For the stagnation day (275), the control simulations result in the same reductions in peak ozone as the uniform reductions.

A second finding is that the model appears to show a synergistic effect between stationary and mobile source control. For example, on Day

---

*Initial concentrations used in modeling were reduced from the base case in proportion to reductions in emissions in all cases.

275, the RACT simulation results in an 8 percent decrese in peak ozone and FMVPC, a 32 percent decrease when each is applied separately. However, when the two strategies are combined, the model yields a 49 percent reduction in peak ozone. This finding may be associated with nonlinearity in the HC/O_3 response curve, i.e., HC control becomes more effective as the HC/NO_x ratio decreases and ozone formation is increasingly limited by HC concentration.

Reductions in boundary concentrations representing parallel upwind controls were found to have a substantial effect on peak ozone concentration for the 2 transport days (159 and 195). On Day 159, reduction in boundary concentration in conjunction with FMVPC and RACT resulted in an additional 5 percent reduction in peak ozone. For Day 275 (stagnation) the model appears to be insensitive to changes in boundary concentrations. On this day, ozone transported into the region was lower than on most other days and the effect of precursor buildup associated with urban emissions tends to overwhelm the effect of transported ozone and precursors.

Changes in NO_x emissions also affect model estimates of peak ozone reduction. For Day 195, the FMVPC simulation was run for HC reductions alone and for the case in which both HC and NO_x emissions are reduced in accord with current statutes. Note that in the cases for which NO_x control is included, the computed reduction in peak ozone is diminished by about 5 percent This finding is similar to that reported in the section on uniform reduction sensitivity tsts.

The changes in emissions associated with the control strategies and uniform reductions not only reduce the magnitude of the peak ozone concentration, but also change the position of the peak in time and space. As Figure 40 illustates, there is a strong tendency for the position of the peak to migrate downwind as the level of control increases. For 2 of the 3 days, the time of the predicted peak is later in the day with increasing control.

As in the case of the uniform emission reduction simulations, the control strategy simulations demonstrate that the effects of control vary strongly from day to day. For example on Day 195, the combination of RACT and FMVPC led to a 30 percent reduction in peak ozone, whereas on Days 275 and 159, the same combination of controls resulted in a more than 45 percent reduction of peak ozone. Moreover, the estimates of control requirements are quite different for the 3 days. The day-to-day variation in HC/O_3 response probably reflects reality. Each day has unique source-receptor relationships, photochemical potential and boundary concentrations.

For Days 275 and 195 the analysis indicates that RACT and the FMVPC applied in St. Louis (and in upwind cities) may be sufficient to meet the ozone standard. On the other hand, the results for Day 159 suggest that control beyond RACT, FMVPC and I/M may be required. (I/M was tested only on one day (195); on this day the estimated effect of I/M on peak ozone was relatively small, about 3 percent). One should note, however, that for Day 159, the model predicted peak ozone concentrations occur in the northwest corner of the region, an area without ozone monitors.

In interpreting the above results, we have made no formal attempt to relate the findings to the statistical (expected exceedance) form of the ozone NAAQS. The use of resource-intensive photochemical grid models precludes modeling a large number of days that would be required for a strict determination of control requirements relative to the statistical form of the standard. However, the 3 days tested include several of the days with highest ozone observed in 1976. (Days 275, 195 and 159 had peak observed ozone concentrations of 244, 223 and 172 ppb respectively). The 3 days represent a good cross section of the types of days associated with high ozone. The most stringent control requirements were found on Day 159; however, the predicted peak for this day was found in the northwestern portion of the modeling region where there were no monitors to evaluate the maximum predicted concentration of 312 ppb. Monitoring coverage for Days 275 and 195 was more adequate. Thus, one might be tempted to use the estimates of control requirements for Days 195 and 275, i.e., 50-60 percent NMHC emission reduction achieved largely through a combination of RACT and FMVPC. While the study indicates that Inspection and Maintenance results in a small (several percent) reduction in peak ozone, I/M may be necessary to assure that the full benefits of FMVPC are realized.

The reader is cautioned, however, that the results are based on 1976 emissions and air quality data. Thus, the design concentration and the estimated control requirements may not be in exact agreement with those based on more recent assessments.

6.4 Uncertainties

While it is presently difficult to quantify the uncertainties associated with the analysis, it is possible to identify major areas of uncertainty. As we have shown, the estimates of control requirements are very sensitive to the slope of the HC/O_3 curve. The curves differ from day to day and are complex functions of precursor and ozone transported into the region, dilution, the particular mix of emissions that occurs as air is advected between grid cells and the reactivity of the precursor mix. Any errors (for example, inadequacy of the chemical mechanism, errors in the speciation of NMHC emissions or in estimates of boundary concentrations) will result in errors in the HC/O_3 response curves, and in our estimates of the control required to meet the ambient ozone standard.

Specification of boundary concentrations for future years is particularly difficult. While the assumption that parallel efforts are being made in upwind cities, one must assume the portion of incoming pollutants are anthropogenic. Moreover, we can only make approximations as to how control efforts in distant cities affect ozone and precursor concentrations in air that has been transported over hundreds of kilometers. The uncertainty associated with boundary concentrations is likely to increase as emissions are "turned-down" and peak ozone concentrations grow increasingly sensitive to boundary concentrations.

Unfortunately, there is no readily available way to test the veracity of the HC/O_3 response curves. However, it may be possible (for St. Louis or for other cities) to track changes in ozone and in emissions over a multi-year period and to compare the observed relationship with that shown by the model.

The principal difficulty in such an approach is that it is often difficult to separate the effects of meteorology from that of emissions.

as possible with regard to meteorology. In assessing emissions-related reductions in ozone, model results from meteorologically similar days should be used.

7.0 Conclusions

The purpose of this chapter is to highlight the primary findings of the study with regard to model performance, model senstivity and the model's estimates of control requirements for the St. Louis AQCR. The chapter also integrates the information presented in earlier chapters in order to address the issues of uncertainty and the model's tendency to underpredict ozone at high concentrations. Finally the chapter discusses the feasibility of the Airshed Model approach for regulatory analyses and makes recommendations regarding the use of the model.

7.1 Conclusions on Model Performance

An evaluation of the Airshed Model for St. Louis was conducted using the latest EPA version of the model and the RAPS data base. The resulting ozone concentration estimates were compared using statistical procedures (performance measures) recommended by the AMS Workshop on Model Evaluation.

In general, the results indicate that the model is sufficiently accurate for use in control strategy simulations. Specific findings are discussed below:

a. Model Bias ($\overline{O-P}$) was used to assess the model's abilty to estimate observed ozone concentrations over the full range of ozone values. The analysis indicates that there is no overall pattern of under- or overestimation for the 20 days when all of the data pairs are used; most of the bias values are within ±20 percent of the zero value. There is, however, a marked shift toward underprediction for the analyses which use higher ozone concentrations.

b. Consistent with the finding in (a), the Airshed Model was found to have a systematic tendency to underestimate peak and near-peak ozone concentrations. This conclusion is based on a number of performance measures recommended by the AMS and by Cox.

c. The selection of performance measure has a pronounced effect on perception of model bias. The measures of peak accuracy based on a single residual (O_{max} - P_{max}) tend to overstate the degree of underprediction. Because these measures are based on the location and/or time of the observed maximum, temporal and/or spatial displacements result in a positive bias (underprediction) even if the model correctly predicts the magnitude of the observed peak. On the other hand, the measures are obtained by averaging (O_{max}-P_{max}) residuals over all hours for a temporally paired comparison and over all sites for a spatially paired comparison. These are more robust and free of this inherent bias. These "A" measures indicate that the average bias for spatially paired residuals is 14 ppb (about 11 percent). The predicted spatially averaged maxima for nearly all of the days fall within ±30 percent of the corresponding observed maxima.

d. The model accurately represents temporal variation of ozone; however, the model's ability to replicate spatial patterns varies from day to day. While the model is able to locate the general area of highest concentrations for most days, it tends to underestimate the size of the NAAQS exceedance zone. A lack of monitoring sites in the areas downwind of St. Louis limit the assessment of the model's spatial accuracy.

e. The model was found to estimate 24-hour average NMHC and NO_x concentrations accurately for the 20-day data set. The lack of bias indicates that the overall emission inventories are fairly accurate; however, no conclusions may be drawn with regard to the accuracy of the spatial, temporal or species distributions in the inventories.

7.2 Model Sensitivity

7.2.1 Findings

Conclusions resulting from a large number of sensitivity tests (described in Chapter 5) are summarized as follows:

a. The sensitivity of the Airshed Model to changes in model inputs shows large day-to-day variation, variation which demonstrates a high degree of interaction among different input parameters.

b. Uniform changes in hydrocarbon emissions result in nonlinear changes in peak ozone predictions which are in the same direction. However, the relative magnitude of the change in peak ozone is invariably less than that for emissions. Peak ozone concentrations are more sensitive to uniform reductions in hydrocarbon emissions than are area-wide ozone predictions.

c. Compared to a reduction in NMHC emissions alone, simultaneous reductions in both NMHC and NO_x emissions appear to lower the reduction of peak model ozone. Conversely, a reduction in hydrocarbon emissions accompanied by an increase in NO_x emissions, tends to enhance the reduction of peak ozone. These conclusions, however, were obtained at only a single (42%) reduction in HC emissions and for a limited set of NO_x changes. No conclusions can be drawn regarding the sensitivity of nitrogen dioxide predictions to changes in NO_x or the effect on carryover or long-range transport of ozone precursors.

d. Peak ozone predictions are a function of the absolute amount of NMHC and NO_x emissions and not merely of the NMHC/NO_x ratio. Equal reductions in both NMHC and NO_x emissions result in lowered peak ozone.

e. Differences in the reactivity of hydrocarbon emissions which are representative of emission inventories in different cities, produce modest differences in peak ozone predictions. It follows that the photochemical potential in each city will vary according to the species distribution of its emissions.

f. Despite the small fraction that carbonyls represent in the total hydrocarbon emissions, these oxygenated organics play a very significant role in contributing to peak ozone predictions.

g. Radical shifts in the spatial and temporal distribution of emissions produce significant changes in peak ozone predictions. Spreading out, or diluting, emissions in time and space reduces peak ozone predictions.

h. The importance of nonuniform spatial and temporal emissions patterns are illustrated by the effect which large across-the-board changes in emissions have in shifting the time and location of the peak ozone prediction. These shifts are associated with differences in the trajectory and emissions burden of the air parcel arriving at the time and location of the peak. The burden of emissions in turn reflects variations in the temporal and spatial distribution of emissions.

i. Changes in the height of the mixed layer can result in unexpected and very significant changes in peak ozone predictions. This behavior is associated with a complex interaction among ozone and precursors aloft, elevated emissions sources, and the height of the mixed layer.

j. Changes in peak ozone predictions are nearly directly proportional to changes in photolysis rates (which in turn are nearly directly proportional to total solar radiation).

7.2.2 Recommendations for Further Sensitivity Analyses

In Chapter 5 gaps in our knowledge of Airshed Model sensitivity were identified. The following analyses are recommended to fill these gaps:

a. The sensitivity of Airshed predictions of both peak and area-wide ozone and nitrogen dioxide levels from combined changes in both hydrocarbon oxides of nitrogen emissions should be assessed. Specifically, both increases and decreases in oxides of nitrogen at various levels of hydrocarbon reductions should be examined.

b. The sensitivity of peak ozone predictions to the spatial and temporal resolution of emissions should be evaluated. Emissions grid squares should be enlarged such that adjacent grid squares in the base case are averaged, thereby diluting precursor concentrations in areas of high emissions density. Similarly, the time interval at which emissions are updated (presently hourly) should be lengthened, thereby diluting precursor concentrations associated with peaks in emitting actvities.

c. Initial conditions, boundary conditions along the borders of the modeling region, and boundary values aloft should be scrutinized with respect to their effect on both peak and area-wide ozone predictions. Attention should be given initial conditions for hydrocarbons, oxygenated organics, nitric acid, and organic nitrates, which act as reservoirs of photochemical activity, particularly on stagnation type days when pollutant carryover is significant. The effect of ozone and hydrocarbons being advected into the modeling region along the borders should be examined, particularly on transport type days when advection is most pronounced. The significance of aloft concentrations of ozone, hydrocarbons, and oxygenated organics, which all serve as sources of reactive materials, should be assessed on a day when aloft concentrations are relatively high and a large diurnal rise in the depth of the mixed layer occurs and entrainment is maximized.

d. The sensitivity of the Airshed Model to changes in the wind field needs to be explored. The response of the model to both changes in the richness of the basic data (radiosonde, pibal, surface wind speed, direction, and temperature sensors) and to the method (interpolation and divergence reduction or diagnostic wind modeling) by which the wind field is generated from the basic data should be analyzed.

e. The effect of different choices of grid cell structure on model predictions should be systematically investigated. Changes in the horizontal dimensions of grid cells on both transport and stagnation type days and in the vertical dimension on days of prominent wind shear should be examined.

f. The role of biogenic emissions in modifying the effect of changes in angthropogenic emissions of both hydrocarbons and oxides of nitrogen needs to be elucidated with regard to its effect on peak and area-wide ozone concentrations. Specifically, combined hydrocarbon and oxides of emissions changes should be made at various estimated levels of biogenic organic compounds.

7.3 Conclusions with Regard to Control Requirements

In order to estimate control requirements, a series of simulations were conducted in which NMHC emissions were reduced uniformly for all sources. Specific control strategies (i.e., RACT for stationary sources and FMVPC and I & M for mobile sources) were also tested separately and in combination. In all cases, the authors determined the reduction in peak model ozone regardless of location associated with each simulation. This method is preferable to tracking the peaks at specific monitoring sites because it utilizes the entire modeling domain and offers greater assurance that the predicted control requirements will benefit the entire region and not merely shift the problem downwind. To account for model bias in the control strategy simulations, the model was used in a relative sense; it was assumed that the relative error (percent bias) remains constant as emissions are "turned down." In this method, no explicit calibration is required for the base case and control case scenarios.

Specific findings are as follows:

a. Reductions in hydrocarbon emissions were found to result in substantial (but less than 1:1) reductions in model predictions of peak ozone concentration. The sensitivity of the model to reduction in hydrocarbon emissions varies from day to day. We found, for example, that the day with the highest observed ozone concentration was not the day with the greatest control requirements. This day-to-day variation in sensitivity probably reflects reality. Each day has unique source-receptor relationships, photochemical potential and boundary conditions. Thus, it is essential to apply the model for a number of days with varying conditions.

b. The sensitivity and control strategy analyses suggest that the most effective strategies are those which rely on substantial across-the-board reductions in NMHC emissions. The model shows a synergistic effect between stationary and mobile source emissions reductions such that the combined effect of RACT and FMVPC is greater than the sum of the separate reductions. The sensitivity analyses do indicate that modest reductions in peak ozone may be accomplished through significant changes in species distribution (reactivity of NMHC) or through the spreading out of emissions; however, the most effective strategy appears to be associated with substantial reductions in total NMHC emissions, a finding which supports current EPA policy.

c. Reductions in boundary concentrations representing parallel control efforts in upwind cities were found to have a substantial effect on peak ozone concentration for transport days, but a negligible effect on stagnation days in St. Louis.

d. Simulations in this study suggest that reduction of NO_x emissions may increase HC control requirements; however, only a small number of tests for 3 days at one level of HC reduction (HC/NO_x ratio) were conducted. Secondly, as discussed previously, the model's handling of NO_x emissions from point sources is inadequate. A complicating factor is that reductions in NO_x emissions may result in several benefits: reduced urban NO_2, reduced levels of nitrate and a potential reduction in ozone concentrations in regions downwind of the area modeled.

e. The emissions and air quality data used are based on 1975-1976 information. Thus, the current analysis cannot be used to formulate a specific control program. Nevertheless, the simulations suggest that both the Federal Motor Vehicle Pollution Control and RACT for stationary HC sources are minimally required for attainment of the ozone NAAQS for sizeable urban areas.

7.4 Errors and Uncertainties

In this section, we review findings related to model error and uncertainty. Chapter 4 clearly demonstrates that the Airshed Model has a systematic tendency to underestimate ozone concentrations, particularly at higher concentrations, for St. Louis. The reasons for this tendency have not been established to date. Nevertheless, the evidence presented in this report points to several possibilities. Two lines of evidence suggest that the carbonyl fraction used for the St. Louis NMHC emissions and background concentrations were erroneously low: (1) the sensitivity analyses indicate that the magnitude of the carbonyl fraction is an important determinant of peak ozone and (2) the value used for St. Louis is substantially lower than the size of the faction measured in a number of urban areas. Whereas SAI now recommends that a value of 5-10 percent carbonyl fraction be used, the fraction used in this study is about 1.5 percent. The sensitivity tests suggest that an increase in carbonyl fraction from this level to about 5 percent (the lower end of the recommended range) can increase peak ozone concentration by 10 percent or more. This amount is comparable to the 11 percent average bias for spatially paired residuals calculated for the 20-day test period.

Several other factors may also contribute toward underprediction of ozone. These include the current model's inappropriate mixing of point source NO_x into entire grid cells, the neglect of vegetative emissions, and errors in advective transfer associated with windfield errors on transport days.

In this study, no attempt has been made to assess the uncertainty associated with the estimates of control requirements. Airshed Modeling is a complex process based on a large number of assumptions and input variables. Uncertainties associated with these parameters and assumptions contribute to the overall uncertainty. While many important variables have not been tested systematically, the sensitivity tests, at least in a preliminary way, point to those variables which have a very strong impact on peak ozone. Among the variables found to be critical are: the distribution of hydrocarbon species (reactivity) and particularly carbonyl fraction, $NMHC/NO_x$ ratio, the photolysis rate, and mixing height. Furthermore, testing with OZIPP/EKMA indicates that predictions are extremely sensitiive to concentrations of precursors transported into the modeling region.[53] Errors in these parameters may lead not only to errors in predicting observed concentrations, but also to errors in the HC/O_3 response curves used to estimate control requirements. Additional factors which may contribute to problems in the HC/O_3 response curves are the designation of future year boundary (background) concentrations and deficiencies in the model treatment of chemistry, point-source diffusion, and vertical mixing. A number of specific tests are suggested in Section 7.2.2.

7.5 Feasibility of the Airshed Approach

The St. Louis ozone modeling project and other studies utilizing photochemical grid models have demonstrated that such programs require large and costly data bases, lengthy lead times and considerable resources and expertise. A typical modeling study for an urban region can take 3 years or more and require resources equivalent to $1-2 million (including data-base collection and preparation).[5] Modeling requires the availability of an air pollution engineer, a systems analyst or advanced programmer, an air pollution meteorologist and an atmospheric chemist. A large computer facility and from 30-70 hours of computer time are also required. In addition, potential users can anticipate that initial modeling may identify anomalous model output, a result which will necessitate a detailed examination of the model set-up and inputs. Several modeling iterations may be required to sort out the problems and delays may be anticipated.

There is no doubt that the three-dimensional grid model approach encompassed in the Airshed Model is superior to simple approaches (e.g., OZIPP/EKMA) in its spatial, temporal and species resolution and in its treatment of physical and chemical processes. However, many uncertainties remain and comparative evaluations of Airshed and the simpler approaches being carried out by EPA have not been completed. Thus, we are not at present able to answer the question posed in the Introduction of this report, do the technical advantages and model performance of Airshed outweigh difficulties inherent in the use of photochemical grid models.

The authors strongly recommend that States considering the use of photochemical grid models thoroughly assess the requirements prior to initiating an Airshed application. Secondly, sophisticated grid models are most appropriate for large metropolitan areas with the most serious ozone problems. These areas are more likely to have the resources, expertise and motivation to complete an Airshed application. Finally, the authors recommend that the Airshed Model be viewed as a long-term air management tool rather than as a "one shot" approach toward ozone control. Given the large expense and lengthy time required to complete the base-case modeling, it makes sense to revise emission projections at several year intervals in order to gauge progress and reassess control requirements on a continuing basis. Moreover, the tool can be used to evaluate the impact of changes in regulations or policy on future air quality.

8.0 REFERENCES

1. Reynolds, S. D., "The Systems Applications, Inc., Urban Airshed Model: An Overview of Recent Developmental Work," EPA-600/3-77-001b, U.S. Environmental Protection Agency, Research Triangle Park, North Carolina, 27711, 1977.

2. MacCracken, M. D., J. D. Wuebbles, J. J. Walter, W. H. Duewer, and K. E. Grant, "The Livermore Regional Air Quality Model," J. App. Met., Vol. 17, pp. 254-272, 1978.

3. Schere, K. L., and J. H. Shreffler, "Final Evaluation of Urban-Scale Photochemical Air Quality Simulation Models," (Draft), Environmental Sciences Research Laboratory, U.S. Environmental Protection Agency, Research Triangle Park, North Carolina 27711, 1982.

4. Fox, D., "Judging Air Quality Model Performance," (A Summary of the AMS Workshop on Dispersion Model Performance, Woods Hole, Mass., Sept. 1980). Bulletin of the Amer. Met. Soc., Vol. 62 No. 5, pp. 599-609, 1981.

5. Layland, D., "Guideline for Applying the Airshed Model to Urban Areas," Publication No. EPA-450/4-80-020, U.S. Environmental Protection Agency, Research Triangle Park, North Carolina 27711, October 1980.

6. Briggs, G. A., "Plume Rise: A Recent Critical Review," Nuclear Safety, Vol. 12, pp. 15-24, 1971.

7. Killus, J. P., et al., "Continued Research in Mesoscale Air Pollution Simulation Modeling--Vol. V: Refinements in Numerical Analysis, Transport, Chemistry, and Pollutant Removal," draft report for Environmental Sciences Research Laboratory, Office of Research and Development, U.S. Environmental Protection Agency, Contract No. 68-02-2216, Systems Applications, Incorporated, San Rafael, California, 1977.

8. Littman, F., "Regional Air Pollution Study: Emission Inventory Summarization," Publication No. EPA 600/4-79-004, U.S. Environmental Protection Agency, Research Triangle Park, North Carolina 27711, 1979.

9. Strothmann, J. A., and F. A. Schiermeier., "Documentation of the Regional Air Pollution Study (RAPS) and Related Investigations in the St. Louis Air Control Region," Publication No. EPA 6004-79-076, U.S. Environmental Protection Agency, Research Triangle Park, North Carolina 27711, 1979.

10. Shreffler, J. H. and R. B. Evans., "The Surface Ozone Record from the Regional Air Pollution Study, 1975-1976." Atm. Environment, Vol. 16, p. 6, 1982.

11. Karl, T. R., "Ozone Transport in the St. Louis Area," Atmospheric Environment 12, 1421-1431, 1978.

12. Karl, T. R., "Day of the Week Variations of Photochemical Pollutants in the St. Louis Area, Atmospheric Environment, Vol. 12, pp. 165-1667, 1978.

13. Karl, T. R., "A Study of the Spatial Variability of Ozone and Other Pollutants at St. Louis, Missouri," Atmospheric Environment, Vol. 14, pp. 681-694, 1980.

14. Schiermeier, F. A., "RAPS Field Measurements Are In," Envir. Sci. Technol. Vol. 12, pp. 644-651 1978.

15. Anderson, G., "Objective Windfield Analysis for Airshed Model in Killus, J. P., et al., "Continued Research in Mesoscale Air Pollution Simulation Modeling--Vol. V: Refinements in Numerical Analysis, Transport, Chemistry, and Pollutant Removal," draft report for Environmental Sciences Research Laboratory, Office of Research and Development, U.S. Environmental Protection Agency, Contract No. 68-02-2216, Systems Applications, Incorporated, San Rafael, California, 1977.

16. Schere, K. L., "Air Quality Model Response to Objectively Analyzed Wind Fields," Fifth Symposium on Turbulence Diffusion, and Air Pollution of the American Meteorological Society, Atlanta, Georgia, March 1981.

17. Shir, C. C. and L. J. Shieh, "Development of the Urban Air Quality Simulation Model with Compatible RAPS Data," EPA-600/4-75-005-a,b, U.S. Environmental Protection Agency, Research Triangle Park, North Carolina 27711, 1975.

18. Cox, W. M., letter to Mr. Richard Londergan, TRC Environmental Consultants, October 20, 1981.

19. Cole, H. S., Newberry, C. F., Cox, W., Moss, G. K., and D. Layland, "Application of the Airshed Model for Ozone Control in St. Louis." U.S. Environmental Protection Agency, Research Triangle Park, North Carolina 27711. Presentated at 75th Annual Meeting of Air Pollution Control Assoc., New Orleans, Louisiana, June 1982.

20. Rehme, K. A., J. C. Puzak, M. E. Beard, F. Smith, and R. J. Paur, "Evaluation of Ozone Calibration Procedures," Publication No. EPA 600-54-80-050, U.S. Environmental Protection Agency, Research Triangle Park, North Carolina 27711, 1981.

21. Fried, A., and J. Hodgeson. Laser Photoacoustic Detection of Nitrogen Dioxide in the Gas-phase Titration of Nitric Oxide with Ozone," Anal. Chem., Vol. 54: p. 278, 1982.

22. Zimmerman, P. R., "Testing of Hydrocarbon Emissions from Vegetation, Leaf, Litter, and Aquatic Surfaces, and Development of a Methodology for Compiling Biogenic Emission Inventories," EPA-450/4-79-004, U.S. Environmental Protection Agency, Research Triangle Park, North Carolina 27711, 1979.

23. Flyckt, D. L., H. H. Westbery, and M. W. Holdren, "Natural Oranic Emissions and Their Impact on Air Quality,": Paper No. 80-69.2, 73rd Annual Meeting of the Air Pollution Control Association, Montreal, Quebec, June 1980.

24. Kamens, R. M., H. E. Jeffries, M. W. Gery, R. W. Weiner, K. G. Sexton, G. B. Howe, "The Impact of α-Pinene on Urban Smog Formation: An Outdoor Smog Chamber Study," Atmos. Environ., Vol. 15, p. 969, 1981.

25. Systems Applications, Inc. "The Sensitivity of Complex Photochemical Model Estimates to Detail in Input Information," EPA-450/4-81-031a, U.S. Environmental Protection Agency, Research Triangle Park, North Carolina 27711, 1981.

26. Dennis, R. L., M. W. Downton and R. S. Press, "Evaluation of Performmance Measures for an Urban Photochemical Model," Draft, June 1982.

27. J. P. Killus, G. Z. Whitten, "A New Carbon-Bond Mechanism for Air Quality Simulation Modeling," EPA-600/3-82-041, U.S. Environmental Protection Agency, Research Triangle Park, North Carolina 27711, 1982.

28. G. Z. Whitten, H. Hogo, M. J. Meldgin, J. P. Killus, P. J. Bekowies, "Modeling of Simulated Photochemical Smog with Kinetic Mechanisms, Volume 1. Interim Report, EPA-600/3-79-001a, U.S. Environmental Protection Agency, Research Triangle Park, North Carolina 27711, 1979.

29. G. Z. Whitten, J. P. Killus, H. Hogo, "Modeling of Simulated Photochemical Smog with Kinetic Mechanisms, Volume 1. Final Report," EPA-600/3-80-028a, U.S. Environmental Protection Agency, Research Research Triangle Park, North Carolina 27711 1980.

30. S. T. Zalesak. "Fully Multi-dimensional Flux-Corrected Transport Algorithms for Fluids," J. Comput. Phys., Vol.31, p. 335, 1979.

31. C. F. Newberry, H. S. Cole, G. K. Moss, "The St. Louis Oxidant Modeling Project: Additional Sensitivity Testing," draft report, Office of Air Quality Planning and Standards, Research Triangle Park, North Carolina 27711, May 1981.

32. H. S. Cole, J. Summerhays, K. MacKay, C. Newberry, "St. Louis Oxidant Modeling Project: Progress Report," Draft Report, U.S. Environmental Protection Agency, Research Triangle Park, North Carolina 27711, September 1980.

33. R. M. Kamens, H. E. Jeffries, M. W. Gery, R. W. Weiner, K. G. Sexton, G. B. Howe, "The Impact of α-Pinene on Urban Smog Formation: An Outdoor Smog Chamber Study," Atmos. Environ., Vol.No. 6, p. 969, 1981.

34. R. R. Arnts, B. W. Gay, Jr., "Photochemistry of Some Naturally Emitted Hydrocarbons, " EPA-600/3-79-081, U. S. Environmental Protection Agency, Research Triangle Park, North Carolina 27711, 1979.

35. Gipson, G., "Comparison of Three Ozone Models: Urban Airshed, City-Specific EKMA, and Proportional Rollback." Office of Air Quality Planning and Standards, U. S. Environmental Protection Agency, Research Triangle Park, North Carolina 27711, 1982.

36. Code of Federal Regulations (CRF) 40, Protection of Environment, Part 51, Revised as of July 1, 1981, pp. 584-585.

37. Peterson, P. R. and R. R. Sakaida, "Summary of Group I Control Technique Guideline Documents for Control of Volatile Organic Emissions from Existing Stationary Sources," EPA-450/3-78-120, U.S. Environmental Protection Agency, Research Triangle Park, North Carolina 27711, June 1979.

38. Braverman, T., "Estimated RACT Emissions Reductions for Point-Source Evaporative HC Emissions in St. Louis," Office of Air Quality Planning and Standards, U. S. Environmental Protection Agency, Research Triangle Park, North Carolina 27711, June 1979.

39. Braverman, T., "Estimated RACT Emissions Reductions for Point-Source HC Emissions in St. Louis from Petroleum Refining, Primary Metals Production, Chemical Manufacturing, and Recently Added Point-Sources," Office of Air Quality Planning and Standards, U. S. Environmental Protection Agency, Research Triangle Park, North Carolina 27711, September 1979.

40. Braverman, T., "Estimated RACT Emissions Reductions for Area-Source Evaporative HC Emissions in St. Louis from Nonindustrial Surface Coating, Gasoline Marketing at Service Stations, and Dry Cleaning Operations," Office of Air Quality Planning and Standards, U.S. Environmental Protection Agency, Research Triangle Park, North Carolina 27711, 1979.

41. Braverman, T., "Revision of RACT Control for RAPS," Memorandum to David H. Barrett, Model Application Section, Office of Air Quality Planning and Standards, U. S. Environmental Protection Agency, Research Triangle Park, North Carolina 27711, October 18, 1979.

42. Code of Federal Regulations (CFR) 40, Protection of Environment, Part 85, Revised as of July 1, 1981, pp. 186-242.

43. Code of Federal Regulations (CRF) 40, Protection of Environment, Part 86, Revised as of July 1, 1981, pp. 242-870.

44. Mayer, N., "Approximate Effects of Mobile Vehicle Emissions Reduction Strategies on Emission Factors," Memorandum to David H. Barrett, Model Application Section, Office of Air Quality Planning and Standards, U.S. Environmental Protection Agency, Research Triangle Park, North Carolina 27711, March 1979.

45. Mayer, N., "Approximate Effects of Motor Vehicle Emission Reduction Schemes on Hydrocarbon and Nitrogen Oxide Emissions in RAPS," Memorandum to David H. Barrett, Model Application Section, Office of Air Quality Planning and Standards, U.S. Environmental Protection Agency, Research Triangle Park, North Carolina 27711, March 1979.

46. "Mobile Source Emission Factors (for low-altitude areas only)," Publication No. EPA-400/9-78-006, Office of Transportation and Land Use Policy, U.S. Environmental Protection Agency, Washington, D.C. 20460 March 1978.

47. Novak, J., Personal commnication. Data Management and Systems Analysis Section, Meteorology and Assessment Division, Environmental Science Research Laboratory, Office of Research and Development, U.S. Environmental Protection Agency, Research Triangle Park, North Carolina 27711, September 1980.

48. "Volatile Organic Compound (VOC) Species Data Manual," Second Edition, Publication No. EPA-450/4-80-015, U. S. Environmental Protection Agency, Research Triangle Park, North Carolina 27711, July 1980.

49. Black, Frank and Larry High, "Procedures to Determine Nonmethane Hydrocarbon Emission Rates from Automobiles," Paper No. 770144, Annual Meeting of the Society of Automotive Engineers, Detroit, Michigan, February 28-March 4, 1977.

50. Black, Frank and Larry High, "Passenger Car Hydrocarbon Emissions Speciation," Publication No. EPA-600/2-80-085, U.S. Environmental Protection Agency, Research Triangle Park, North Carolina 27711, May 1980.

51. Johnson, W. L., "Hydrocarbon Composition, Sulfur, and Manganese Content of U.S. Motor Fuels Sampled for the DuPont 1978 Summer Road Octane Survey," Publication No. PLR--78-68, E.I.duPont de Nemours & Company, Wilmington, Delaware 19898, November 1978.

52. P. G. Hoel, Introduction to Mathematical Statistics, 3rd edition, John Wiley & Sons, Inc., New York, 1962, p. 167.

53. Gipson, Gerald L., "Evaluation of the Carbon-Bond Mechanism for EKMA," Internal Draft Reports, Air Management Technlogy Branch, Office of Air Quality Planning and Standards, U.S. Environmental Protection Agency, Research Triangle Park, North Carolina 27711. Part 1: June 1982; Part 2: July 1982; Part 3: September 1982.

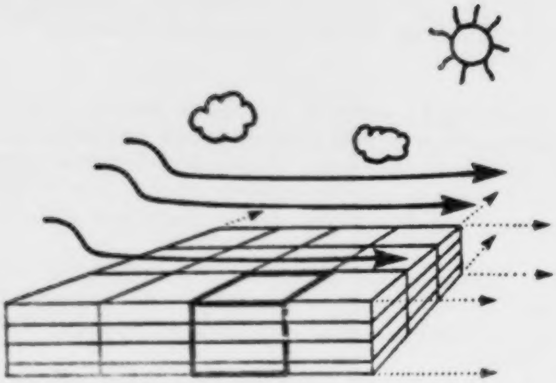

(a) SPECIFICATION OF THE GRID

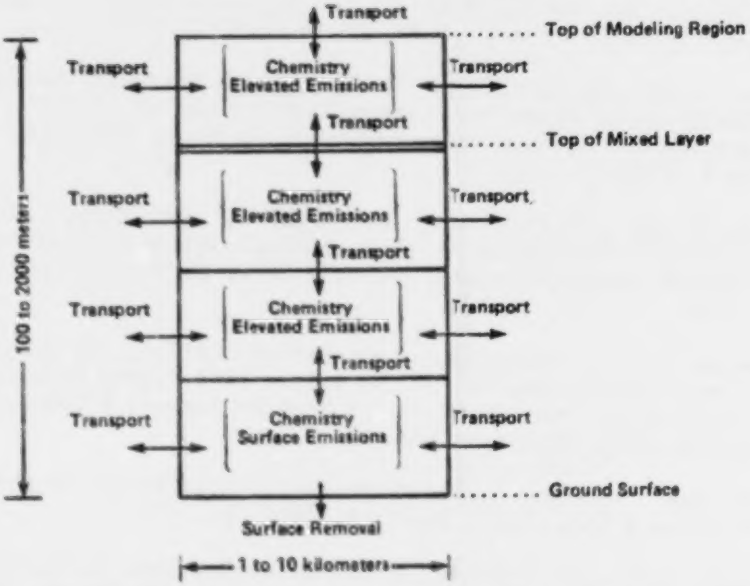

(b) ATMOSPHERIC PROCESSES TREATED IN A COLUMN OF GRID CELLS.

Figure 1. Schematic illustration of the grid used and atmospheric processes treated in the airshed model (adapted from Reynolds, Tesche, and Reid, 1978).

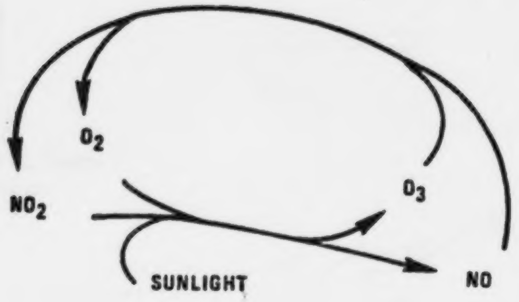

(a) THE NO_2-NO-O_3 CYCLE

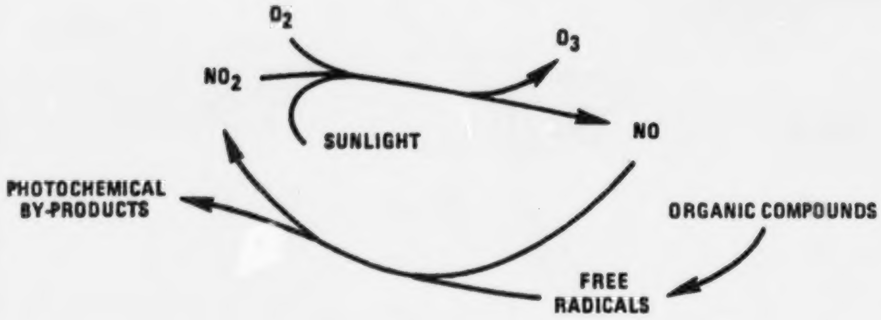

(b) ORGANIC OXIDATION OF NO TO NO_2 WITH OZONE BUILDUP

Figure 2. Photochemical production of oxidants.

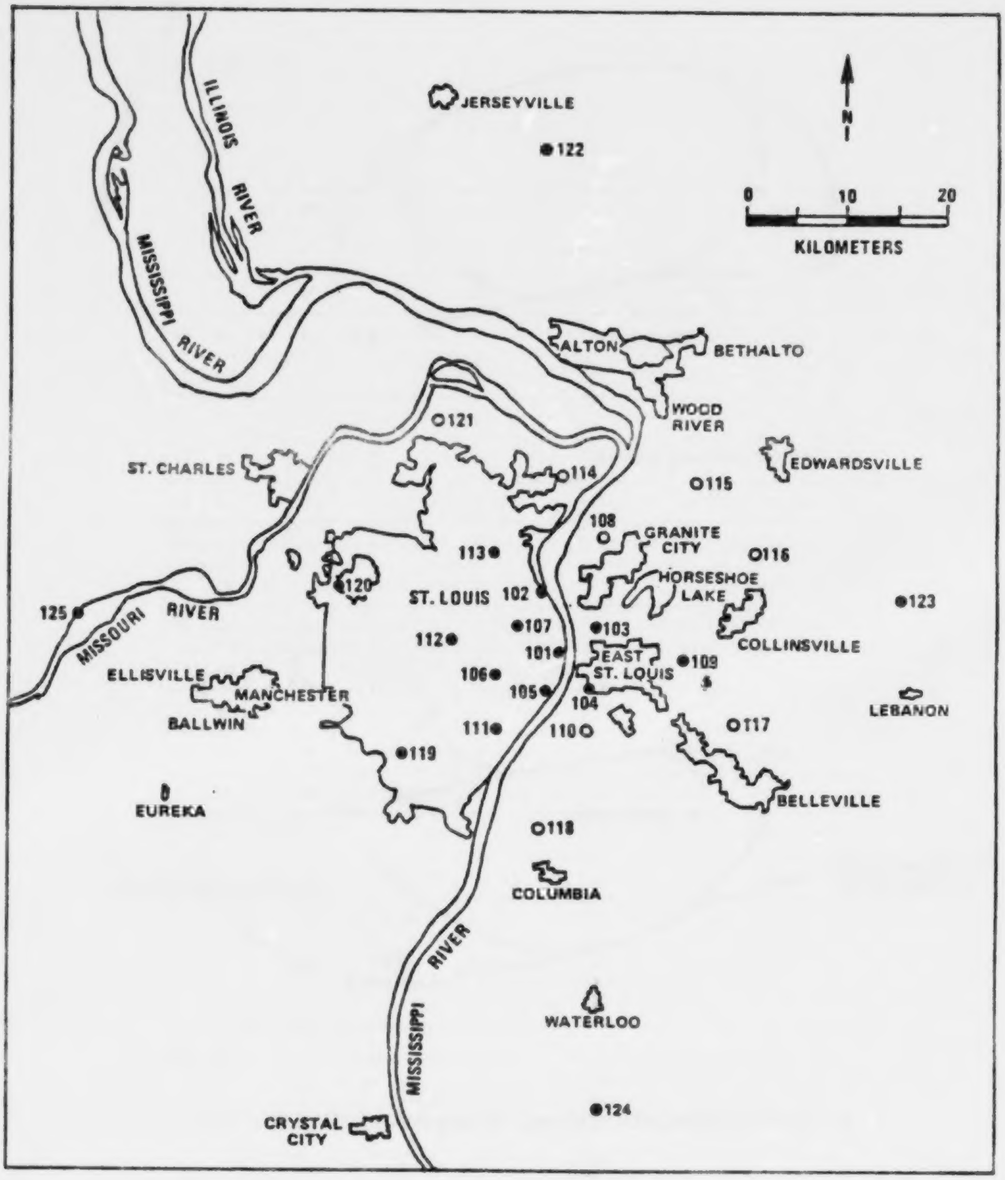

Figure 3. The St. Louis area with locations of the RAPS surface stations.

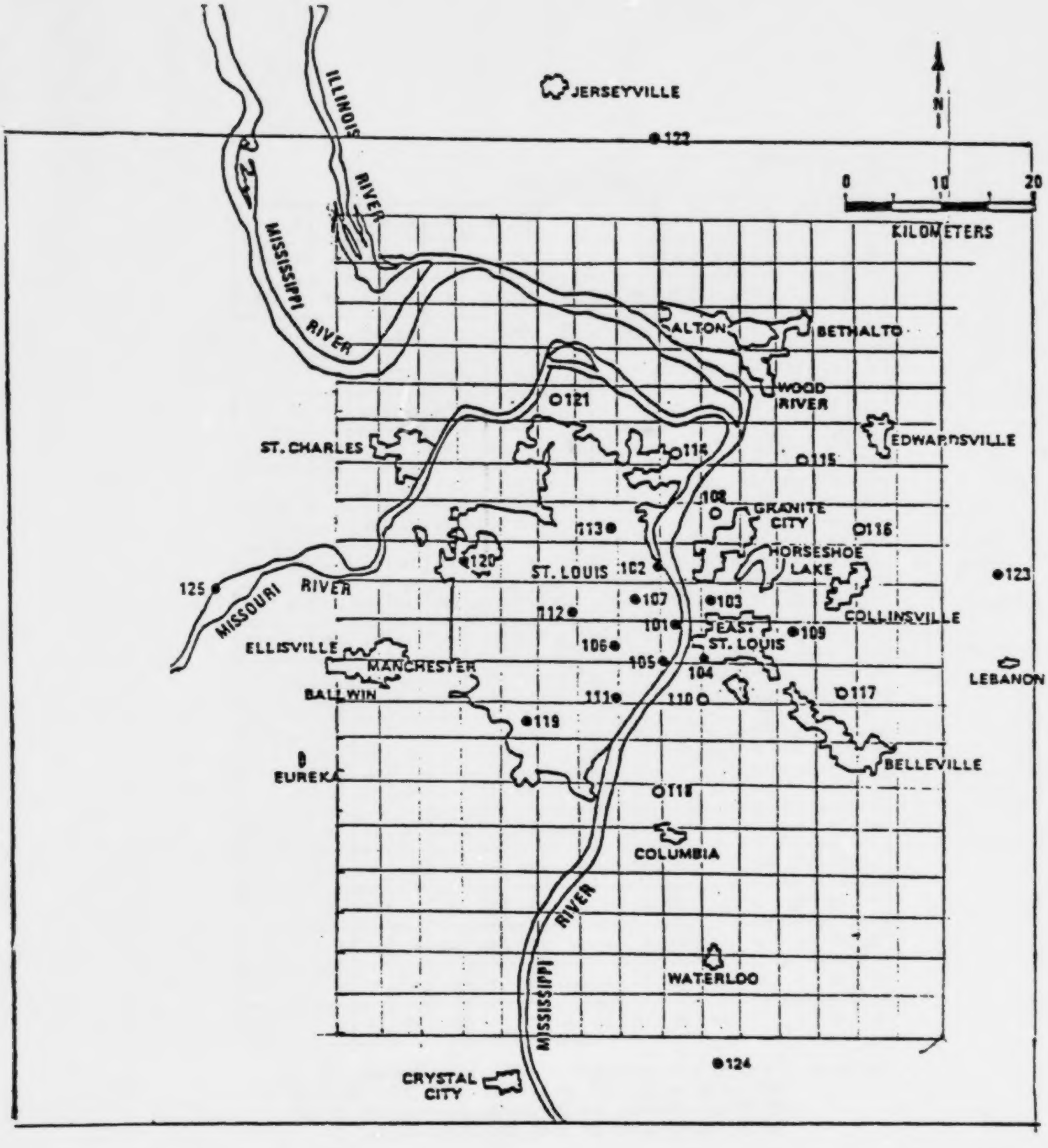

Figure 4. The St. Louis area with locations of the RAPS surface stations and 4 x 4 km modeling grid superimposed.

DAY:195-1976
HR:8

THC EMISSIONS

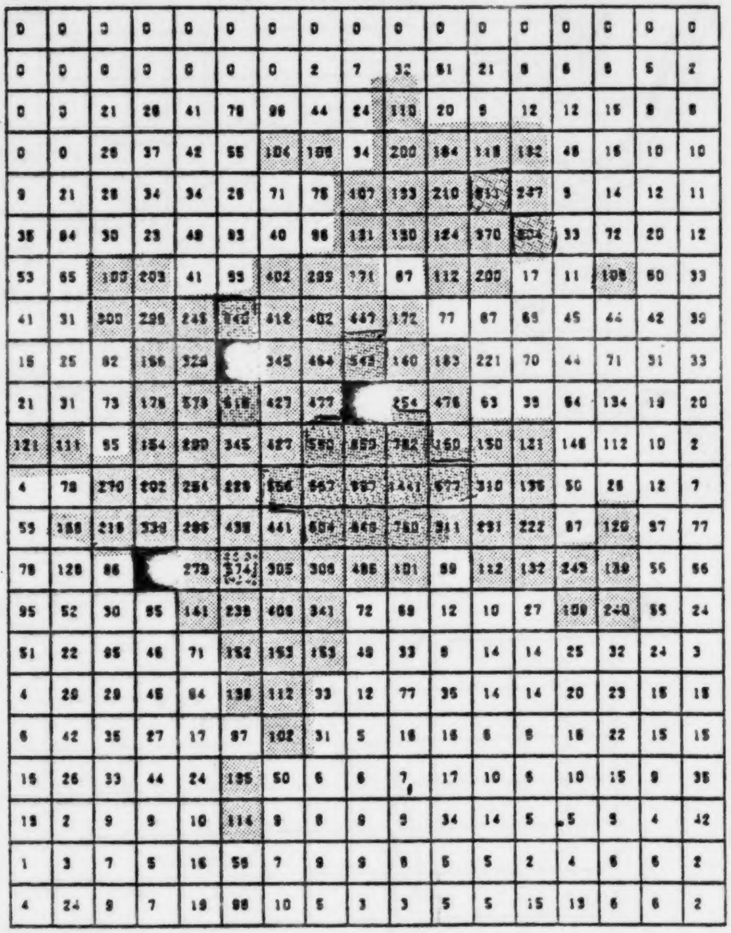

0	0	0	0	0	0	0	0	0	0	0	0	0	0	0	0	0
0	0	0	0	0	0	0	2	7	32	81	21	8	6	8	5	2
0	0	21	28	41	78	96	44	24	110	20	5	12	12	15	8	8
0	0	28	37	42	55	104	188	34	200	184	118	132	48	15	10	10
9	21	28	34	34	28	71	78	107	133	210	813	247	9	14	12	11
38	84	30	23	48	83	40	96	131	130	124	370	604	33	72	20	12
53	65	107	203	41	93	402	299	171	87	112	200	17	11	108	50	33
41	31	300	296	245	840	418	402	447	172	77	87	65	45	44	42	39
15	25	82	156	329	[illegible]	345	464	543	160	183	221	70	44	71	31	33
21	31	73	178	573	618	427	477	[illegible]	254	478	63	39	64	134	19	20
121	111	95	154	299	345	427	590	859	782	160	150	121	146	112	10	2
4	78	270	202	254	228	556	567	987	1441	677	310	136	50	28	12	7
59	188	219	338	296	438	441	604	468	760	311	231	222	87	120	97	77
78	128	86	[illegible]	278	374	305	308	486	101	89	112	132	243	139	56	56
95	52	30	95	141	238	408	341	72	69	12	10	27	109	240	55	24
51	22	95	46	71	152	153	153	49	33	8	14	14	25	32	24	3
4	29	29	45	84	138	112	33	12	77	35	14	14	20	23	18	18
6	42	35	27	17	87	102	31	5	18	16	6	5	18	22	15	15
15	26	33	44	24	195	50	6	6	7	17	10	5	10	15	9	35
19	2	9	9	10	114	9	8	8	9	34	14	5	5	9	4	42
1	3	7	5	16	59	7	9	9	8	5	5	2	4	6	6	2
4	24	9	7	19	98	10	5	3	3	5	5	15	13	6	6	2

Figure 5. Total source emissions of THC, in kilograms, for the RAPS area on Day 195 of 1976 at 0800 CST. Grid cells are 4 km squares; the SW corner corresponds to UTM (x, y) coordinates of Zone 15: (706, 4236).

☐ <100 ☐ 100–500 ▨ 500–1000 ■ >1000

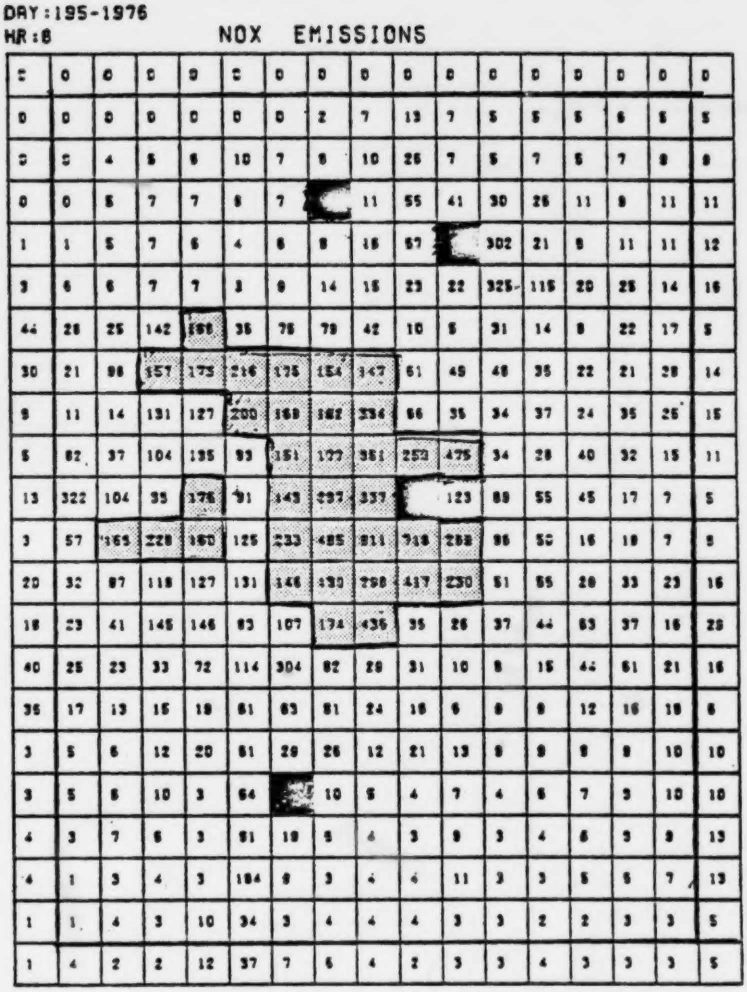

DAY:195-1976
HR:8
NOX EMISSIONS

0	0	0	0	0	0	0	0	0	0	0	0	0	0	0	0	0
0	0	0	0	0	0	0	2	7	13	7	5	5	5	6	5	5
0	0	4	5	6	10	7	8	10	26	7	5	7	5	7	8	9
0	0	5	7	7	8	7	■	11	55	41	30	26	11	9	11	11
1	1	5	7	6	4	6	9	16	57	■	302	21	9	11	11	12
3	6	6	7	7	3	9	14	15	23	22	325	115	20	25	14	16
44	28	25	142	188	35	75	79	42	10	5	31	14	8	22	17	5
30	21	98	157	173	216	175	154	147	61	49	48	35	22	21	28	14
9	11	14	131	127	200	169	182	334	66	35	34	37	24	35	25	15
5	82	37	104	135	93	151	177	351	253	475	34	28	40	32	15	11
13	322	104	35	176	91	143	297	337	■	123	89	55	45	17	7	5
3	57	165	228	160	125	233	485	811	718	268	96	50	16	18	7	9
20	32	87	118	127	131	146	430	798	417	230	51	65	28	33	23	16
18	23	41	145	146	83	107	174	436	35	26	37	44	63	37	16	25
40	25	23	33	72	114	304	82	28	31	10	8	15	44	61	21	16
35	17	13	15	18	61	63	81	24	16	6	8	9	12	16	18	6
3	5	6	12	20	61	29	26	12	21	13	8	9	8	8	10	10
3	5	8	10	3	64	■	10	5	4	7	4	6	7	3	10	10
4	3	7	6	3	91	19	5	4	3	9	3	4	6	3	9	13
4	1	3	4	3	184	8	3	4	4	11	3	3	5	5	7	13
1	1	4	3	10	34	3	4	4	4	3	3	2	2	3	3	5
1	4	2	2	12	37	7	6	4	2	3	3	4	3	3	3	5

Figure 6. Total source emissions of NO_x, in kilograms, for the RAPS area on Day 195 of 1976 at 0800 CST. Grid cells are 4 km squares; the SW corner corresponds to UTM (x, y) coordinates of Zone 15: (706, 4236).

☐ ≤150
▨ 150 – 1000
■ >1000

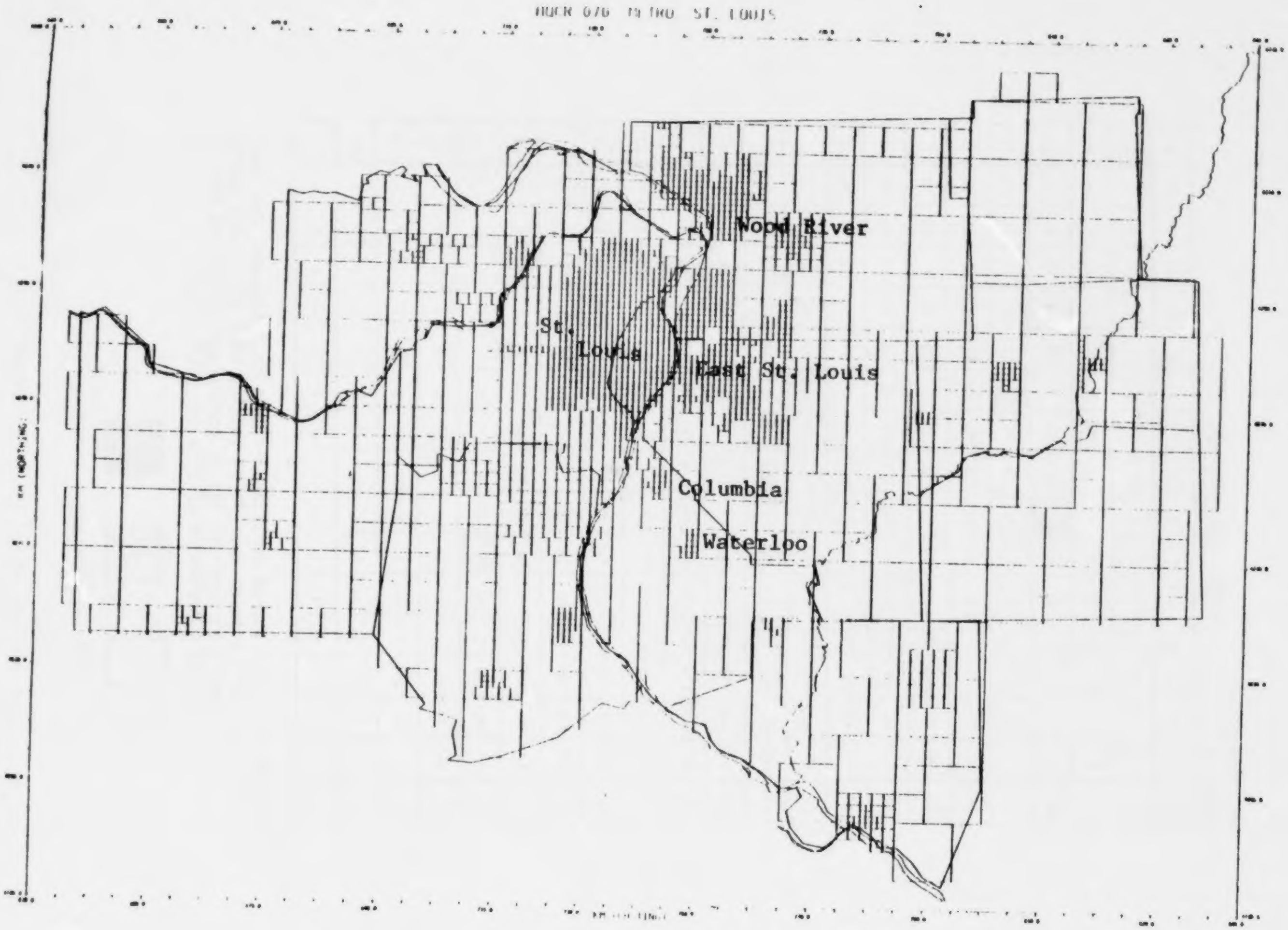

Figure 7. Grid display of the Regional Air Pollution Study Area of St. Louis. Urban and industrial areas are represented by finer grid mesh; rural areas by largest cells; suburban areas have intermediate grid cell sizes.

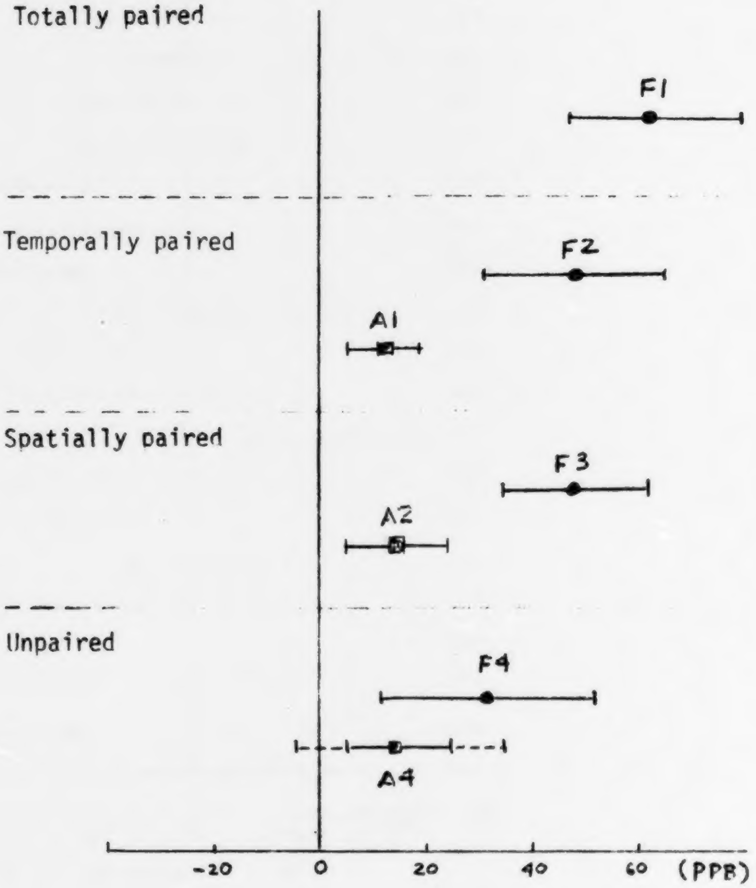

Fig. 8. 20-day average residuals with 95% confidence limits for peak/near-peak measures.

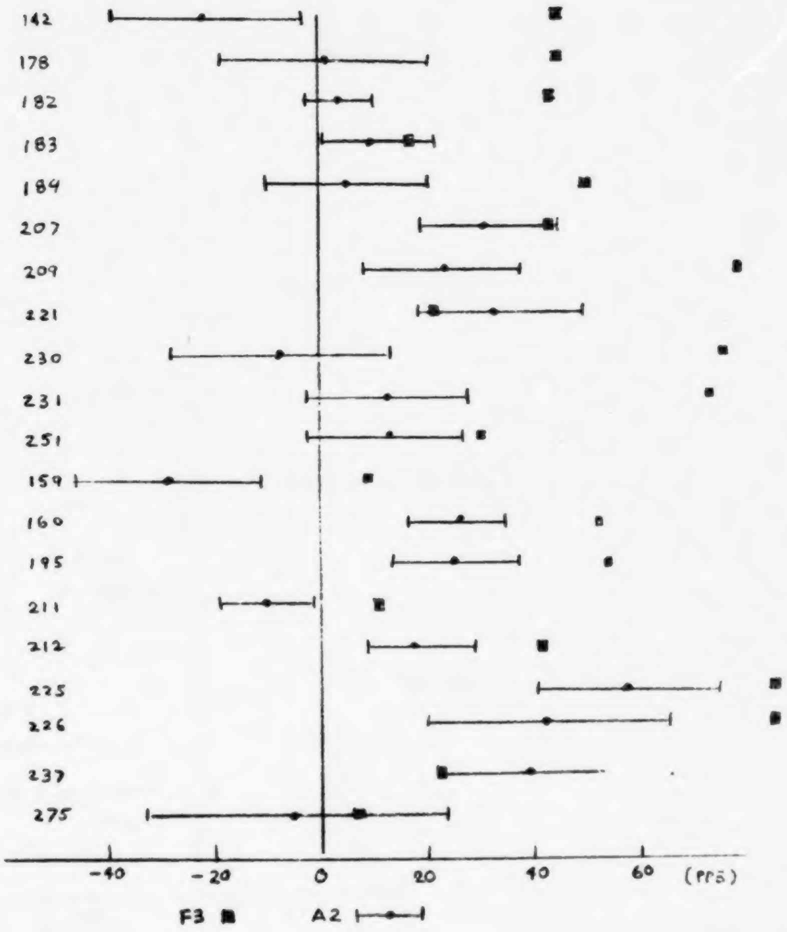

Figure 9. Spatially paired measures for each day.
See text for details.

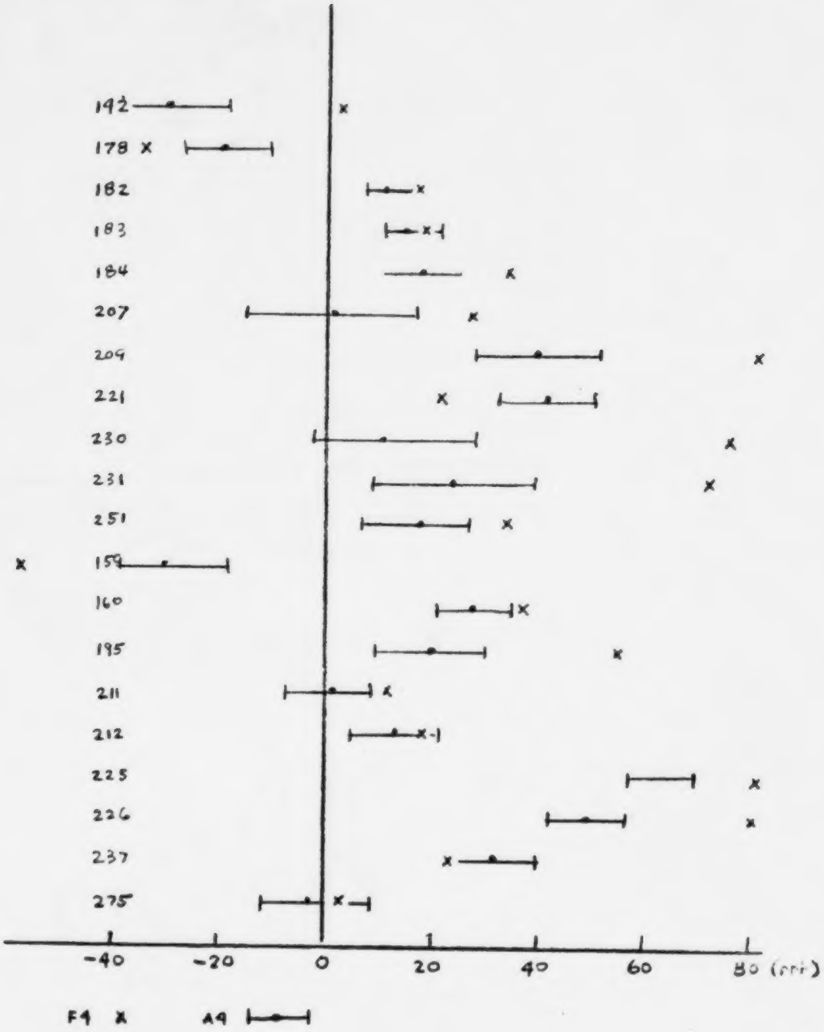

Figure 10. Unpaired measures (F4 and A4) for each day. See text for details.

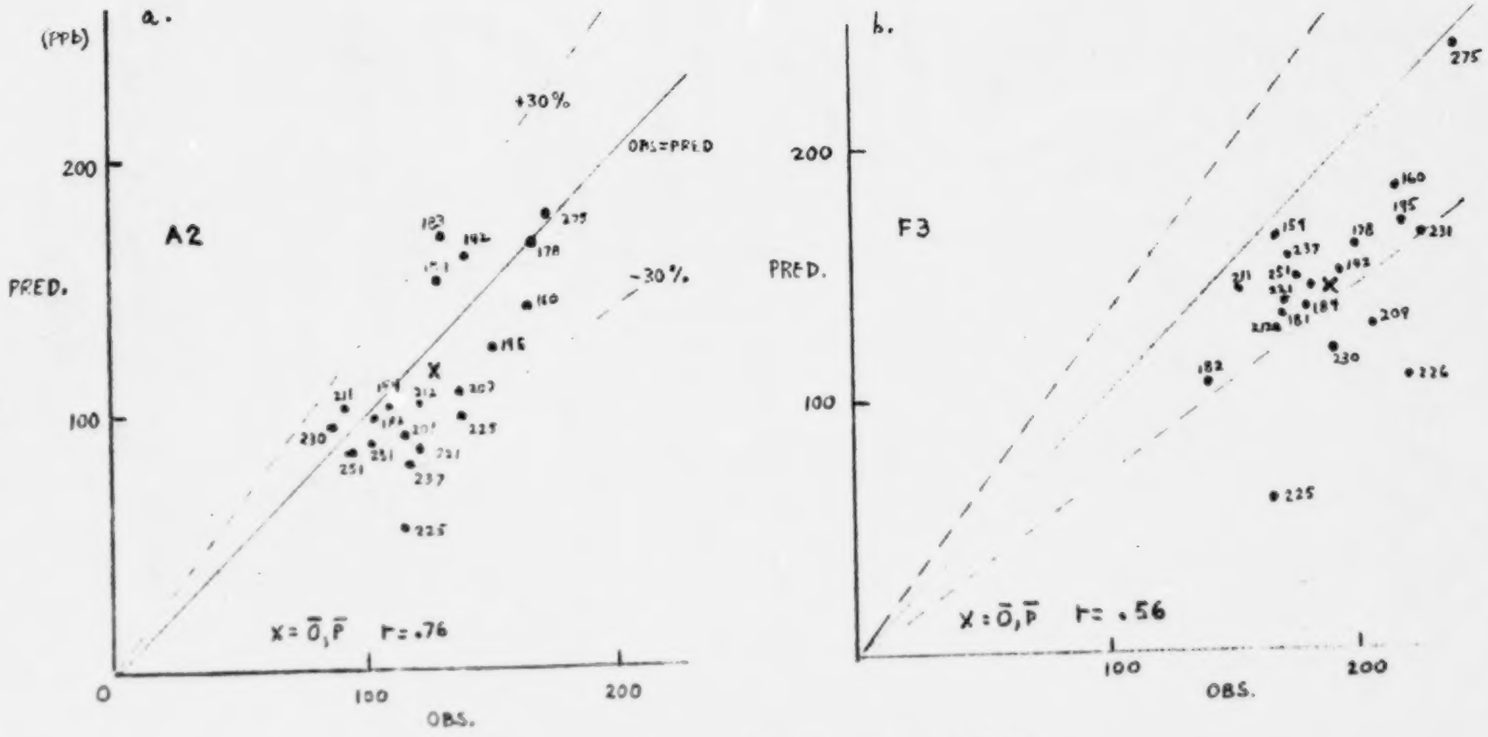

Figure 11a. Scatterdiagrams of predicted vs. observed concentrations.
a. A2 spatially paired measures. b. F3 spatially paired measures.
Julian day numbers given next to each data point.

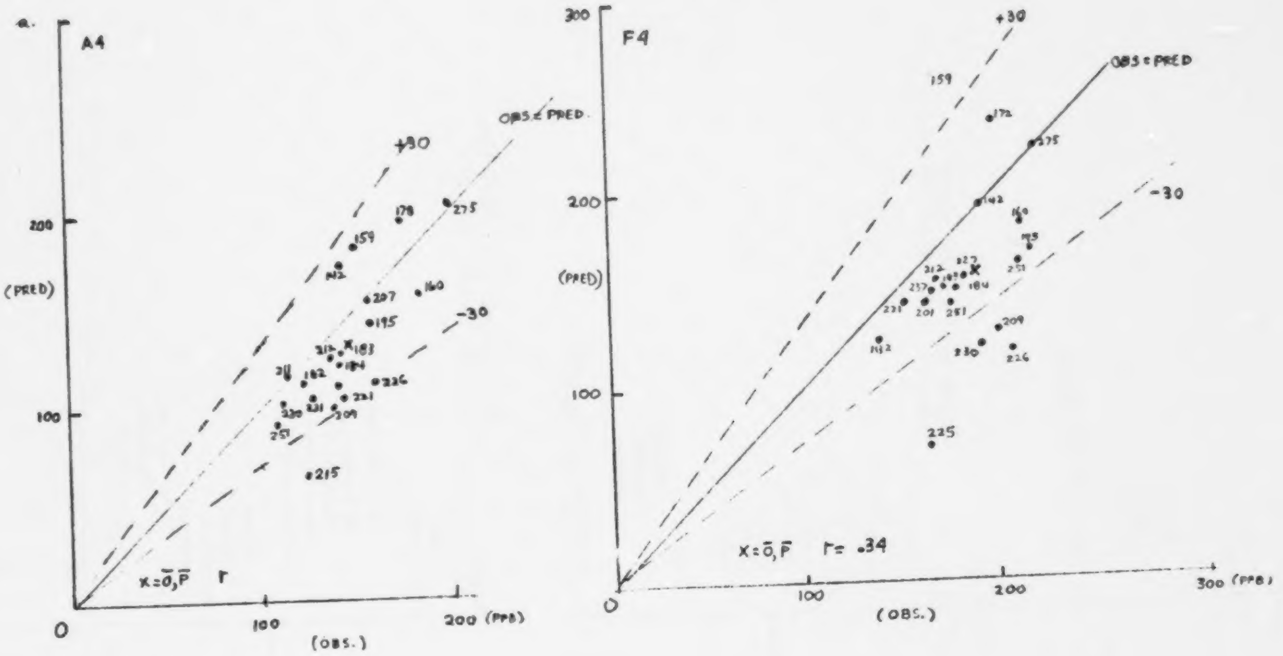

Figure 11b. Scatterdiagrams of predicted vs. observed concentrations for unpaired measures. a. A4 b. F4. Julian day numbers given next to each data point.

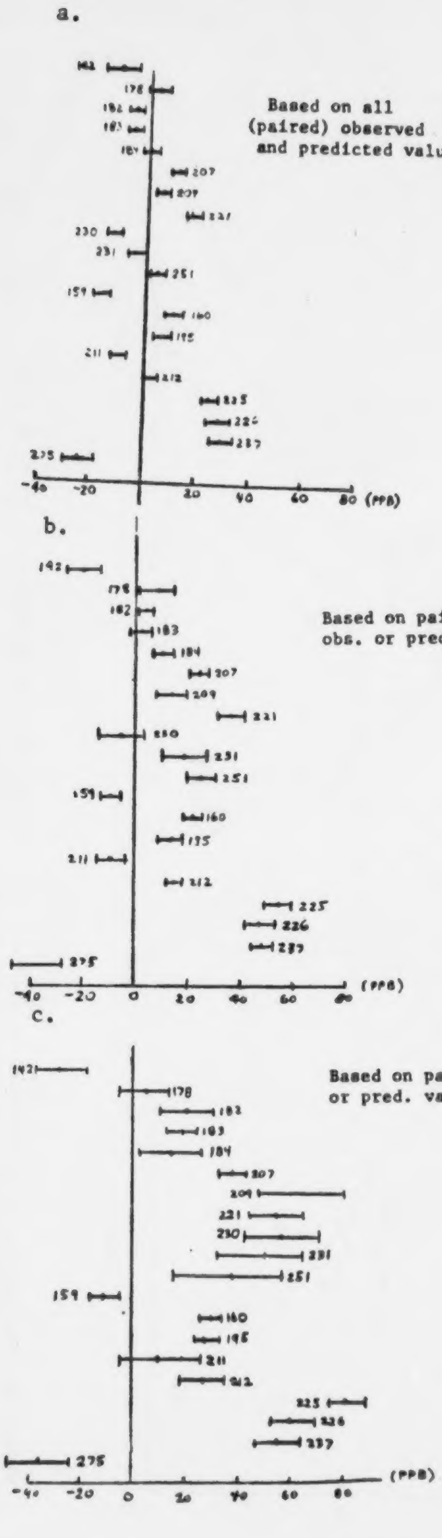

Based on all
(paired) observed
and predicted values.

Based on pairs for which
obs. or pred. values 80 ppb.

Based on pairs for which obs.
or pred. values 120 ppb.

Figure 12. Model Bias (ppb) using all pairs (a), and stratified data sets (b and c).

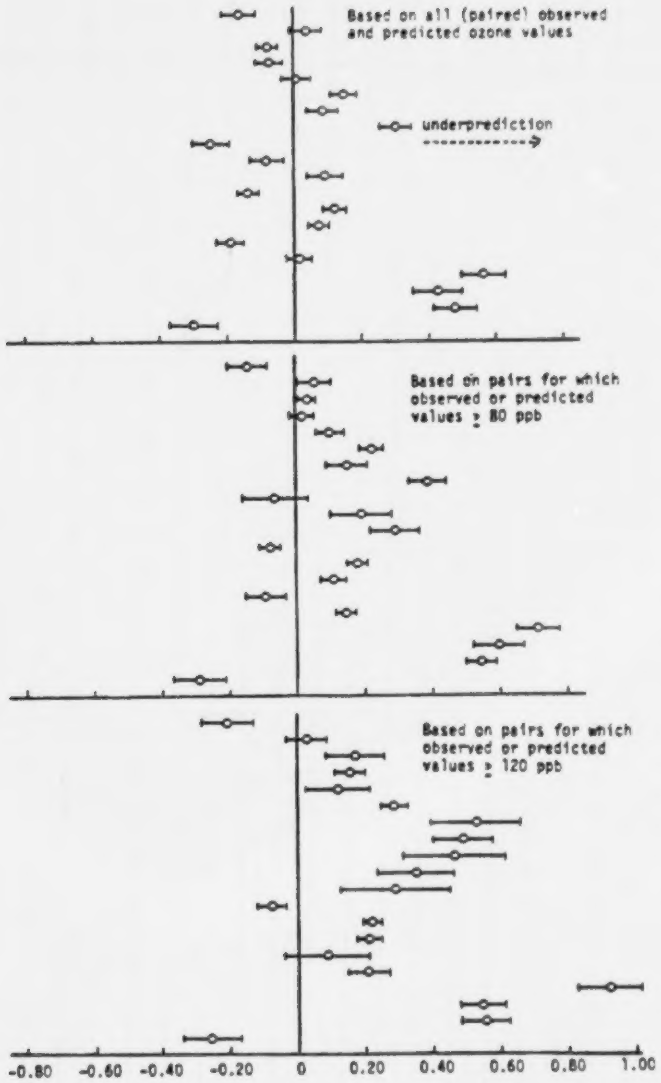

Fig. 13. Normalized Model Bias using all pairs (a), and stratified data sets (b and c). To obtain the normalized bias, mean residuals ($\overline{O}-\overline{P}$) were divided by the term ($\overline{P}+\overline{O}$)/2.

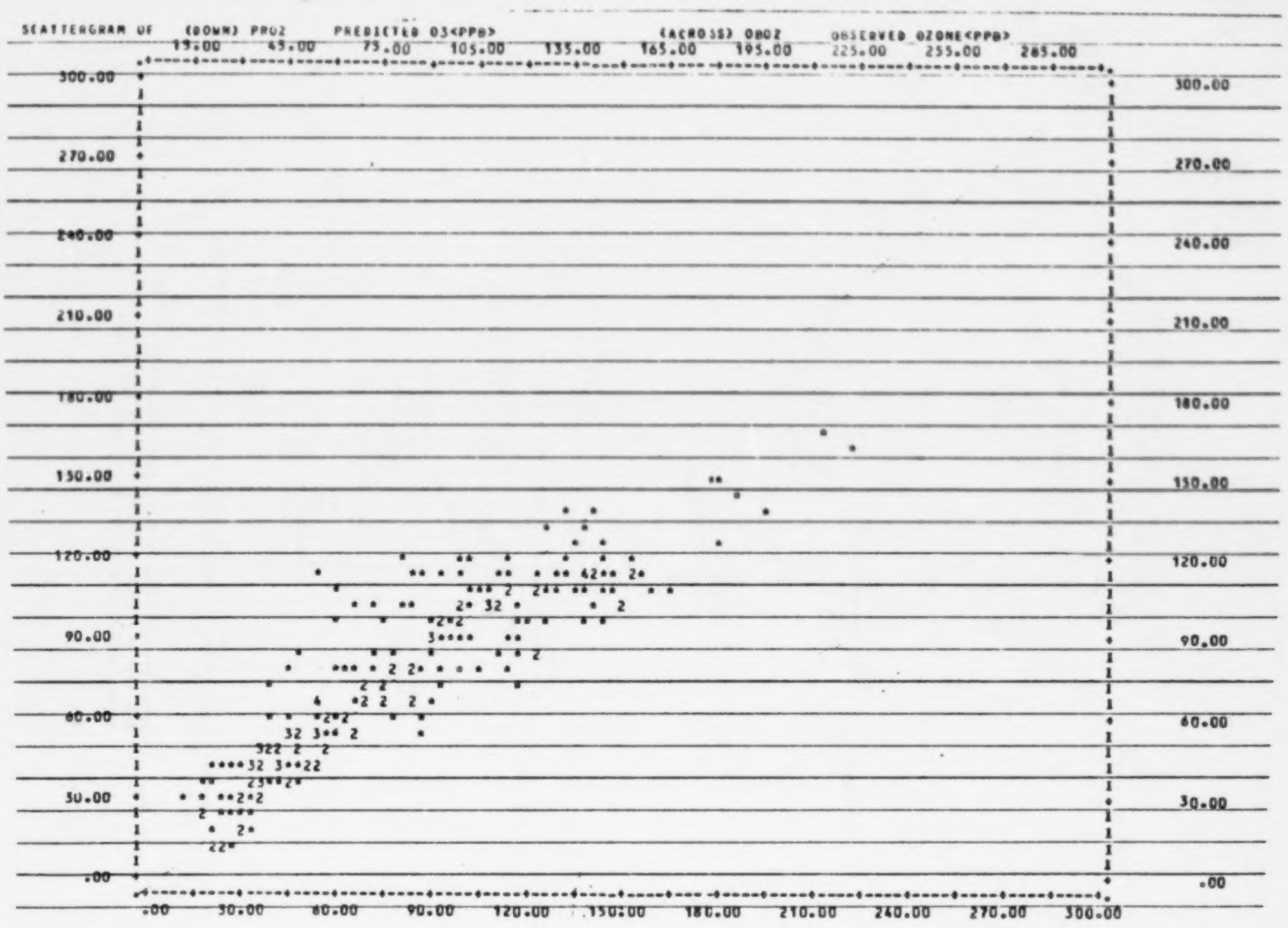

Figure 14. Scatterdiagram of predicted vs. observed ozone concentrations for Day 195.

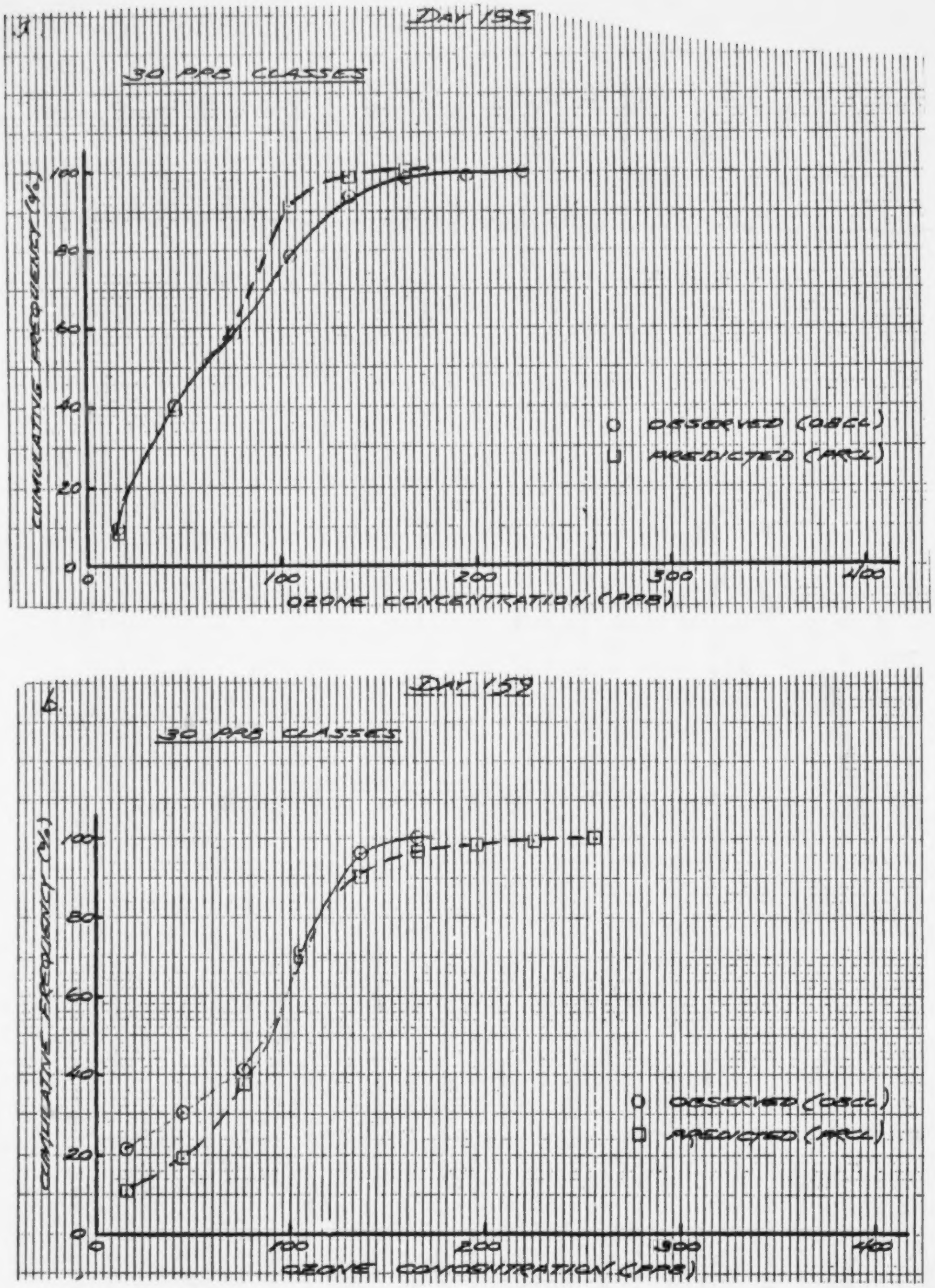

Figure 15. Cumulative frequency distributions of predicted and observed concentration.
a. Day 195 b. Day 159

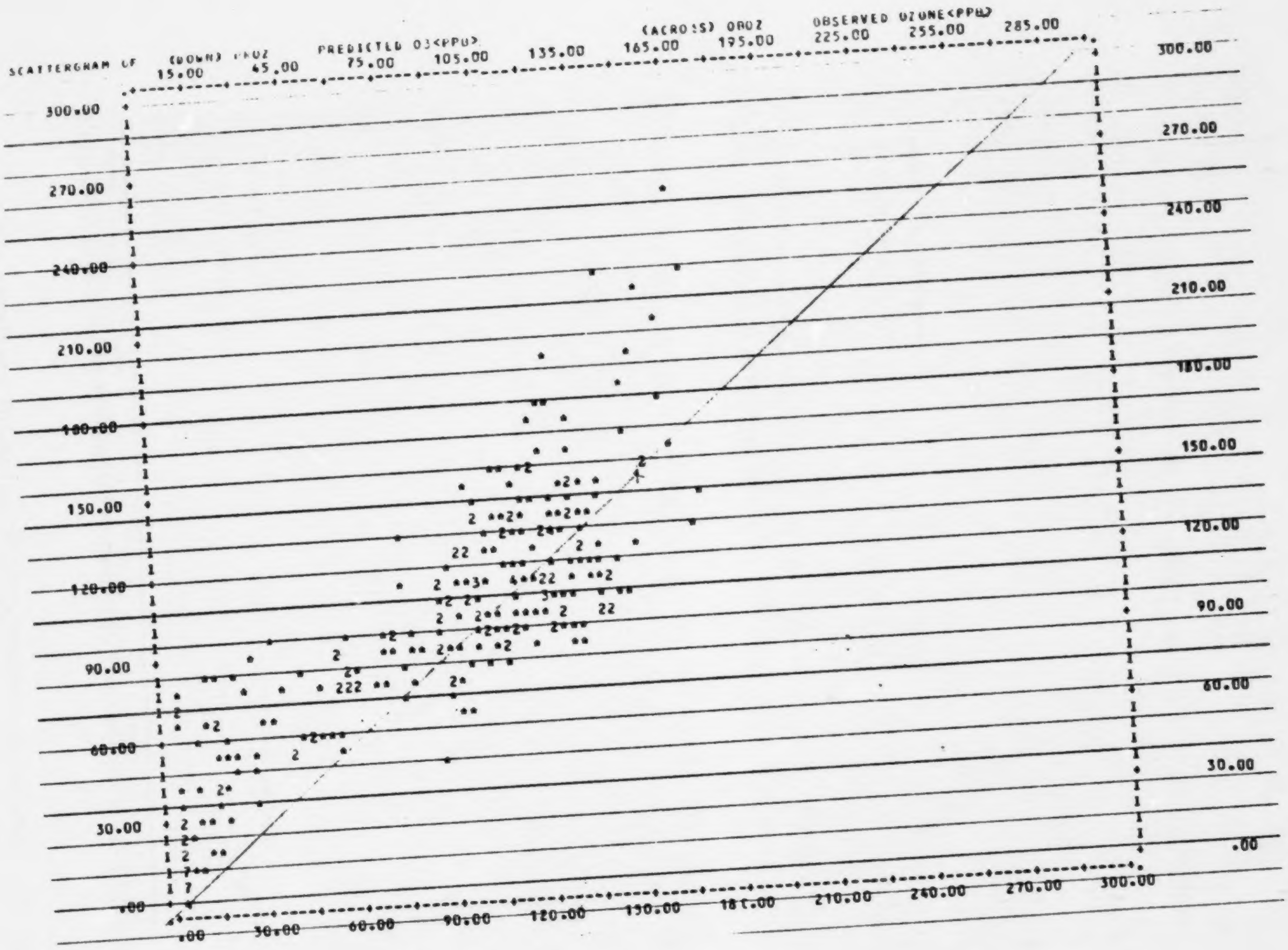

Figure 16. Scatterdiagram of predicted vs. observed ozone concentrations for Day 159.

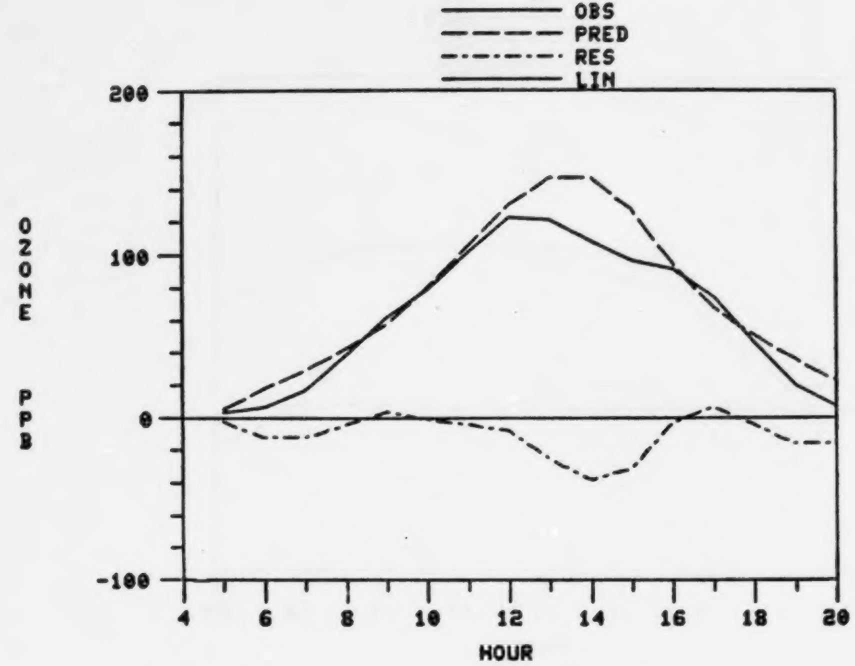

DAY 142

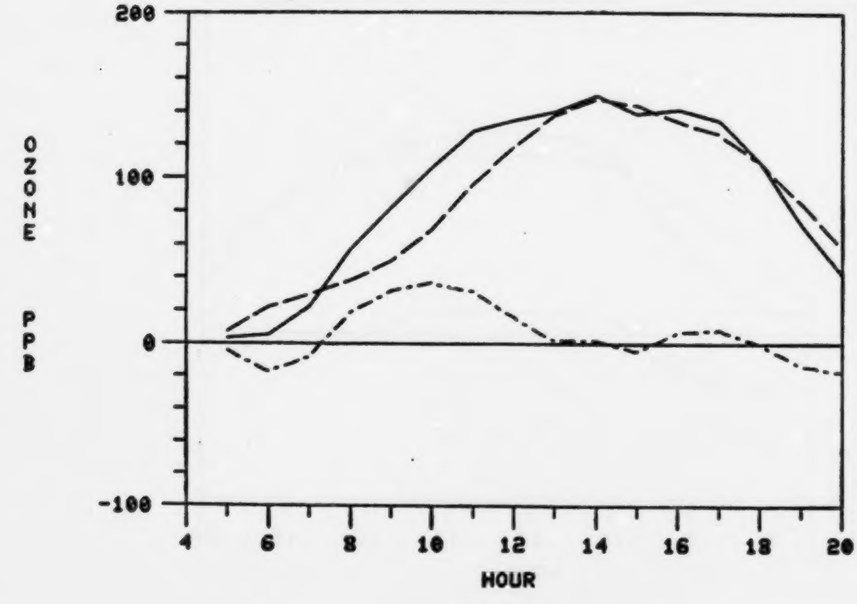

DAY 178

Figure 17. Time series of observed and predicted ozone concentrations and residuals averaged over all stations for each test day.

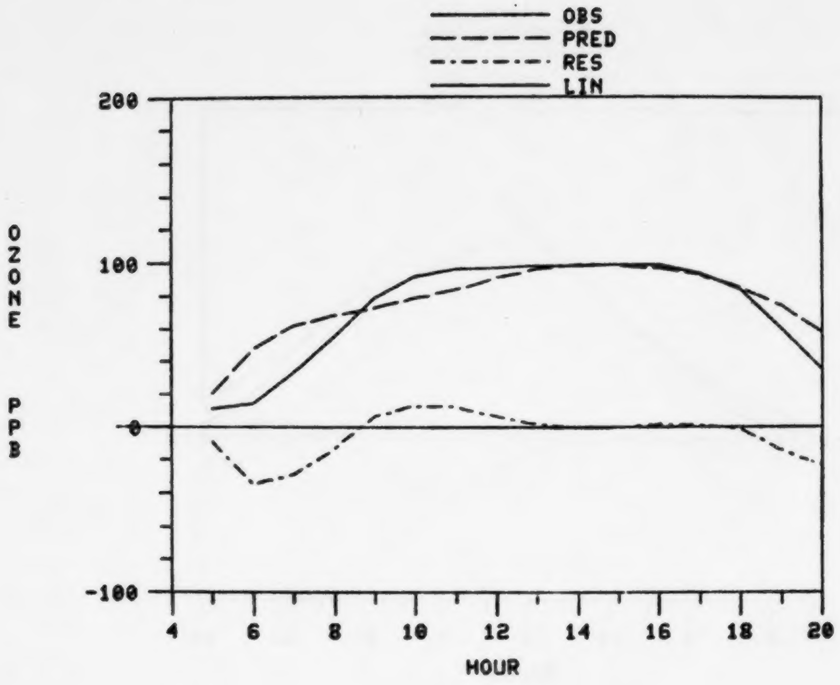

DAY 182

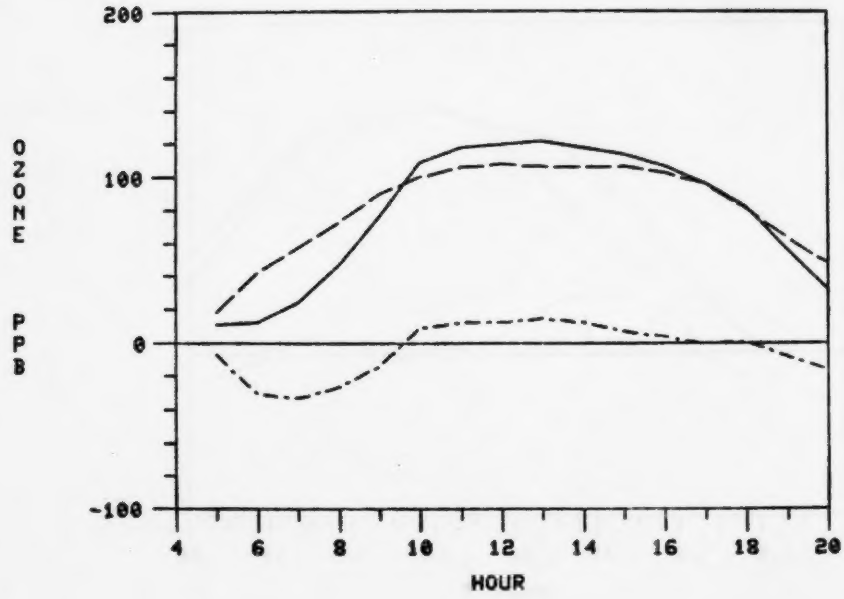

DAY 183

Figure 17 (continued)

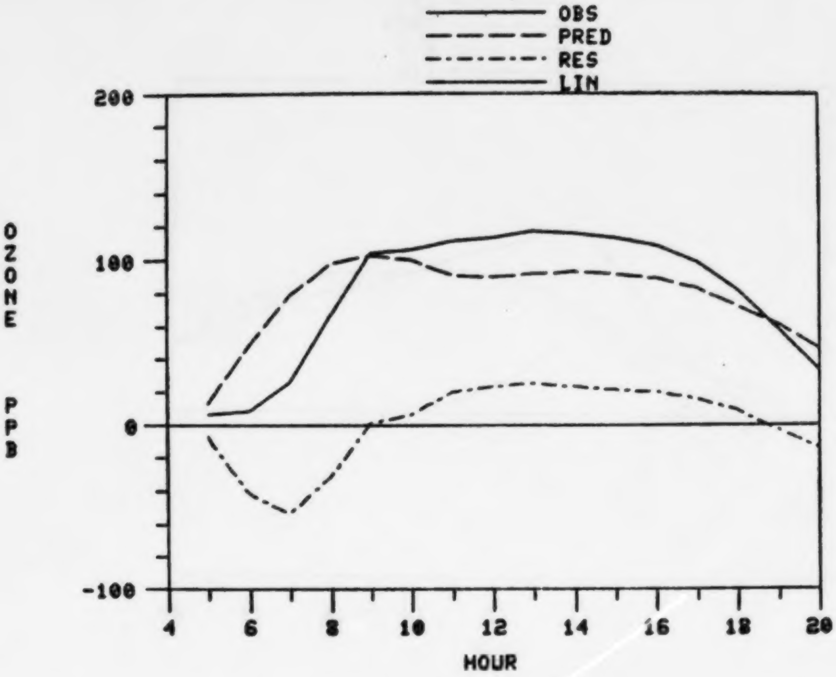

DAY 184

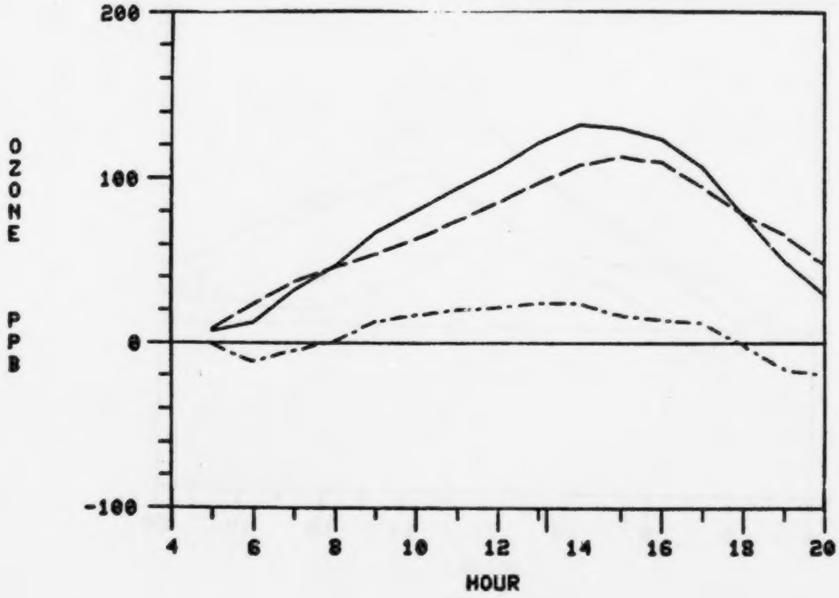

DAY 207

Figure 17 (continued)

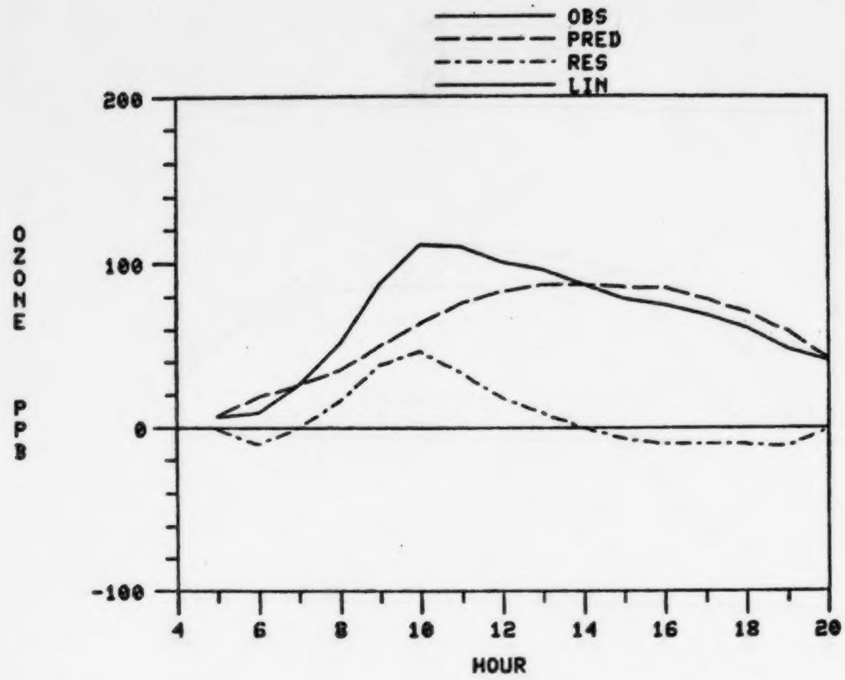

DAY 209

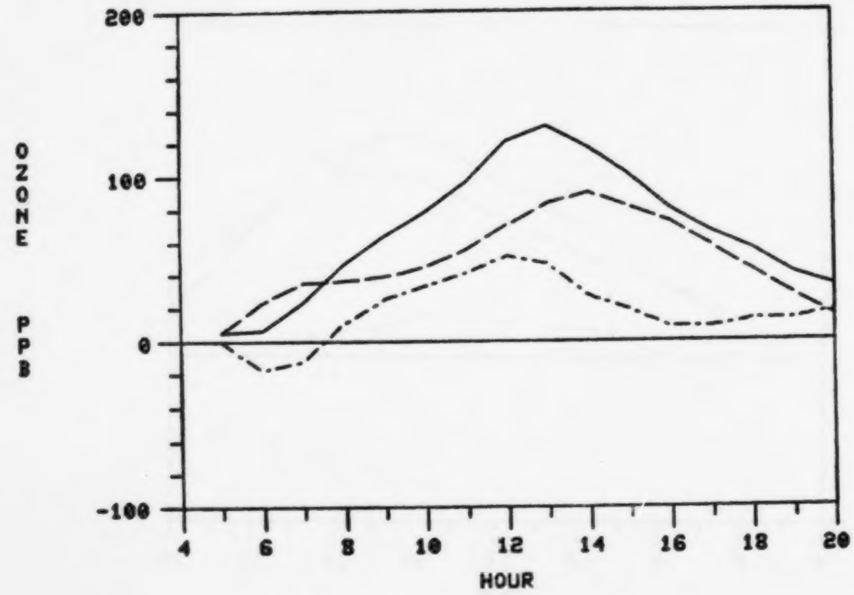

DAY 221

Figure 17 (continued)

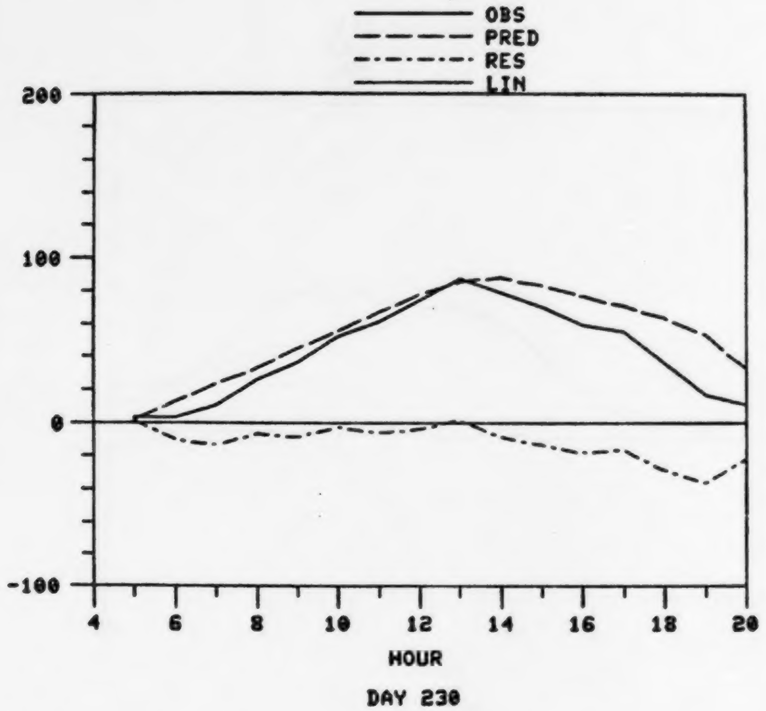

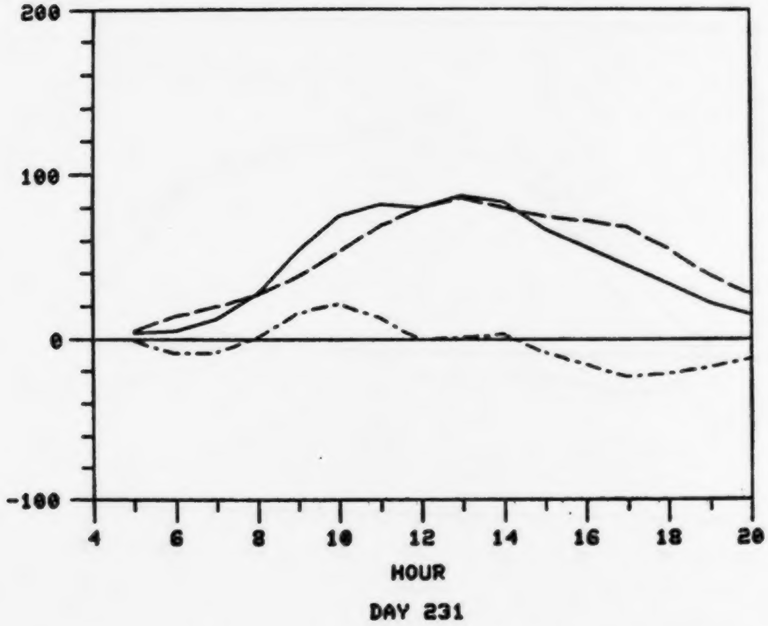

Figure 17 (continued)

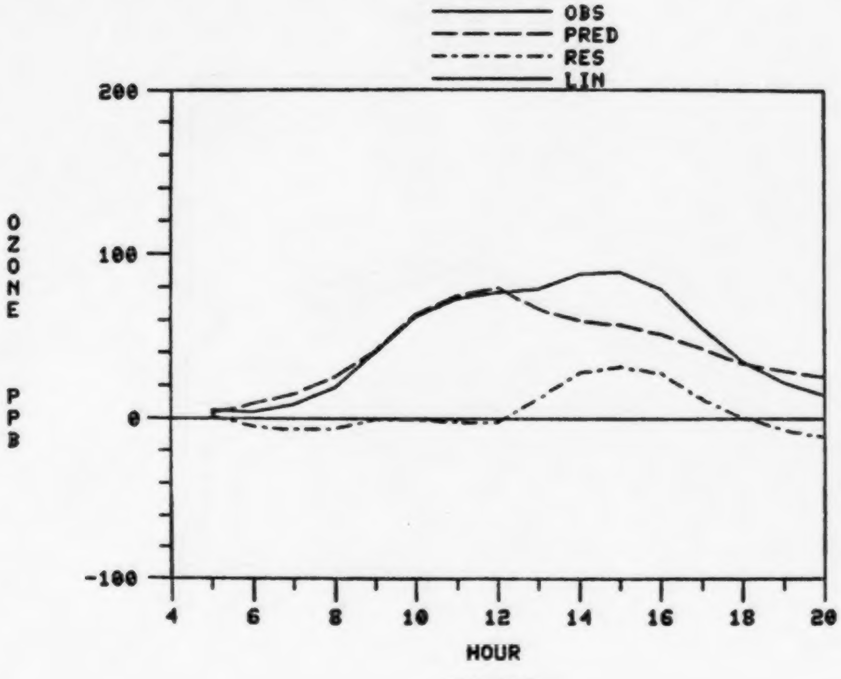

DAY 251

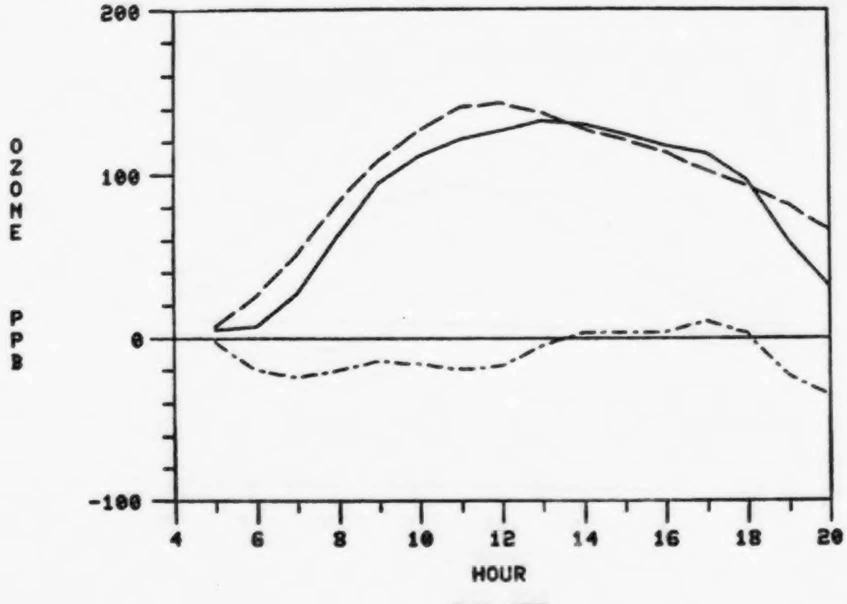

DAY 159

Figure 17 (continued)

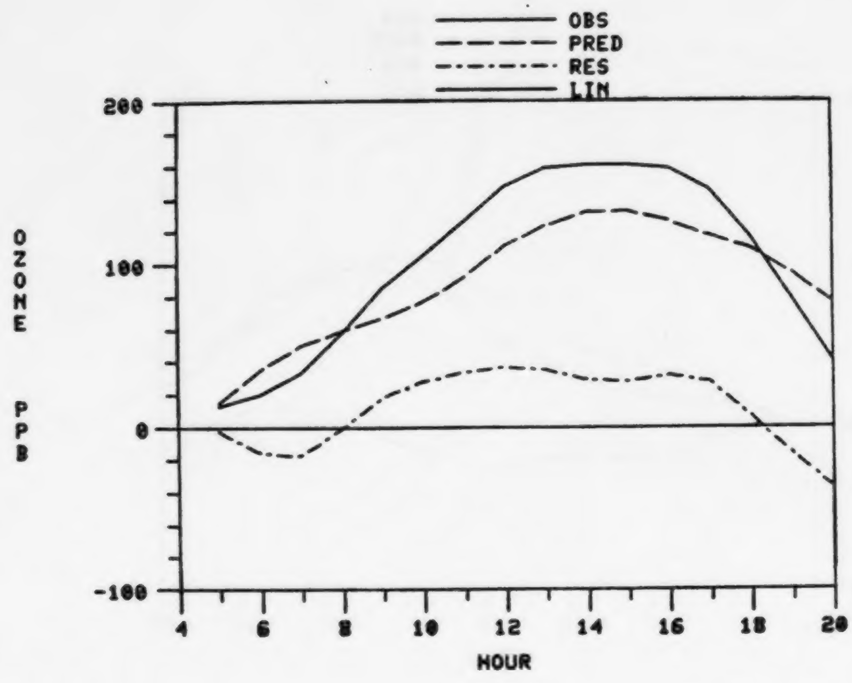

DAY 160

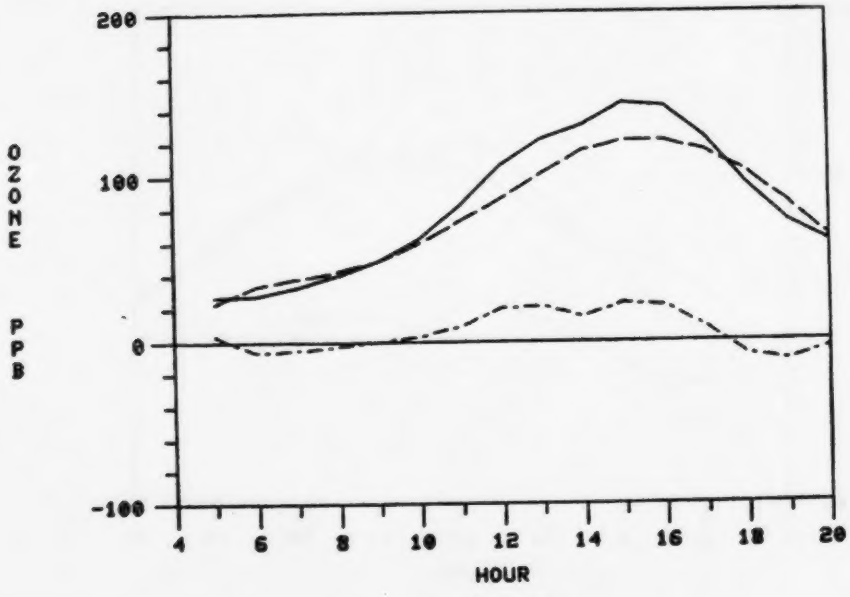

DAY 195

Figure 17 (continued)

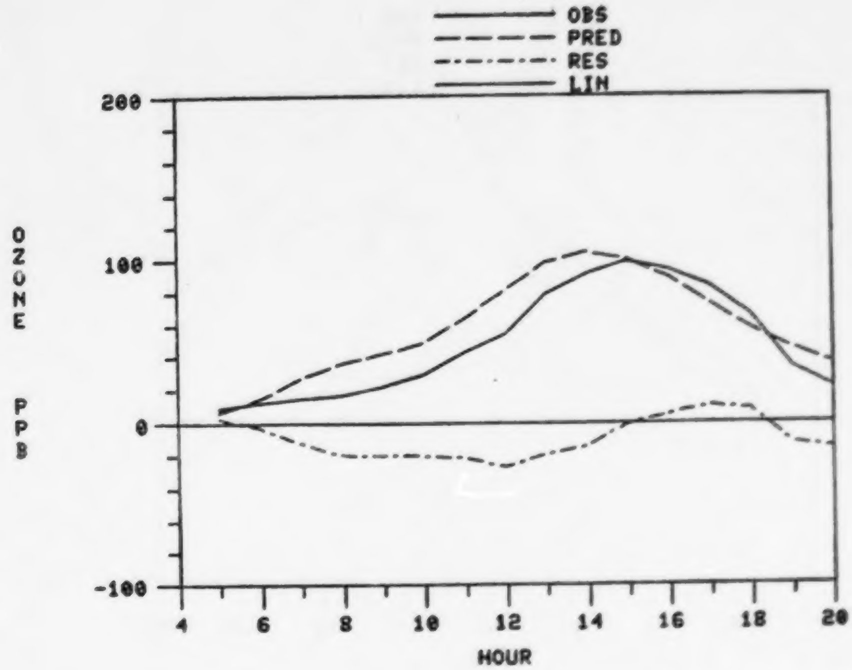

DAY 211

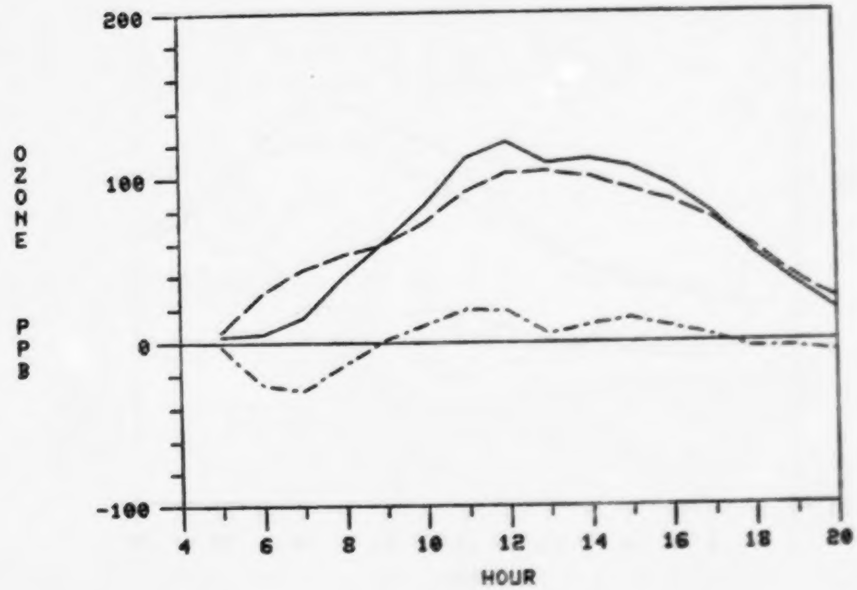

DAY 212

Figure 17 (continued)

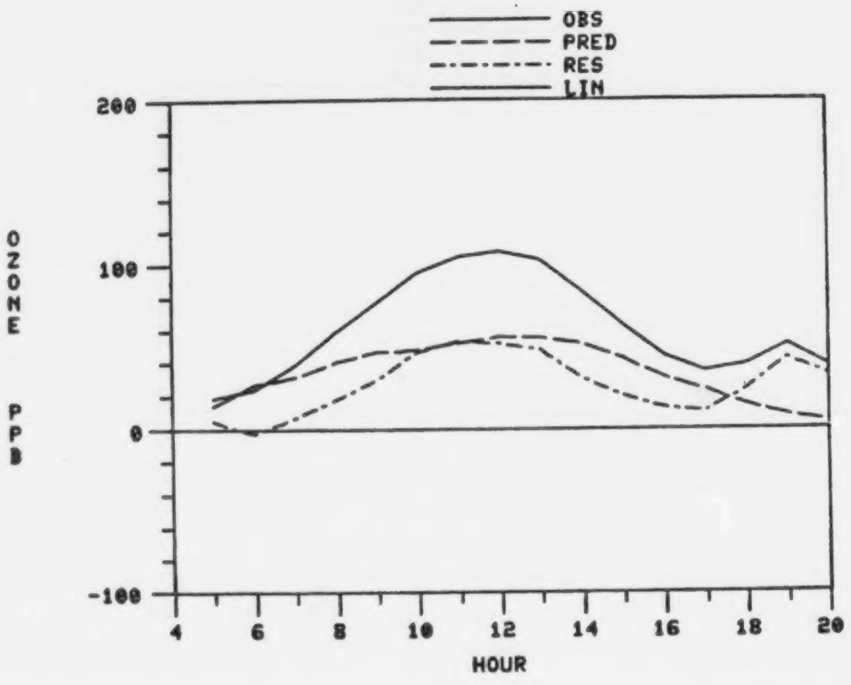

DAY 225

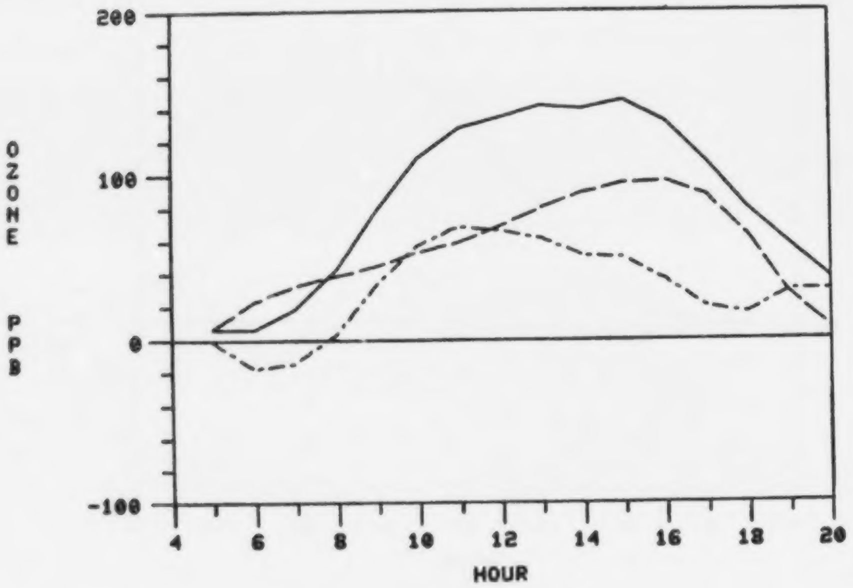

DAY 226

Figure 17 (continued)

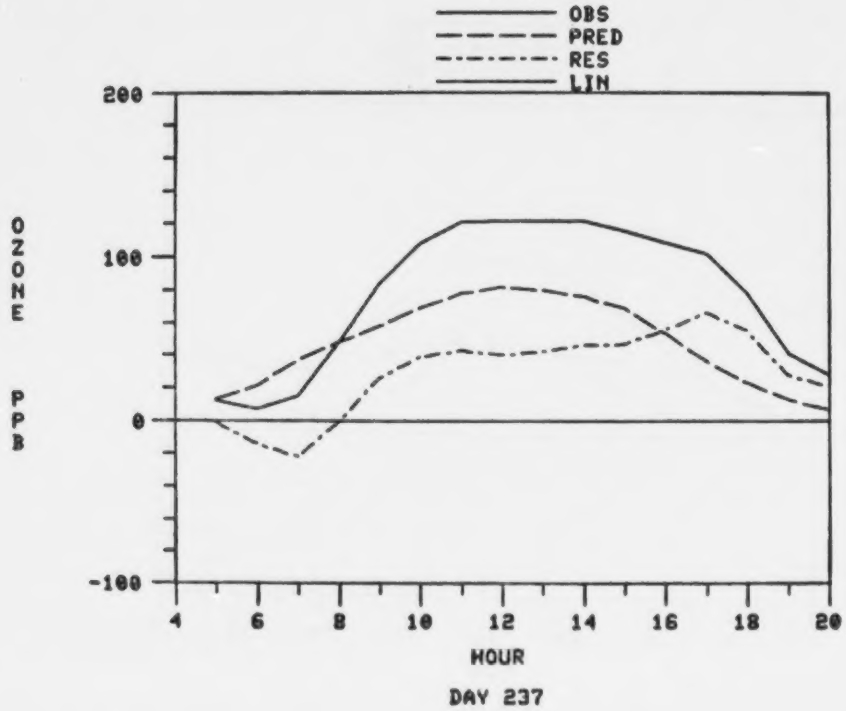

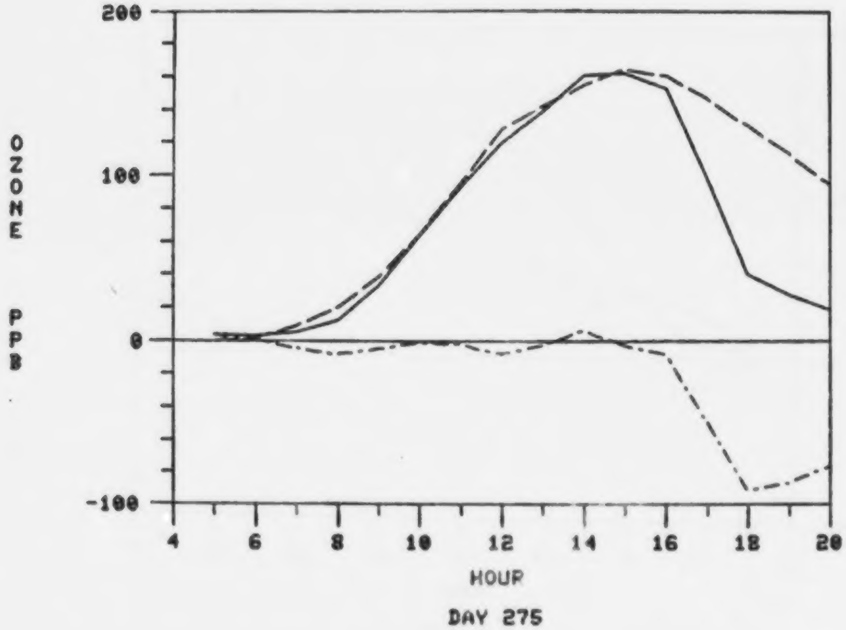

Figure 17 (continued)

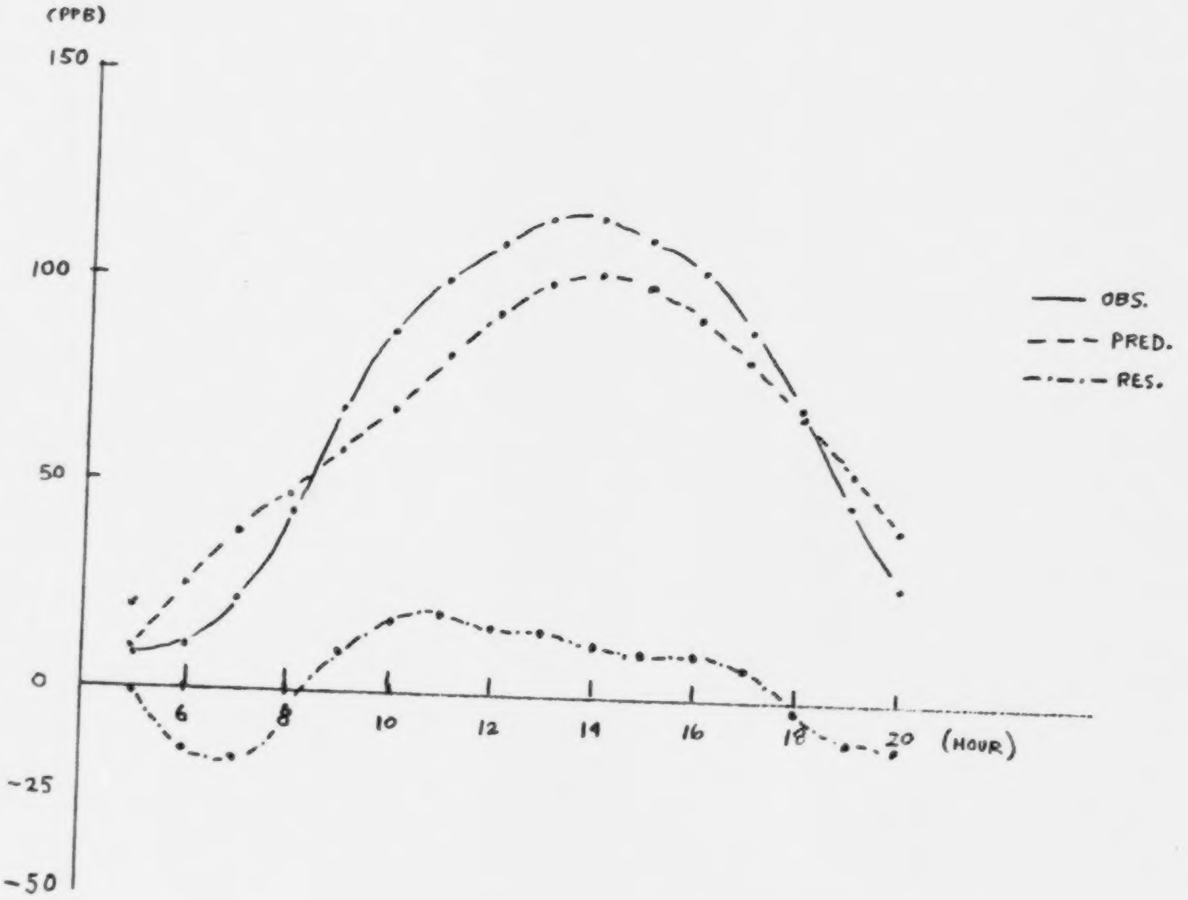

Figure 18. 20-day, all station average time series of observed concentration, predicted concentration and residuals in ppb.

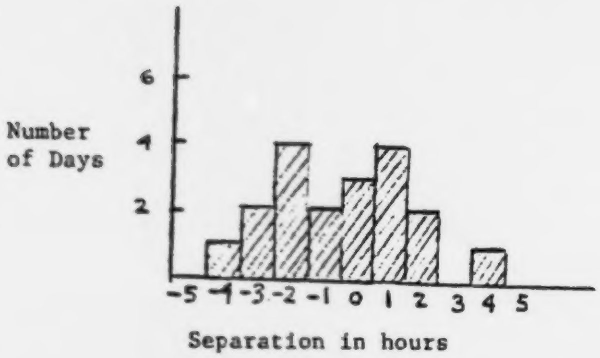

Figure 19. Histogram showing the frequency of lag times between observed and predicted peaks ($t_{obs} - t_{pred}$). (Day 183 excluded because it has multiple peaks.

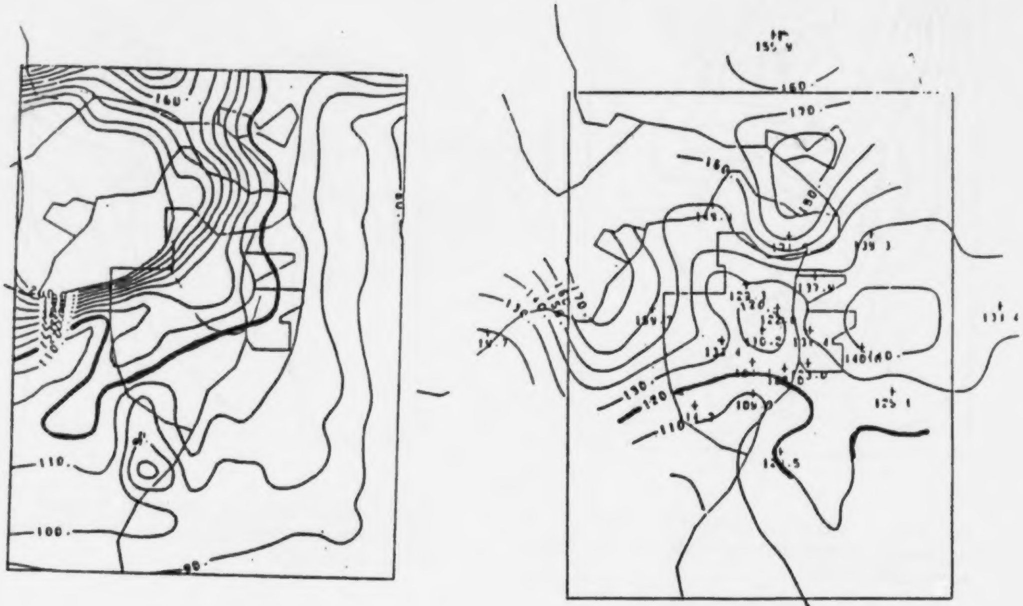

ST. LOUIS JUNE 7, 1976 (DAY 159)
ESTIMATED CONCENTRATIONS OF O_3 (IN PPB)
HOUR 1400-1500

ST. LOUIS JUNE 7, 1976 (DAY 159)
OBSERVED CONCENTRATIONS OF O_3 (IN PPB)
HOUR 1400-1500

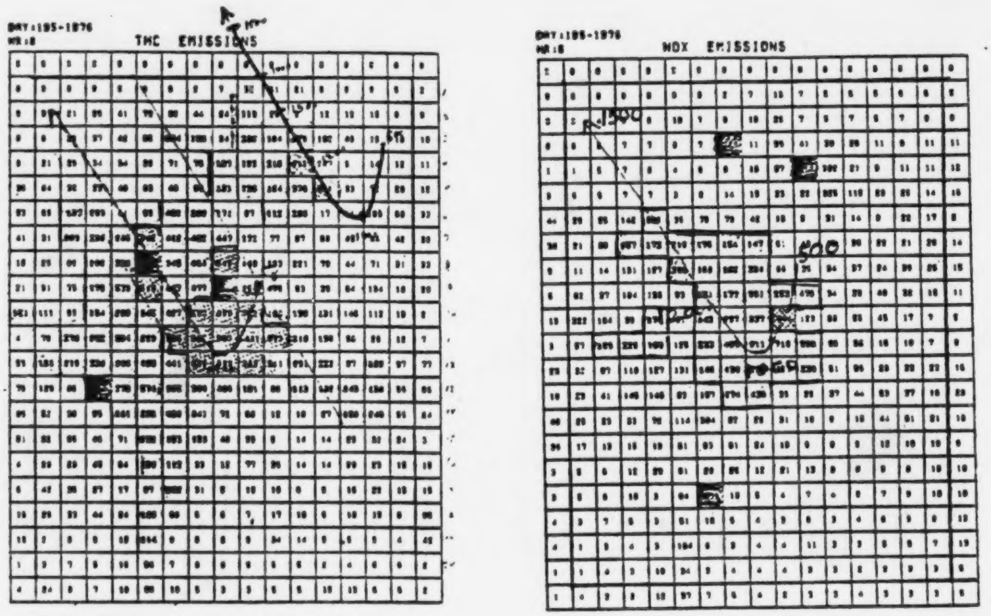

Fig. 20a. Spatial fields of observed and predicted ozone concentrations for hour of peak observed O_3 for Day 159. Rough trajectory estimates are superimposed on THC and NO_x emission density diagrams in the lower insets. Concentrations in ppb.

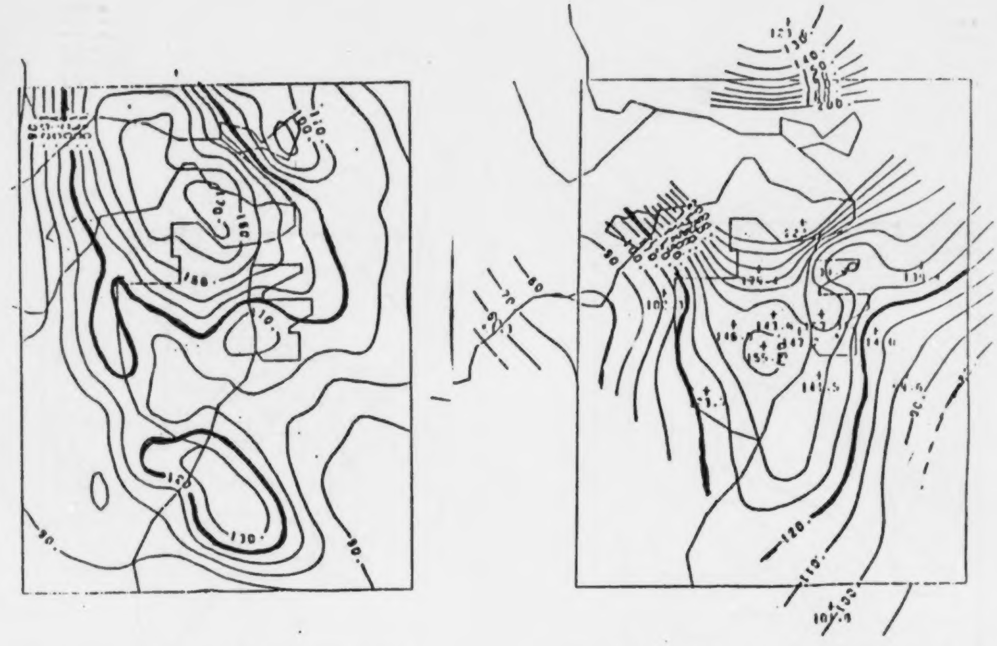

ST. LOUIS JULY 13, 1976 (DAY 195)
ESTIMATED CONCENTRATIONS OF O3 (IN PPB)
HOUR 1500-1600

ST. LOUIS JULY 13, 1976 (DAY 195)
OBSERVED CONCENTRATIONS OF O3 (IN PPB)
HOUR 1500-1600

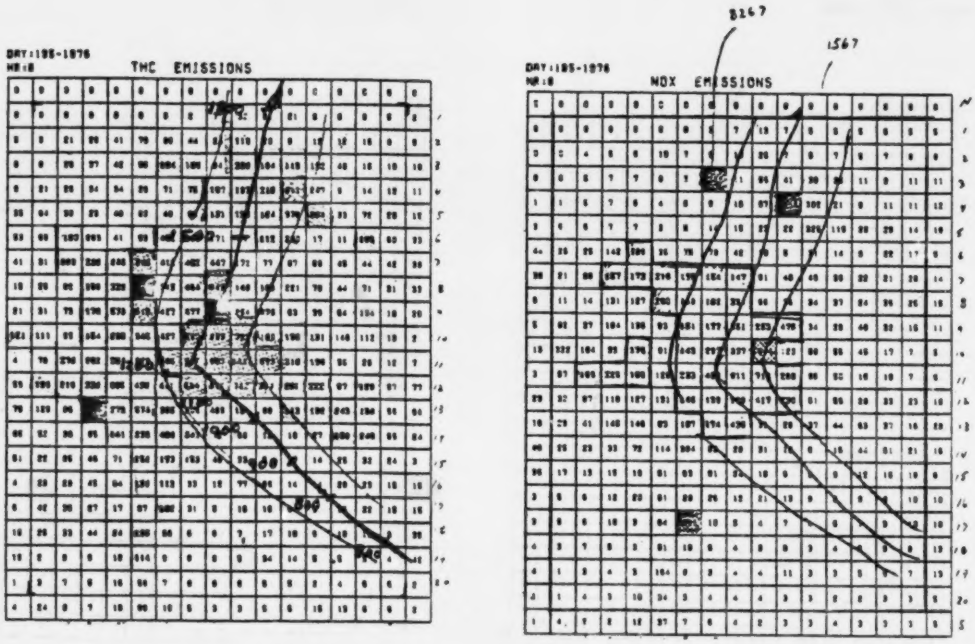

Figure 20b. Spatial fields of observed and predicted ozone concentrations for hour of peak observed O_3 for Day 195. Rough trajectory estimates are superimposed on THC and NO_x emission density diagrams in the lower insets. Concentrations in ppb.

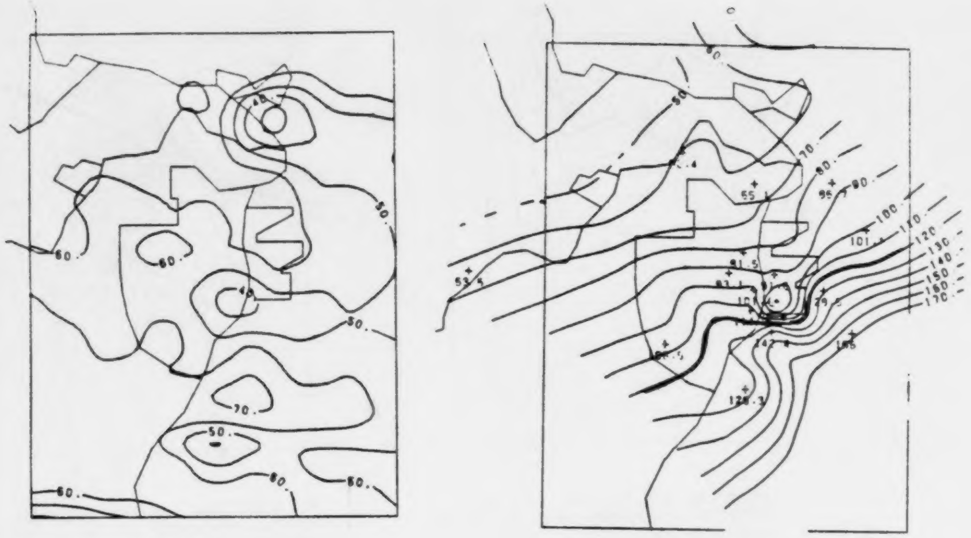

ST. LOUIS AUG 12, 1976 (DAY 225)
ESTIMATED CONCENTRATIONS OF O3 (IN PPB)
HOUR 1300-1400

ST. LOUIS AUG 12, 1976 (DAY 225)
OBSERVED CONCENTRATIONS OF O3 (IN PPB)
HOUR 1300-1400

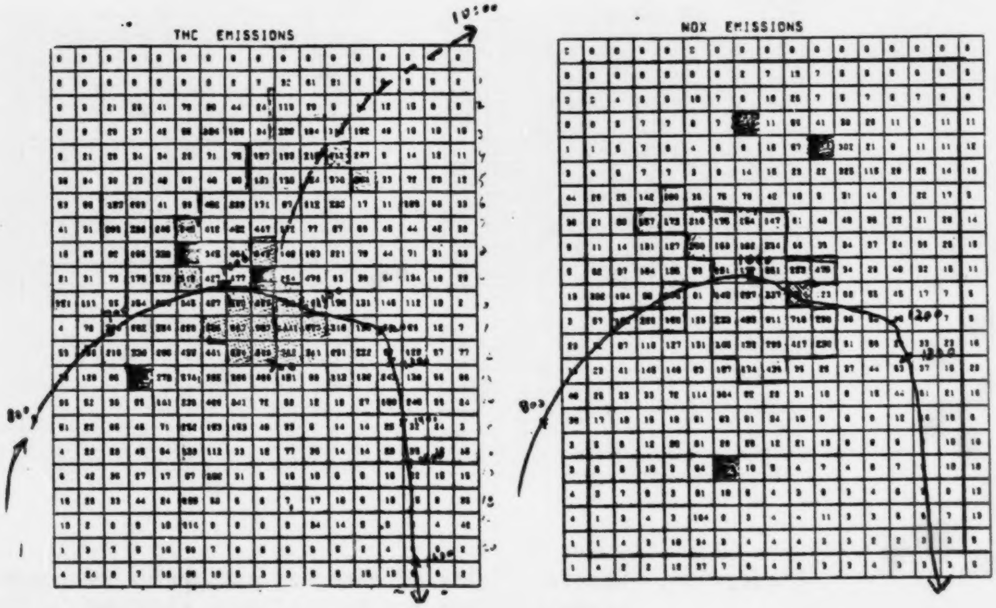

Figure 20c. Spatial fields of observed and predicted ozone concentrations for hour of peak observed O_3 for Day 225. Rough trajectory estimates are superimposed on THC and NO_x emission density diagrams in the lower insets. Concentrations in ppb.

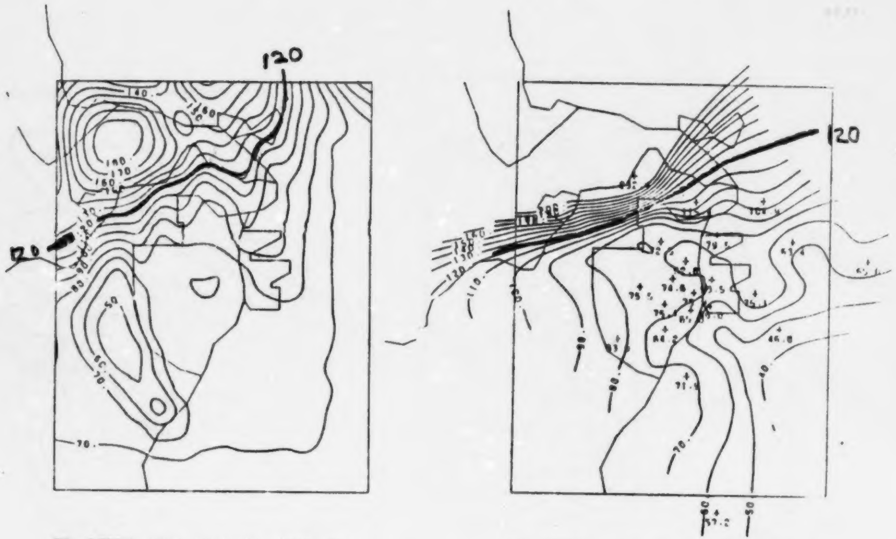

ST. LOUIS AUG. 19 1975 (DAY 231)
ESTIMATED CONCENTRATIONS OF O_3 (IN PPB)
HOUR 1400-1500

ST. LOUIS AUG. 19, 1975 (DAY 231)
OBSERVED CONCENTRATIONS OF O_3 (IN PPB)
HOUR 1400-1500

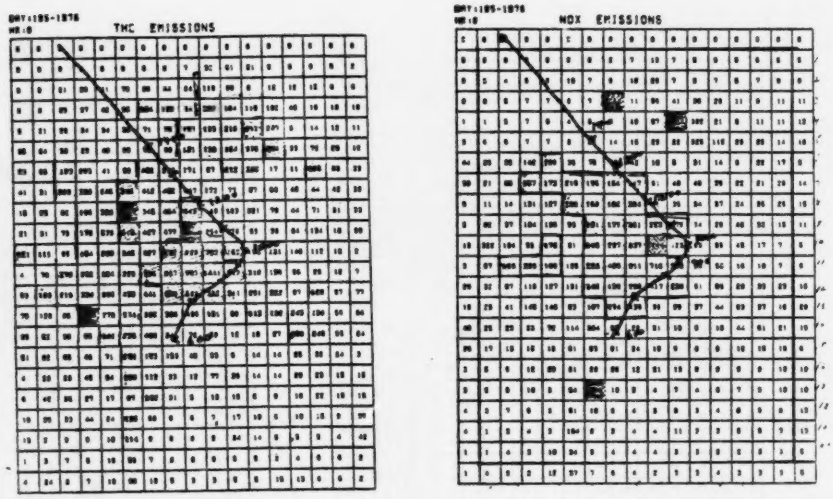

Figure 20d. Spatial fields of observed and predicted ozone concentrations for hour of peak observed O_3 for Day 231. Rough trajectory estimates are superimposed on THC and NO_x emission density diagrams in the lower insets. Concentrations in ppb.

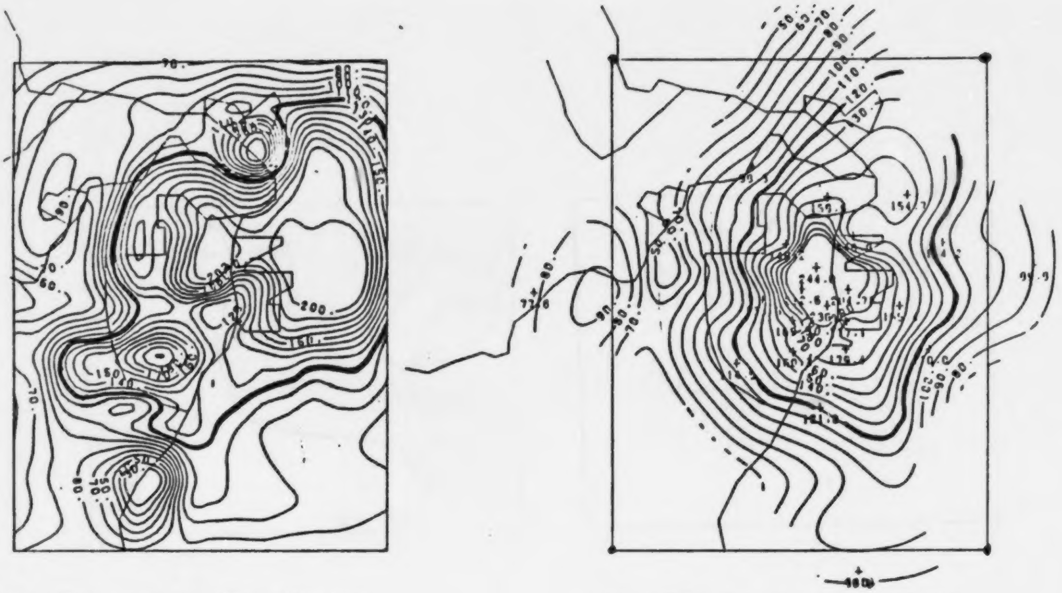

ST. LOUIS OCT. 1, 1976 (DAY 275)
ESTIMATED CONCENTRATIONS OF O_3 (IN PPB)
HOUR 1400-1500

ST. LOUIS OCT. 1, 1976 (DAY 275)
OBSERVED CONCENTRATIONS OF O_3 (IN PPB)
HOUR 1400-1500

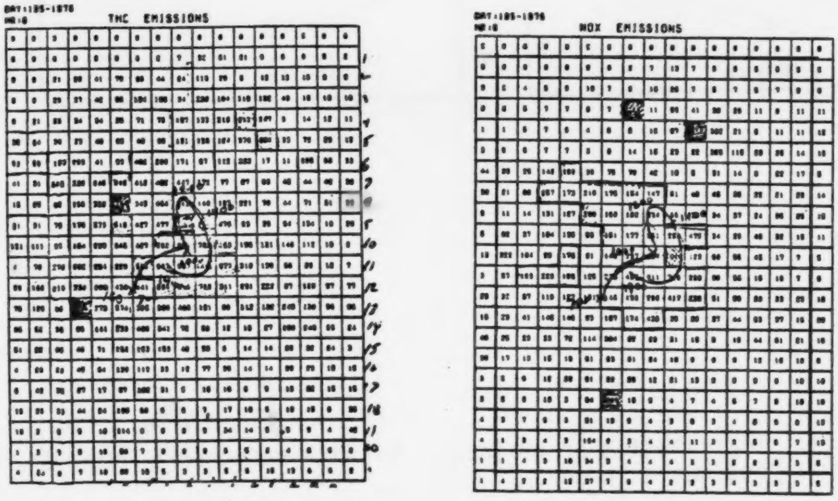

Figure 20e. Spatial fields of observed and predicted ozone concentrations for hour of peak observed O_3 for Day 275. Rough trajectory estimates are superimposed on THC and NO_x emission density diagrams in the lower insets. Concentrations in ppb.

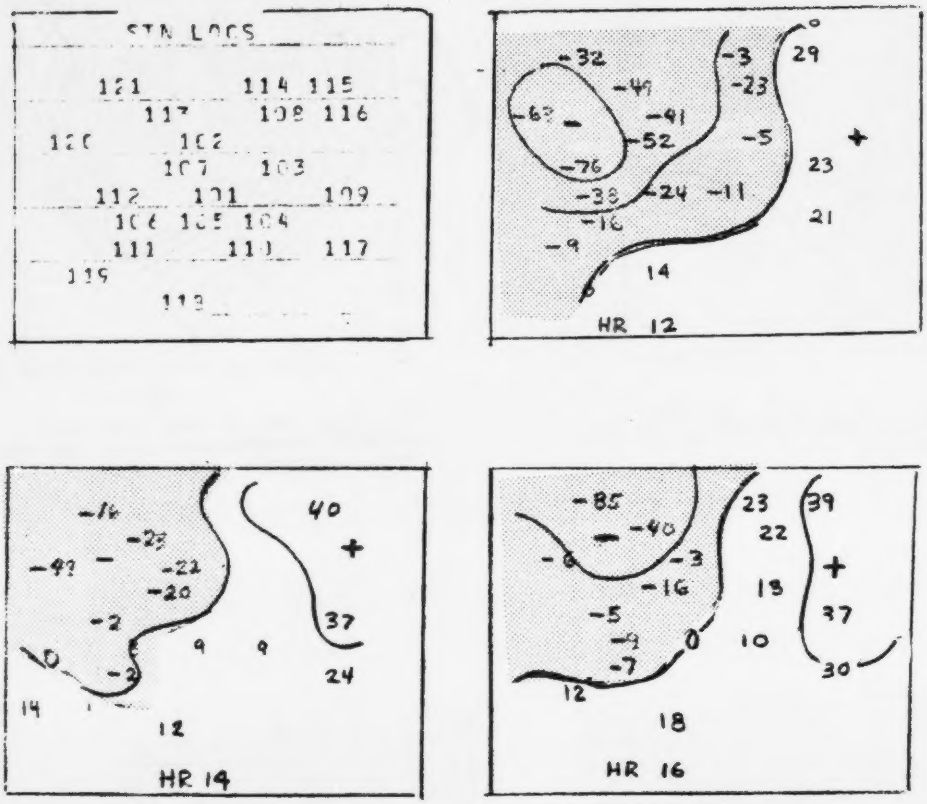

Figure 21. Distribution of residuals for afternoon hours, Day 159. Residuals in ppb.

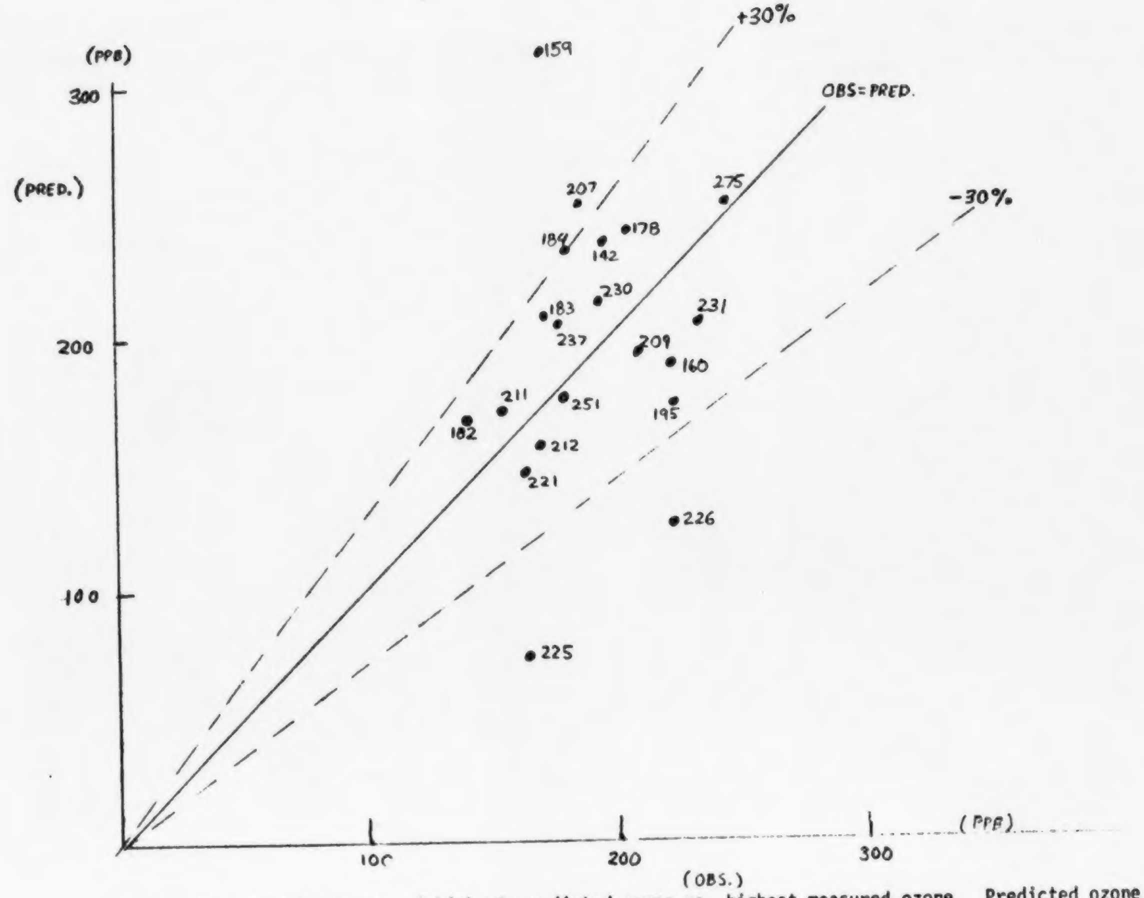

Figure 22. Scatterdiagram of highest predicted ozone vs. highest measured ozone. Predicted ozone from any grid cell in the modeling region (not restricted to monitoring sites).

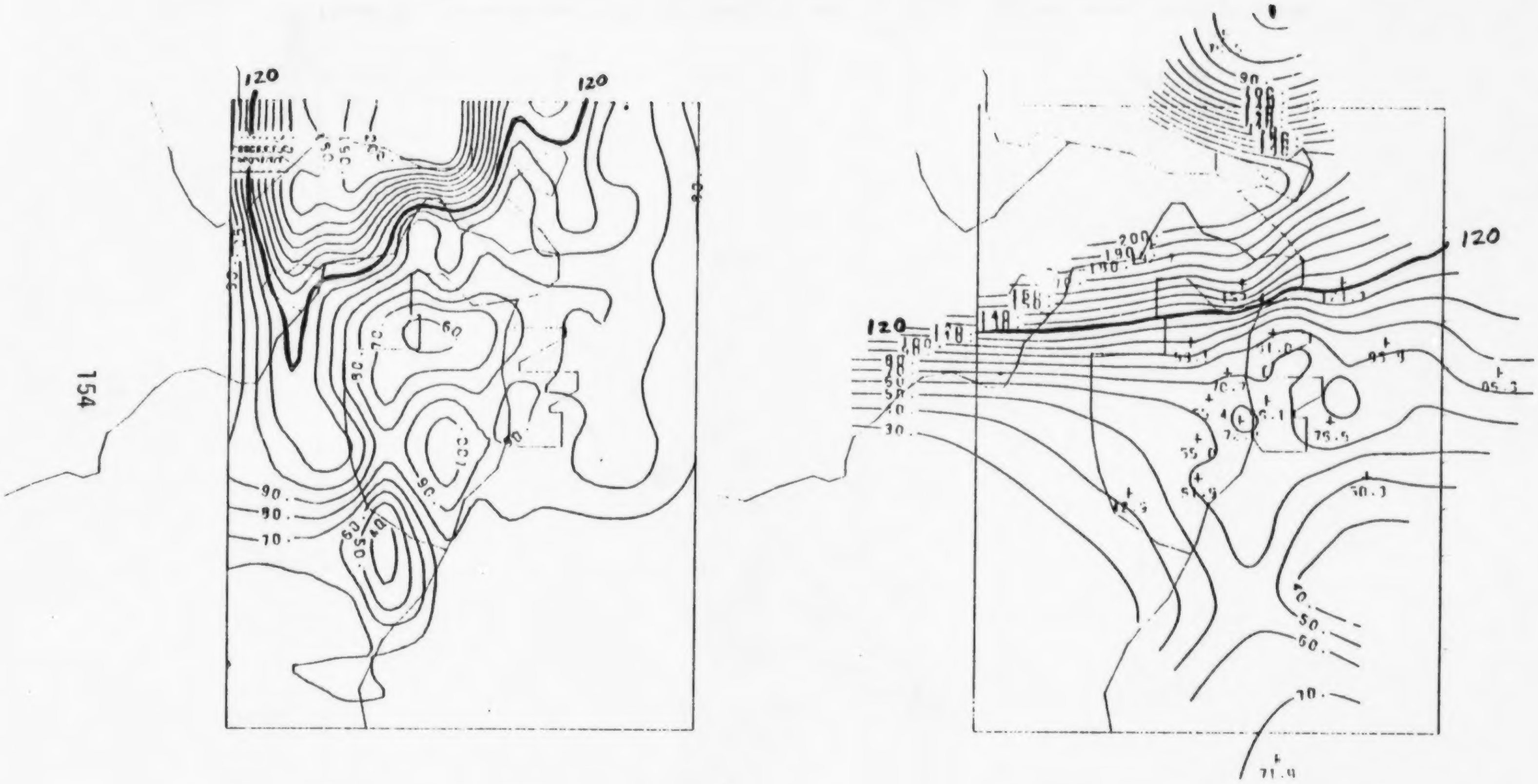

St. Louis Aug. 18, 1975 (Day 230)
Estimated Concentrations of O_3 (in PPB)
Hour 1300-1400

St. Louis Aug. 18, 1975 (Day 230)
Observed Concentrations of O_3 (in PPB)
Hour 1300-1400

Figure 23a. Spatial fields of observed and predicted ozone concentrations for hour of peak observed ozone for Day 230.

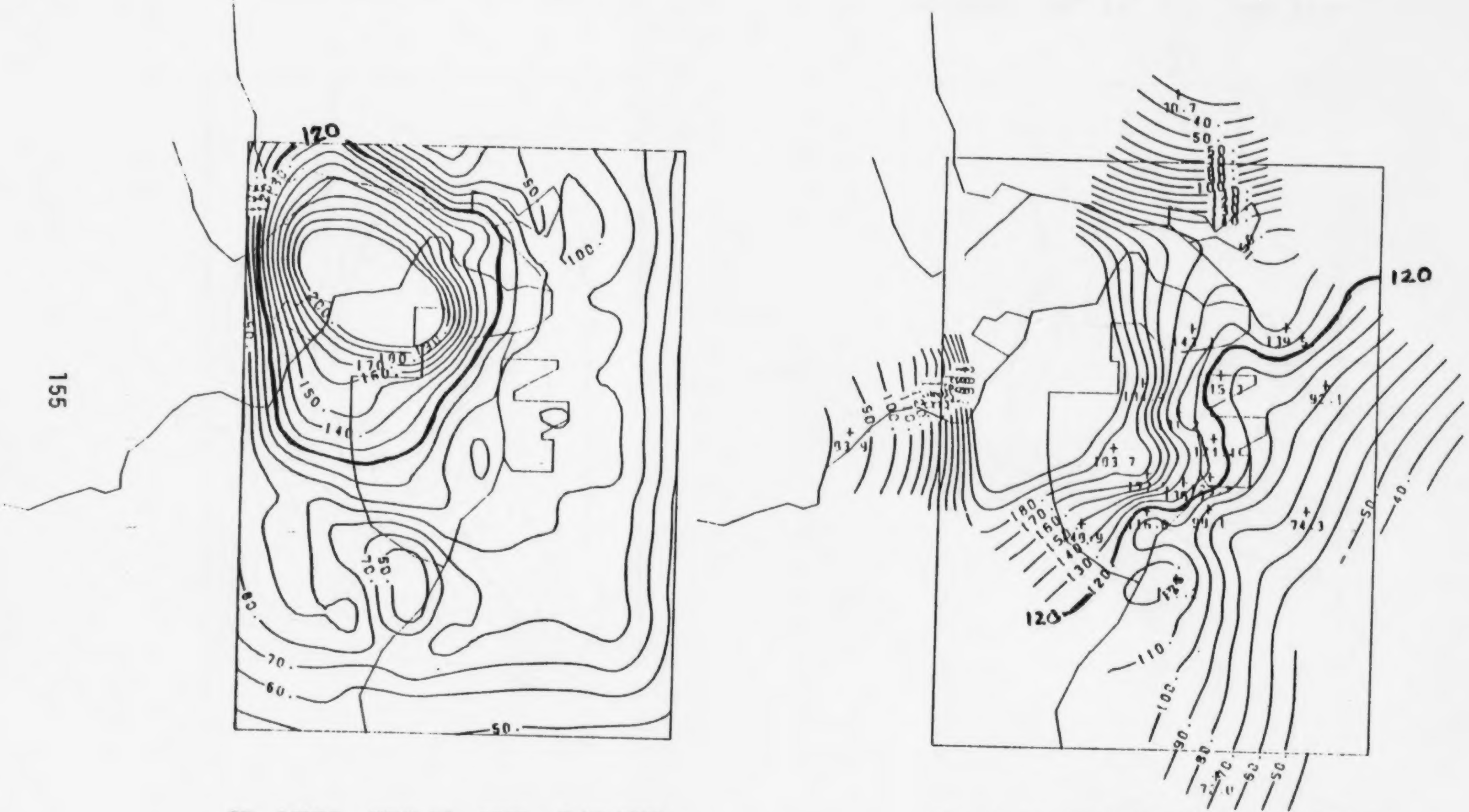

ST. LOUIS JULY 26, 1975 (DAY 207)
ESTIMATED CONCENTRATIONS OF O_3 (IN PPB)
HOUR 1400-1500

ST. LOUIS JULY 26, 1975 (DAY 207)
OBSERVED CONCENTRATIONS OF O_3 (IN PPB)
HOUR 1400-1500

Figure 23b. Spatial fields of observed and predicted ozone concentrations for hour of peak observed ozone for Day 207.

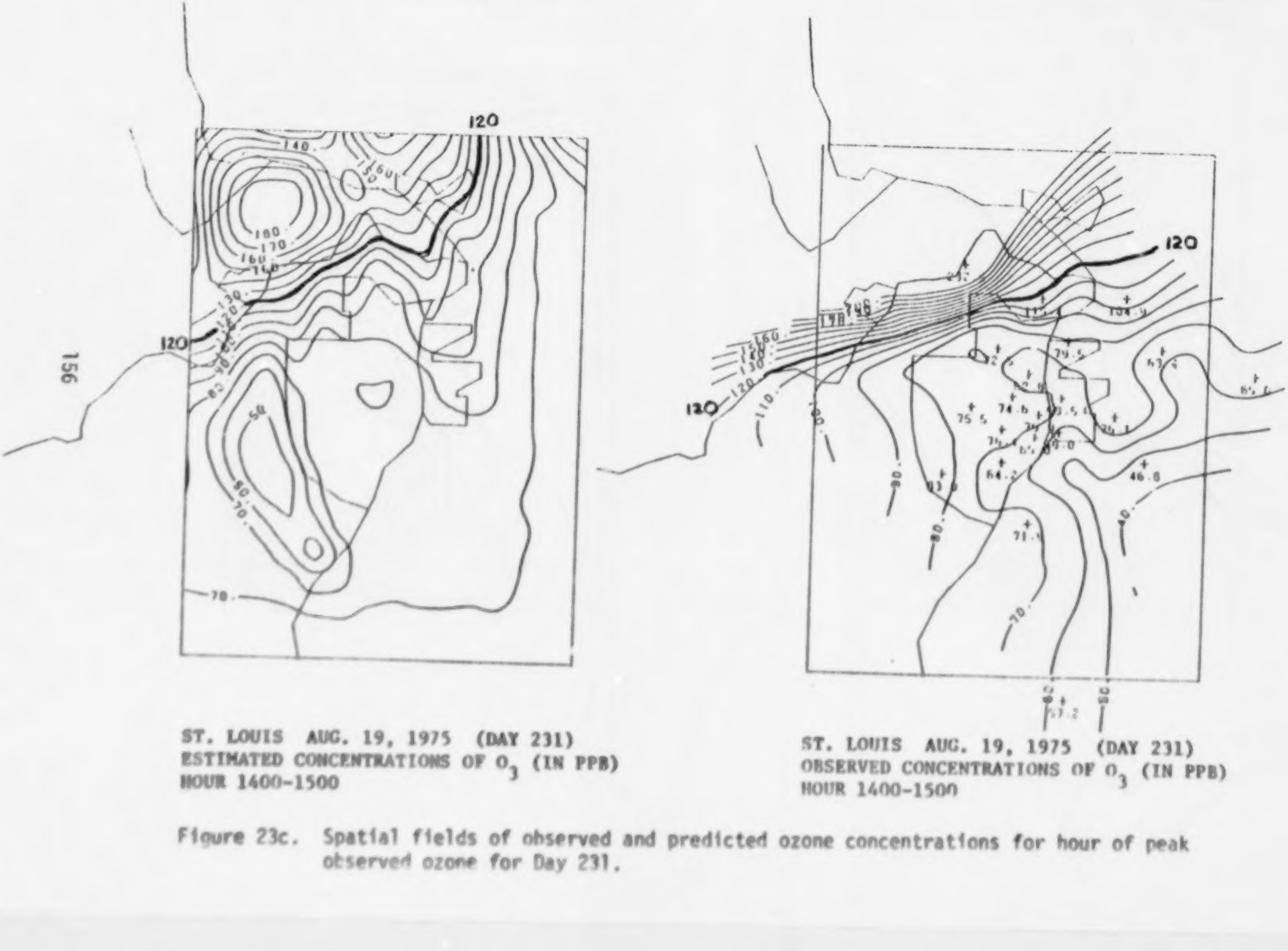

ST. LOUIS AUG. 19, 1975 (DAY 231)
ESTIMATED CONCENTRATIONS OF O_3 (IN PPB)
HOUR 1400-1500

ST. LOUIS AUG. 19, 1975 (DAY 231)
OBSERVED CONCENTRATIONS OF O_3 (IN PPB)
HOUR 1400-1500

Figure 23c. Spatial fields of observed and predicted ozone concentrations for hour of peak observed ozone for Day 231.

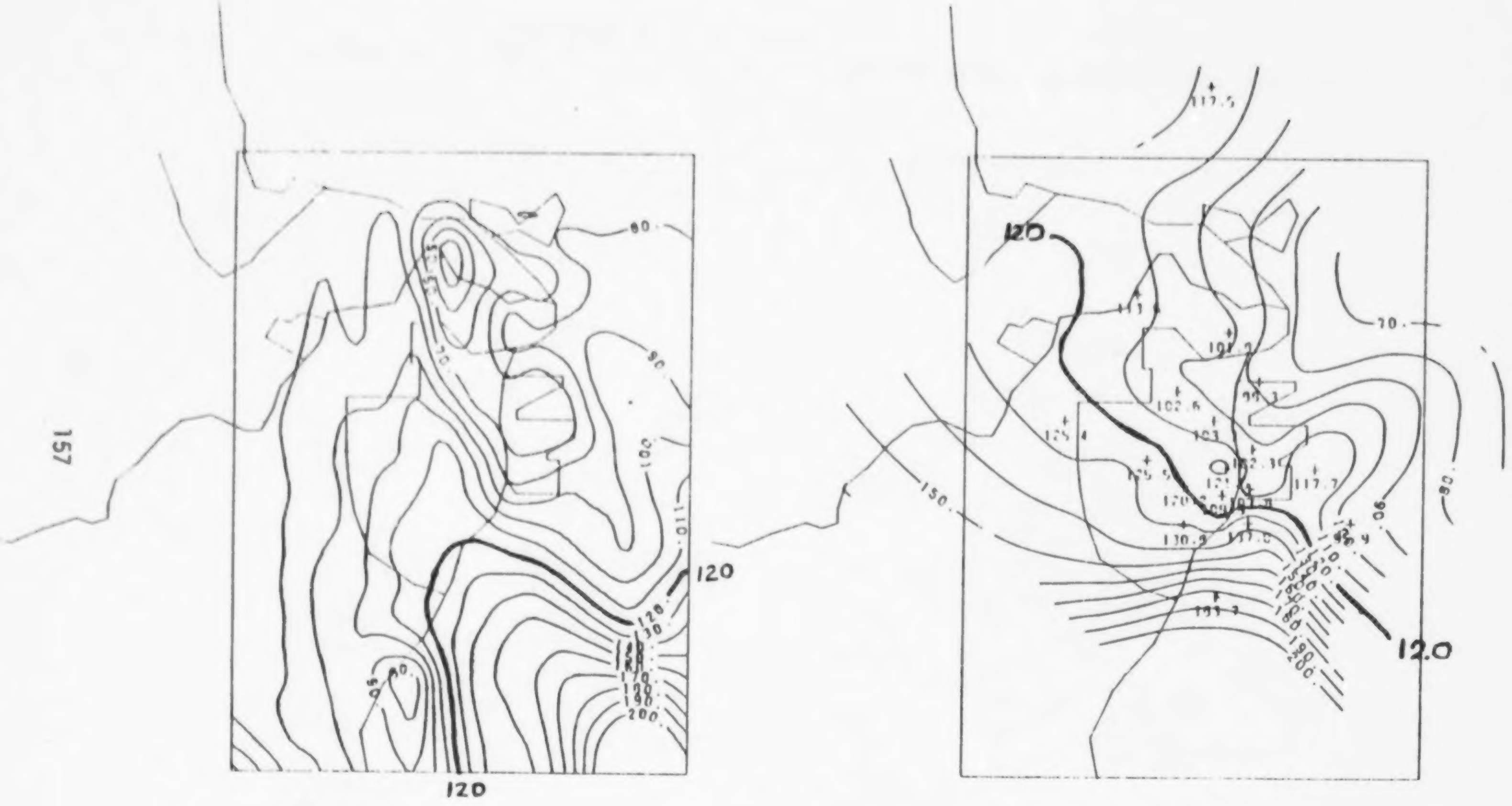

ST. LOUIS JULY 3, 1975 (DAY 184)
ESTIMATED CONCENTRATIONS OF O_3 (IN PPB)
HOUR 1300-1400

ST. LOUIS JULY 3, 1975 (DAY 184)
OBSERVED CONCENTRATIONS OF O_3 (IN PPB)
HOUR 1300-1400

Figure 23d. Spatial fields of observed and predicted ozone concentrations for hour of peak observed ozone for Day 184.

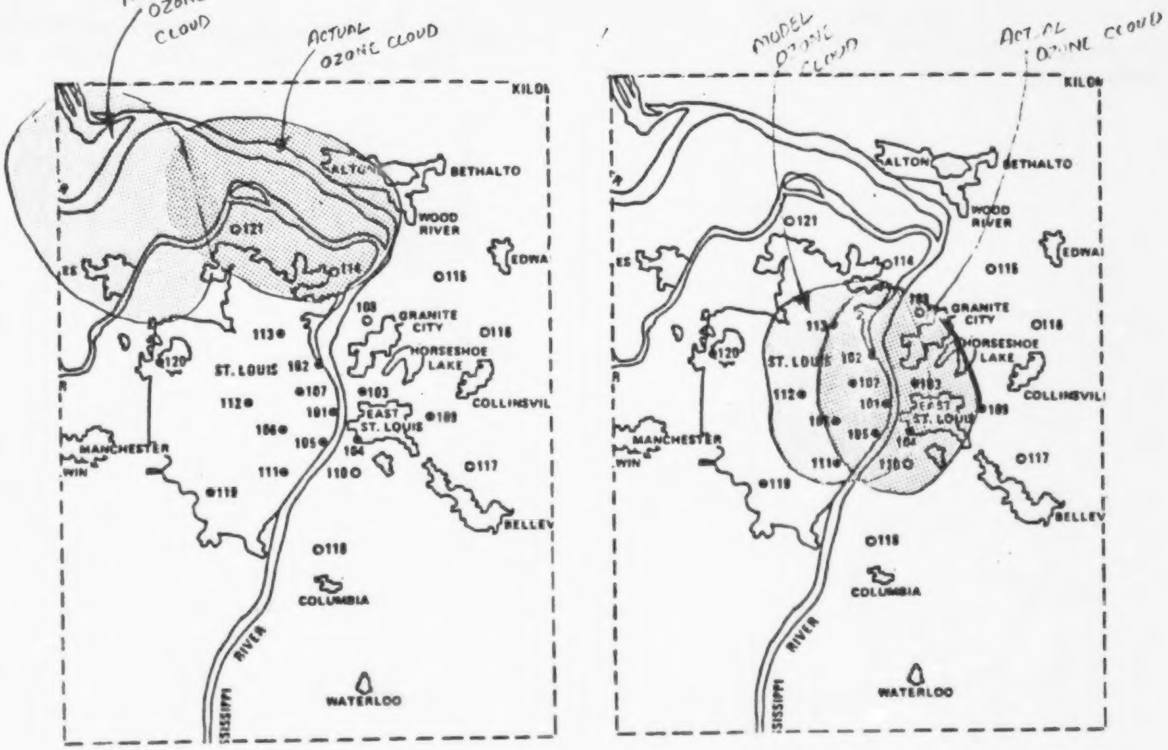

a. Transport Case

b. Stagnation Case

Figure 24. Conceptual diagram demonstrating the effect of advection on spatial displacement of peak ozone.

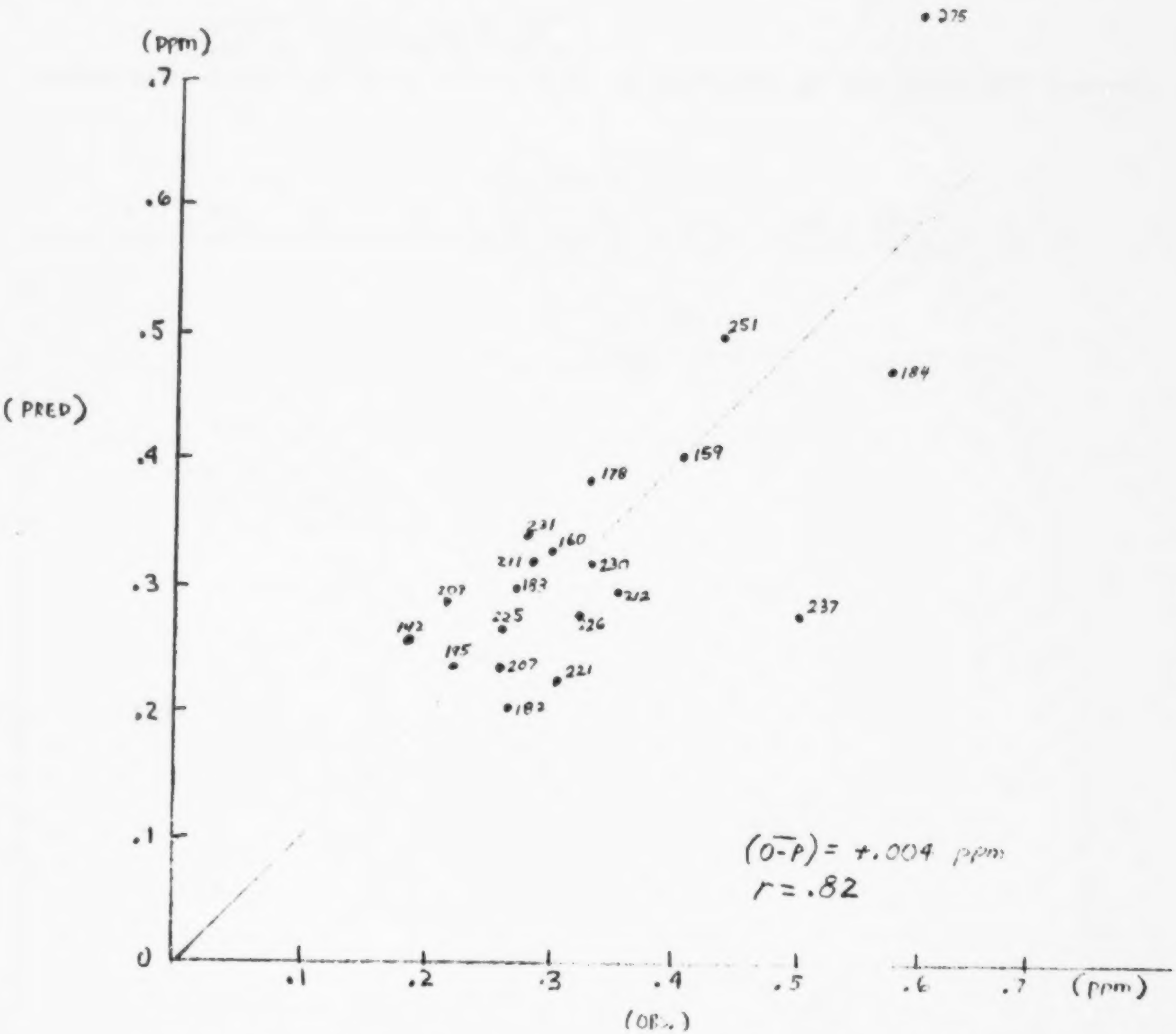

Figure 25a. Scatterdiagram of predicted vs. observed mean NMHC concentrations, averaged over all sites and all hours.
Numbers identify Julian Day.

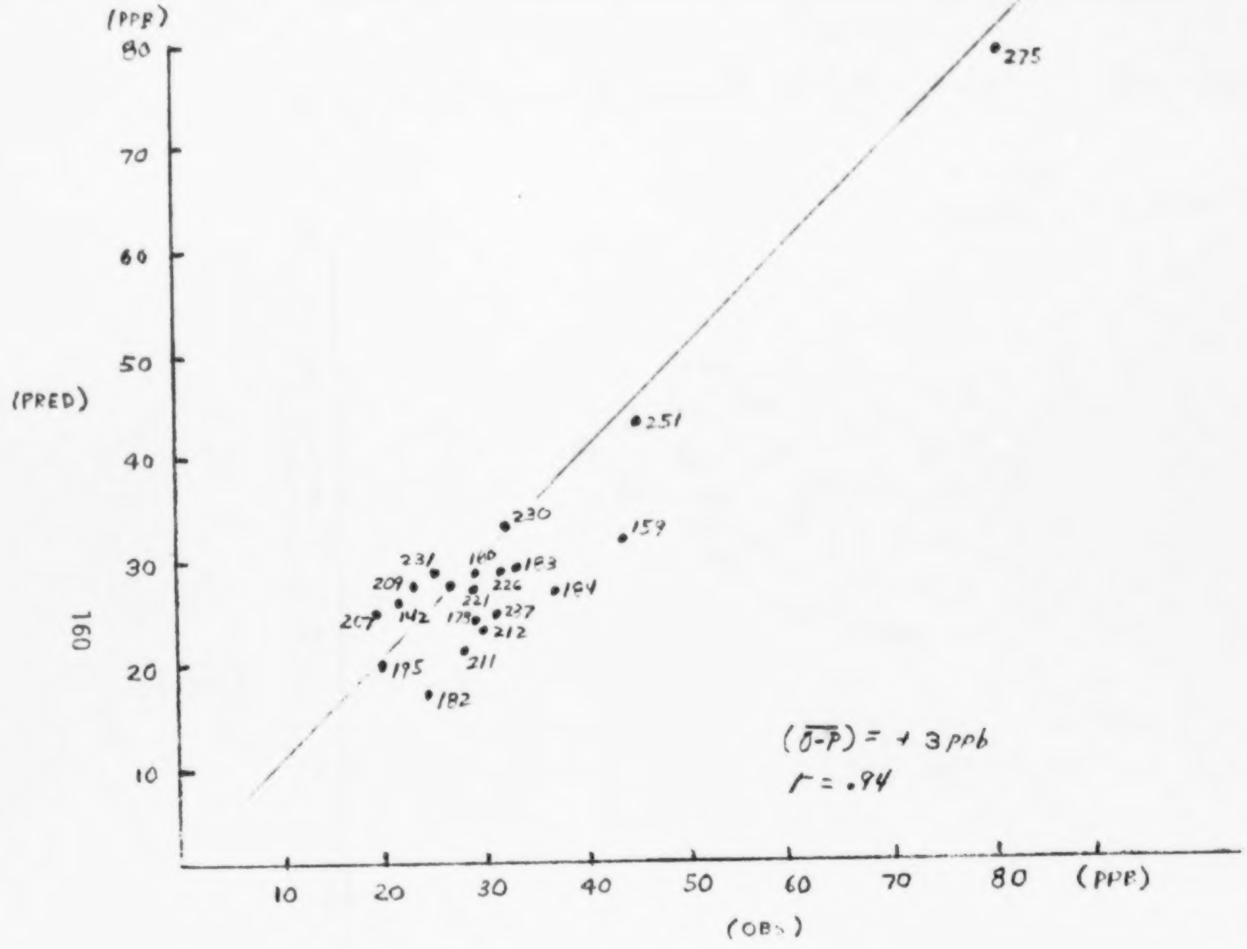

Figure 25b. Scatterdiagram of predicted vs. observed mean NO_x concentrations, averaged over all sites and all hours.
Numbers identify Julian Day.

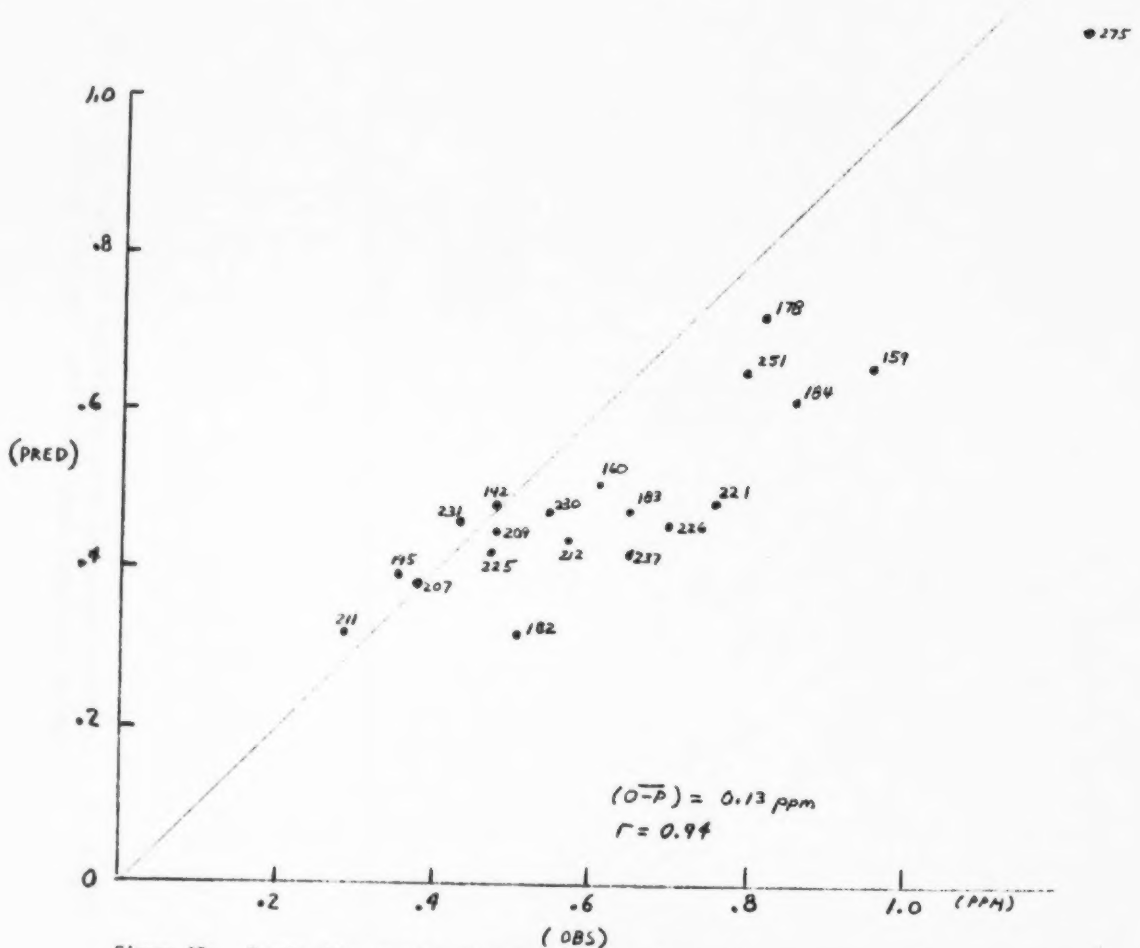

Figure 25c. Scatterdiagram of predicted vs. observed mean CO concentrations, averaged over all sites and all hours. Numbers identify Julian Day.

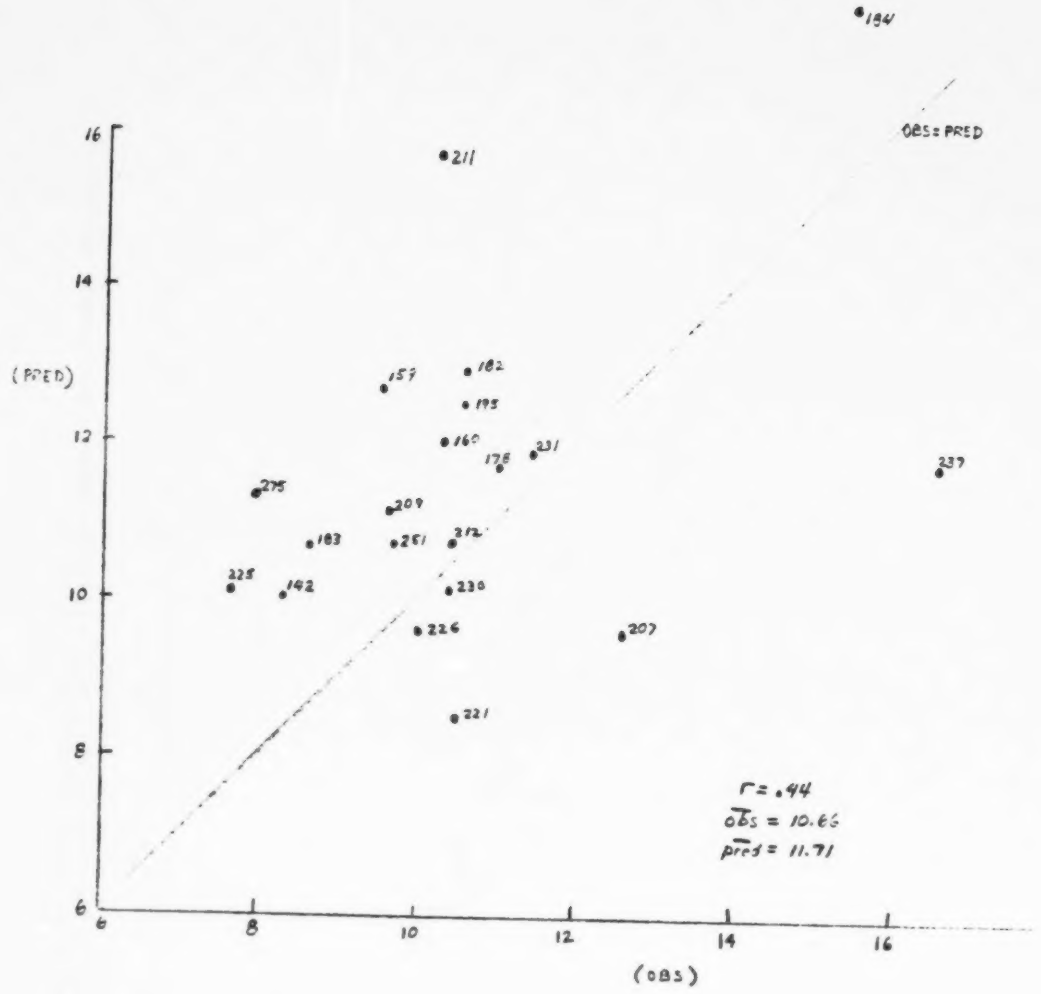

Figure 26. Scatterdiagram of mean predicted vs. observed NMHC/NO_x ratios averaged over all sites for all hours.

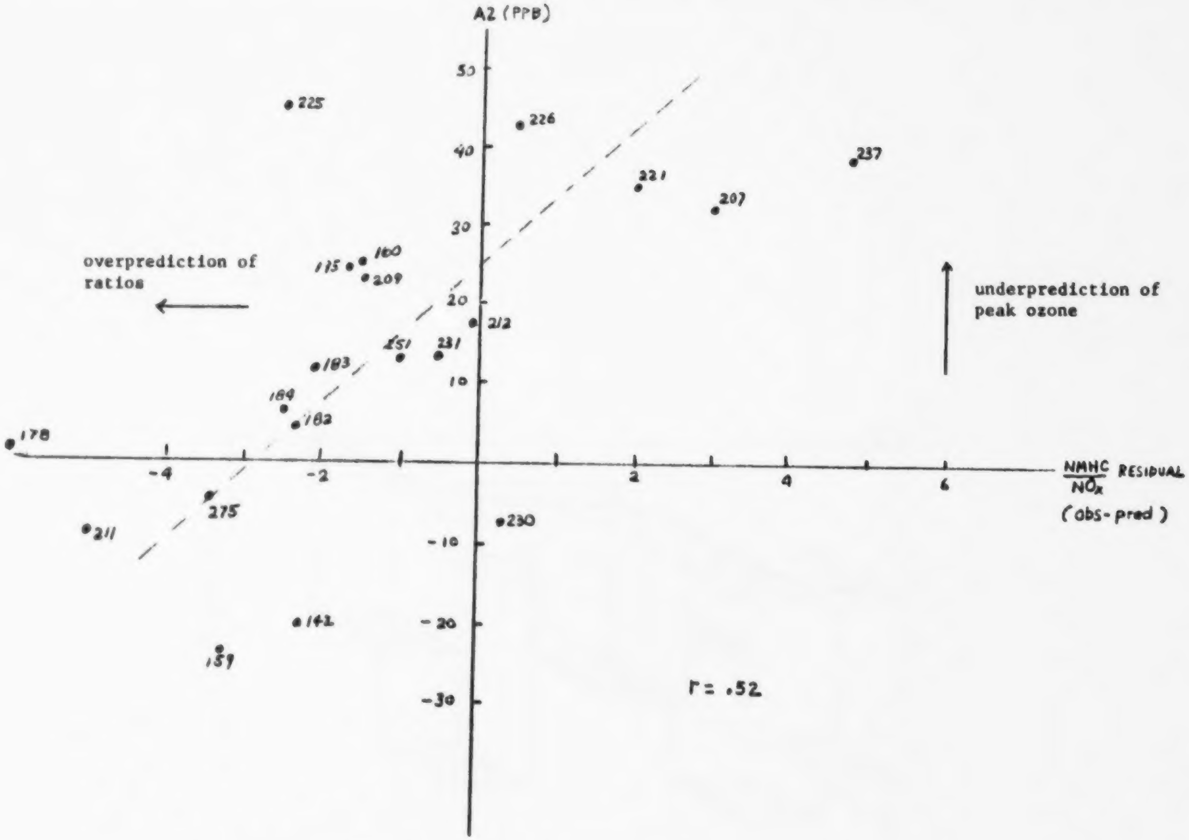

Figure 27. Scatterdiagram of A2 residuals (peak accuracy) vs. residuals of NMHC/NO_x. Positive residuals indicate underprediction.

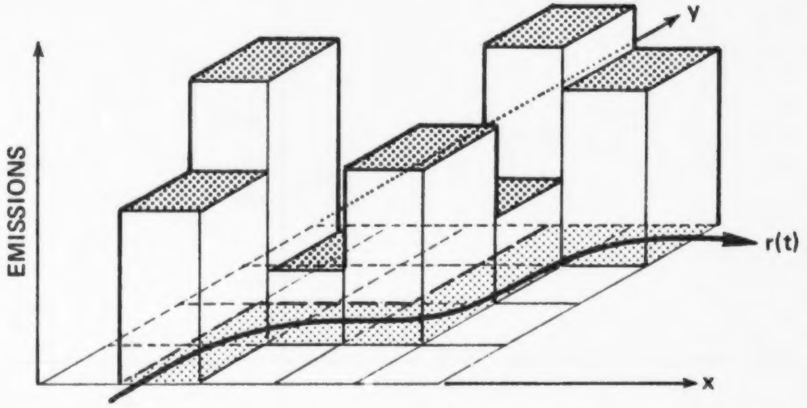

Figure 28. Emissions pattern along a hypothetical trajectory, r (t).

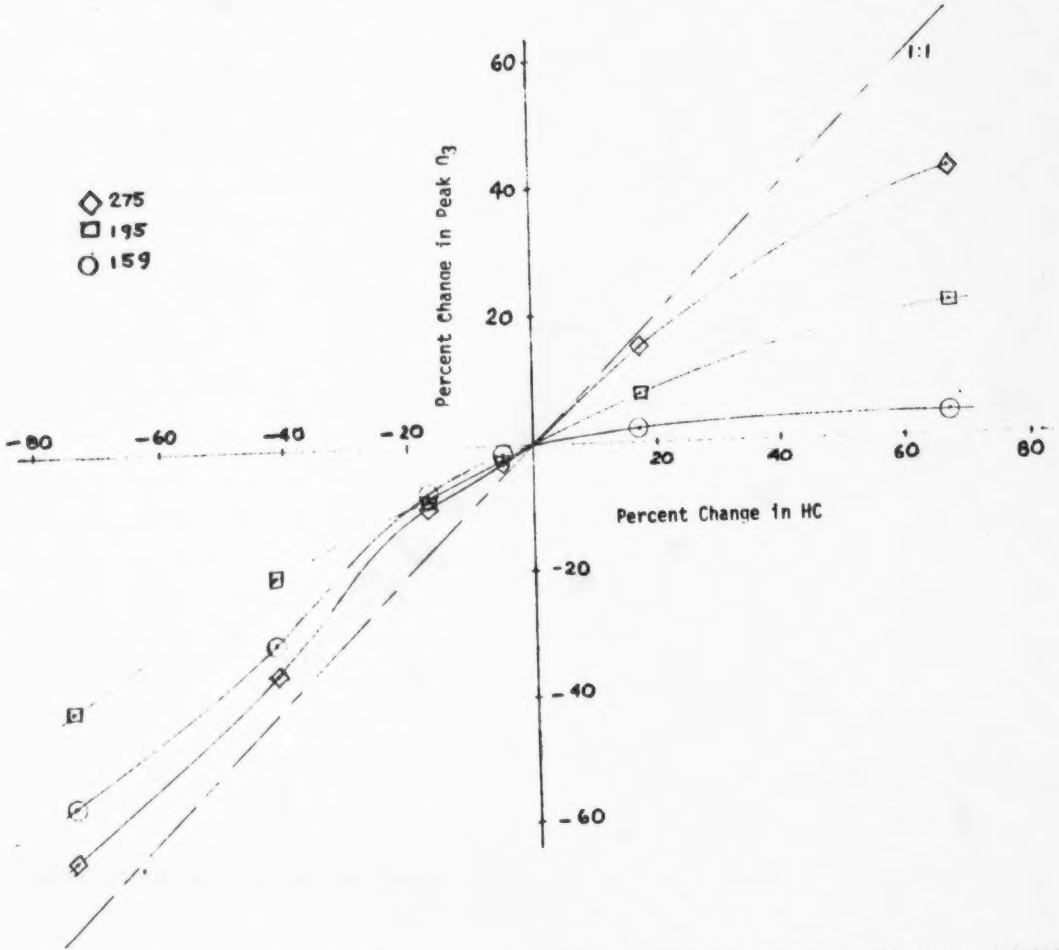

Figure 29. Response to peak ozone predictions to uniform changes in hydrocarbon emissions and initial conditions.

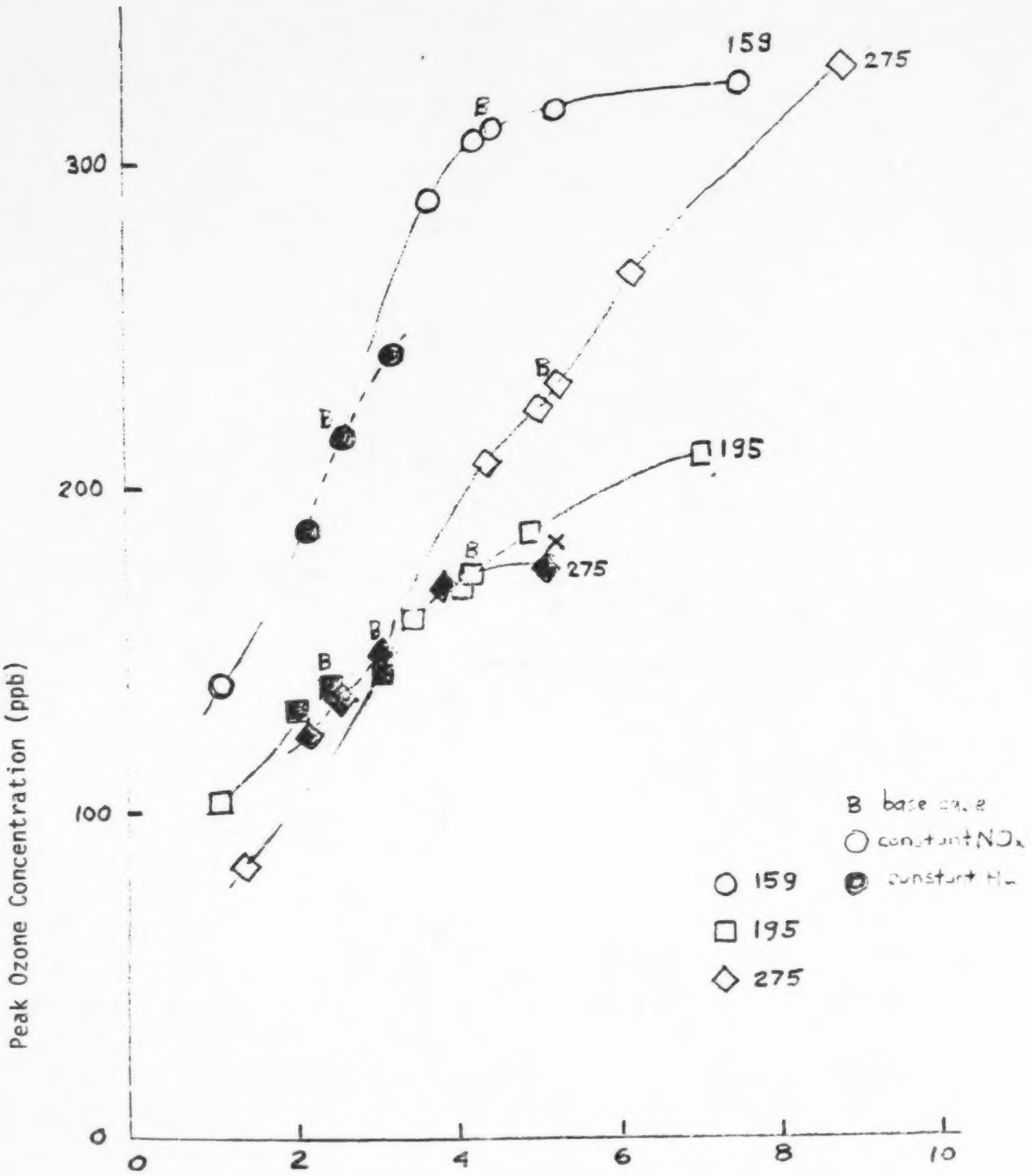

Figure 30. Effect of HC/NO$_x$ Ratio of Emissions on Peak Ozone Predictions (open symbols are constant NO$_x$; solid symbols are constant HC).

a. Day 159

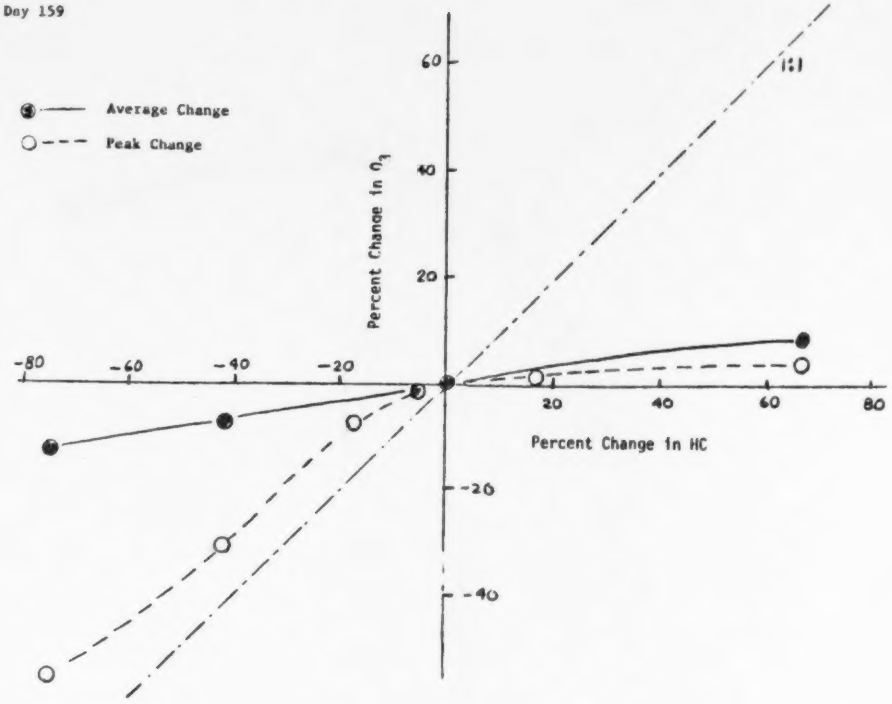

b. Day 195

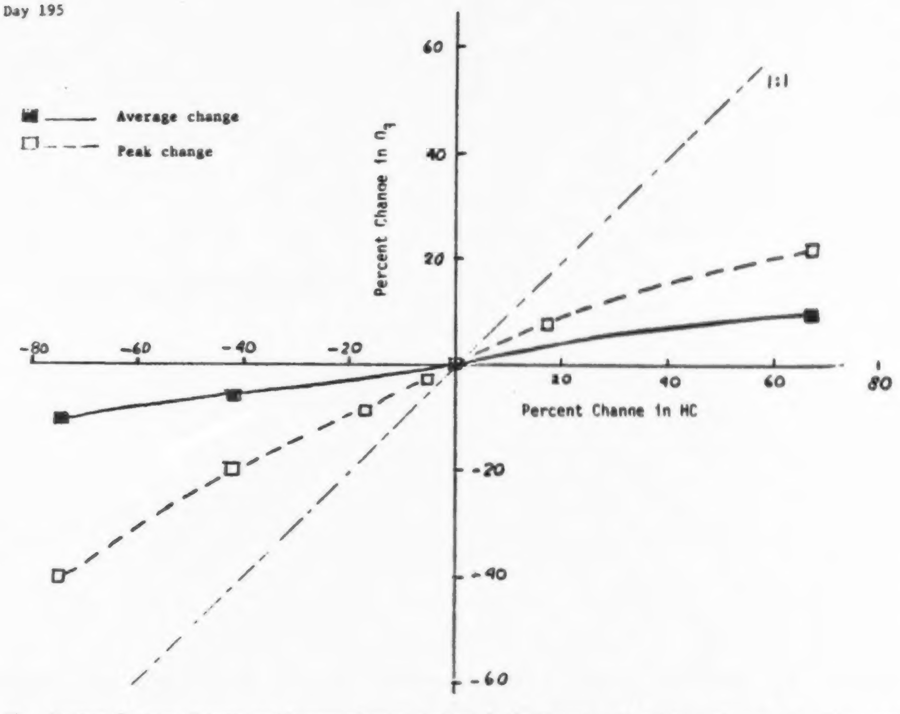

Figure 31. Average Percent Change and Percent Change in Peak O_3 in Response to Uniform Changes in Hydrocarbon Emissions.

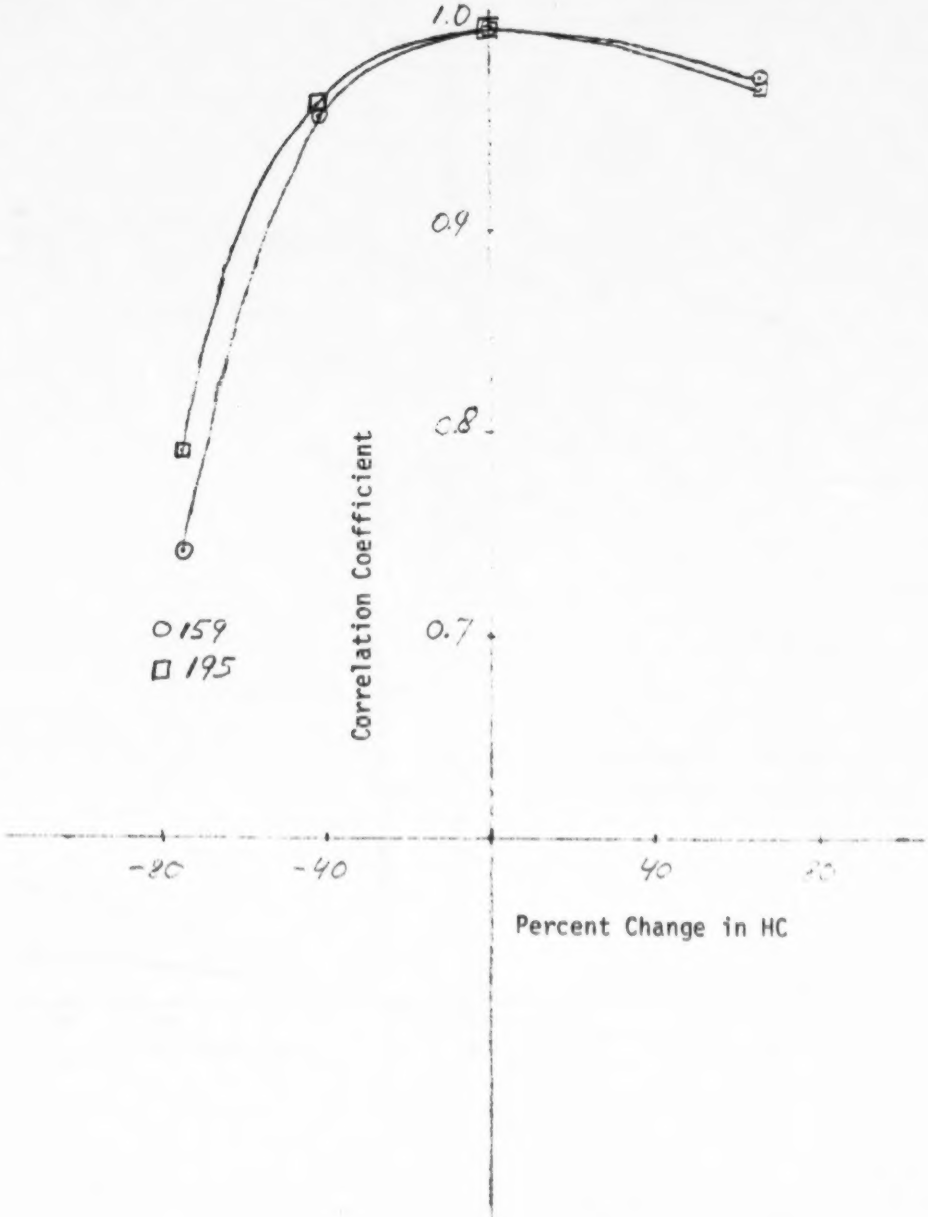

Figure 32. Spatial Correlation Coefficients of Base Case vs. Sensitivity Case Changes in Hydrocarbon Emissions.

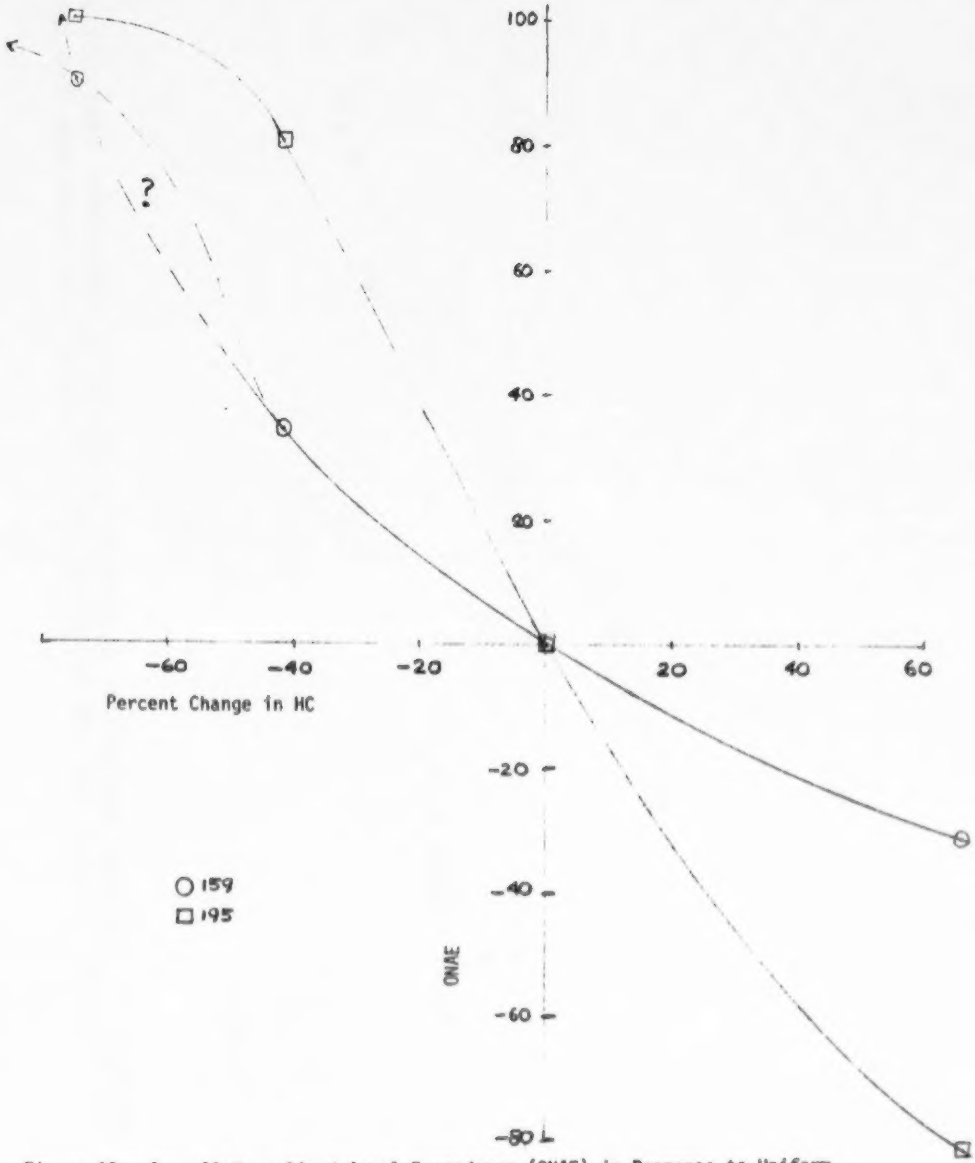

Figure 33. Overall Normalized Areal Exceedance (ONAE) in Response to Uniform Changes in Hydrocarbon.

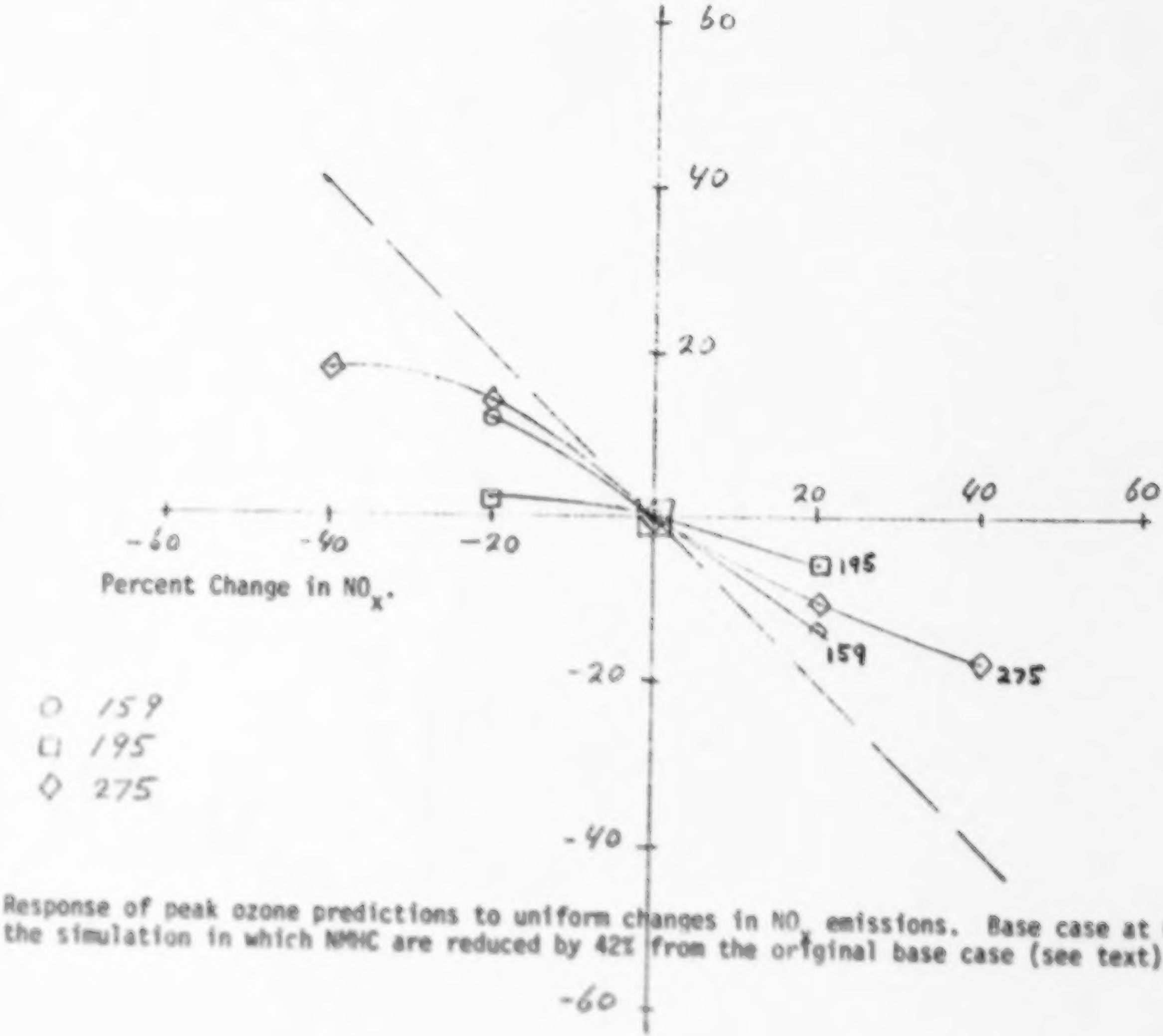

Figure 34. Response of peak ozone predictions to uniform changes in NO_x emissions. Base case at 0,0 is the simulation in which NMHC are reduced by 42% from the original base case (see text).

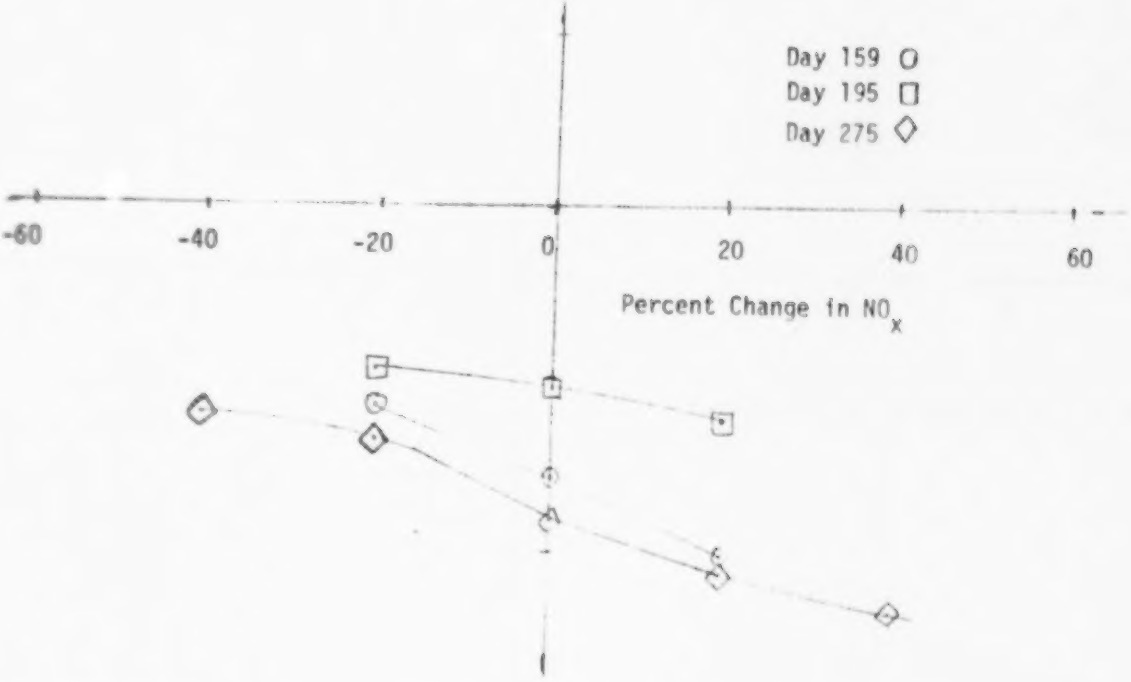

Figure 35. Modification of the effect of a 42% reduction in HC by uniform changes in NO_x.

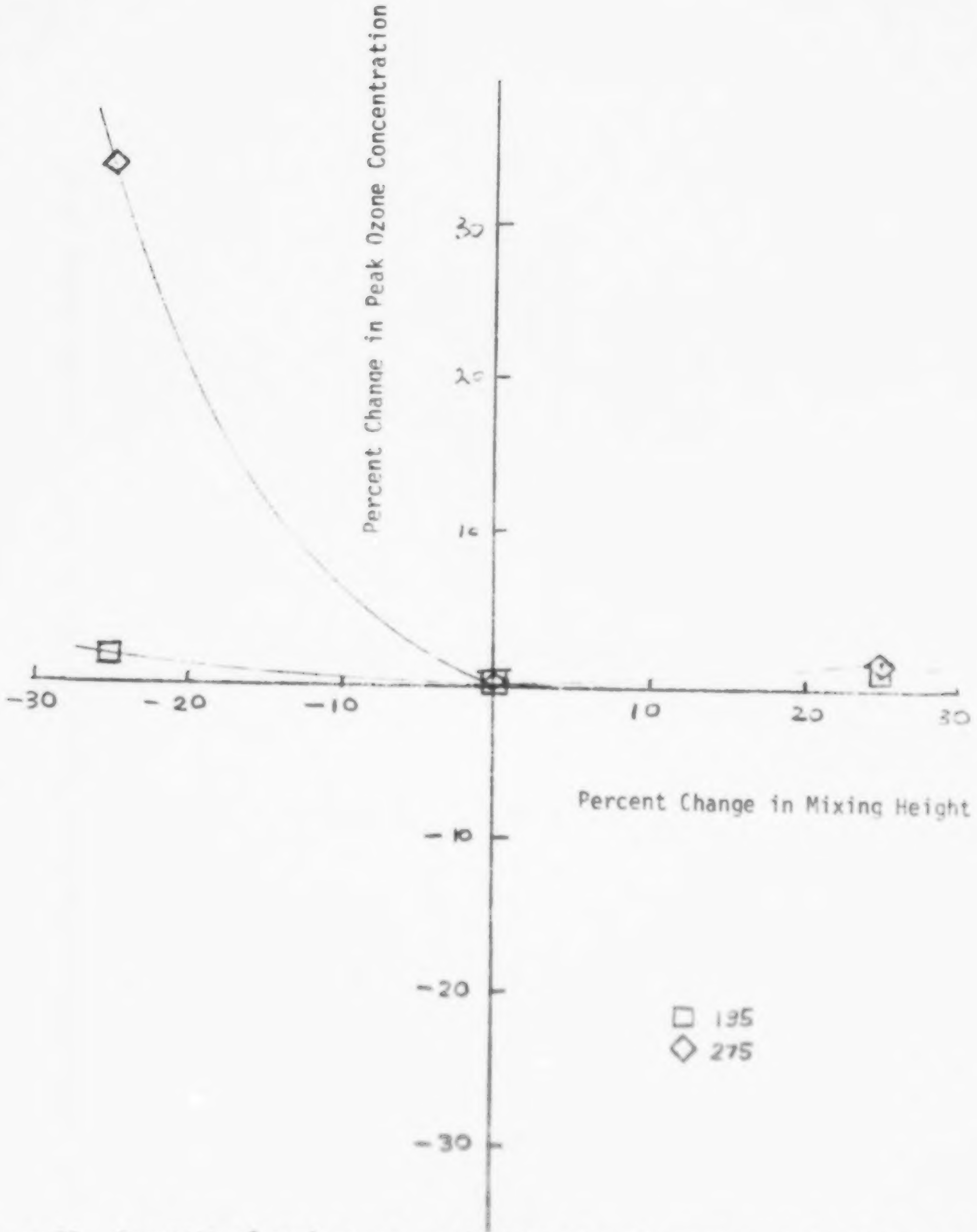

Figure 36. Response of peak ozone predictions to uniform changes in mixing height.

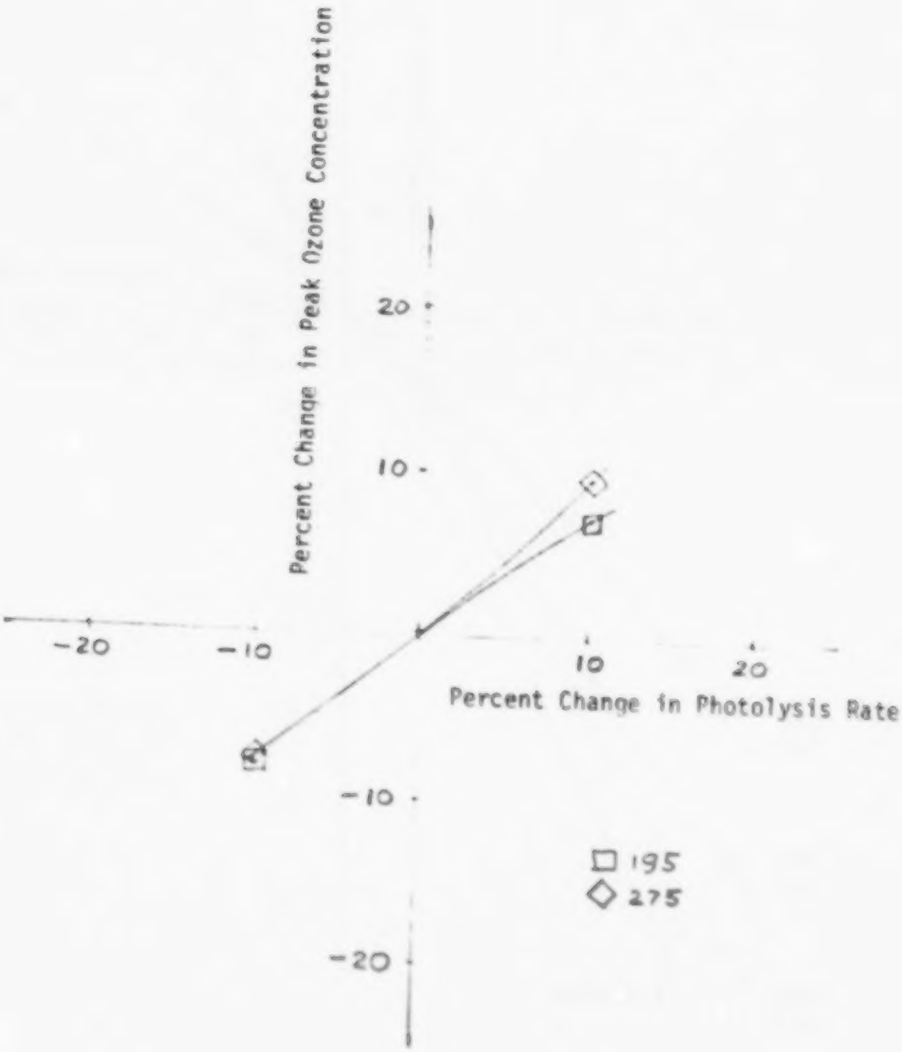

Figure 37. Response of peak ozone predictions to uniform changes in photolysis rate.

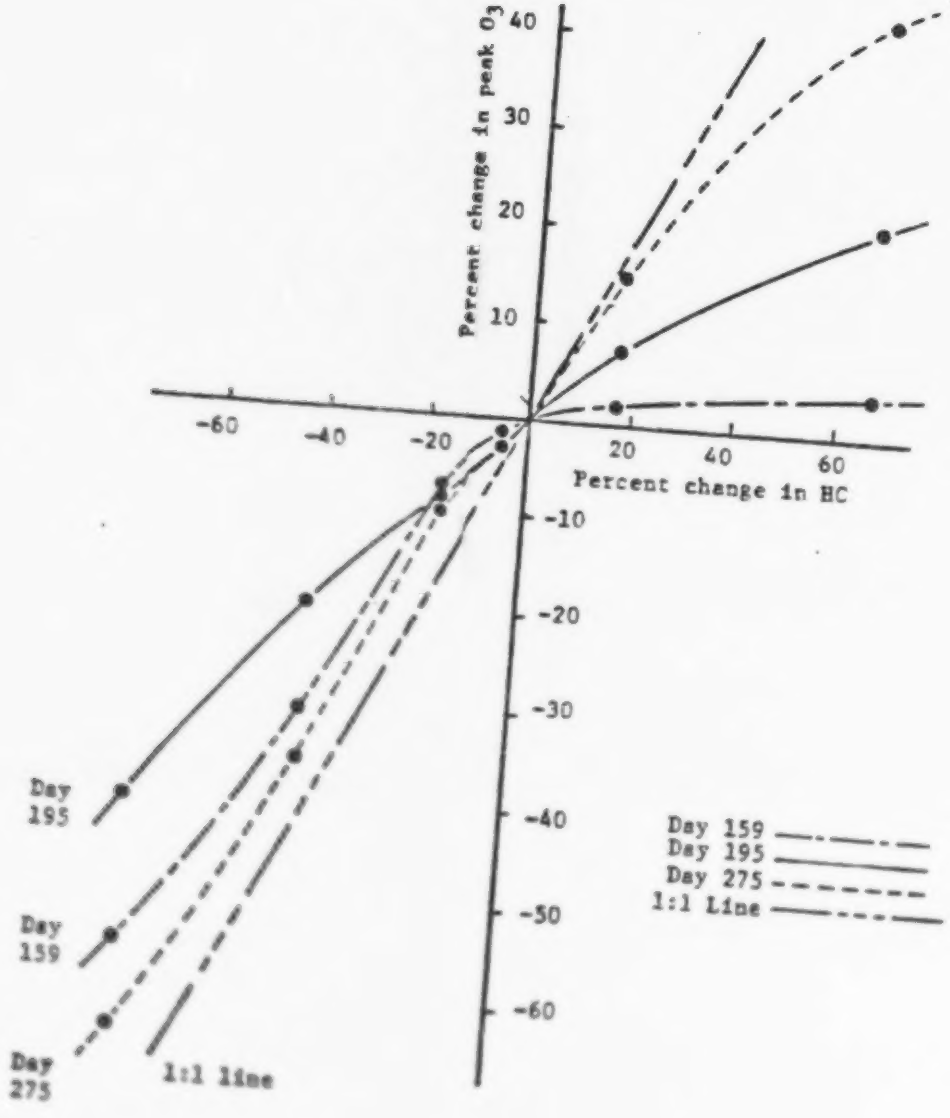

Figure 38. Response of Airshedpeak ozone to uniform changes in HC emissions for 3 ays.

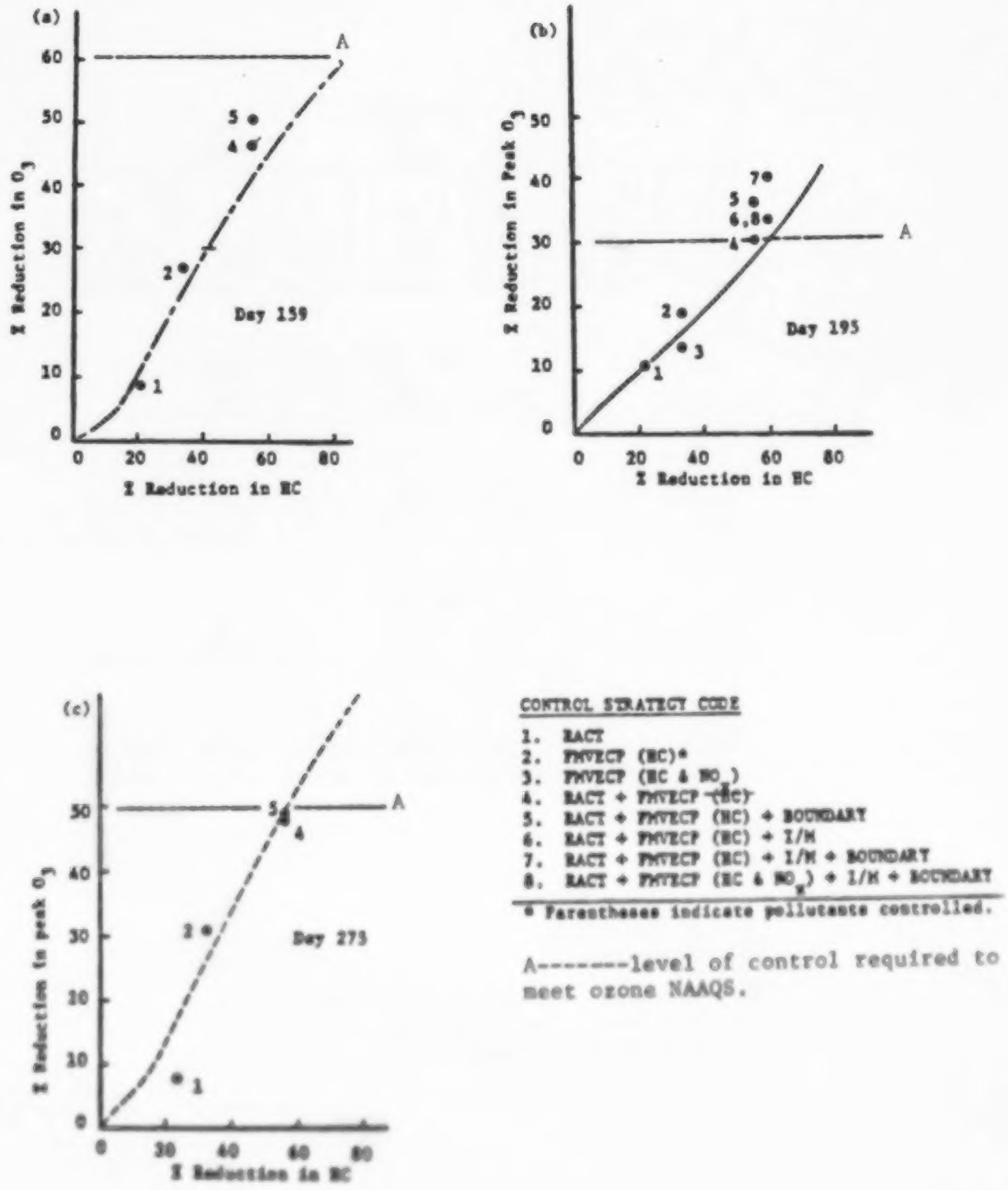

CONTROL STRATEGY CODE

1. RACT
2. FMVECP (HC)*
3. FMVECP (HC & NO_x)
4. RACT + FMVECP (HC)
5. RACT + FMVECP (HC) + BOUNDARY
6. RACT + FMVECP (HC) + I/M
7. RACT + FMVECP (HC) + I/M + BOUNDARY
8. RACT + FMVECP (HC & NO_x) + I/M + BOUNDARY

* Parentheses indicate pollutants controlled.

A--------level of control required to meet ozone NAAQS.

Figure 39. Control strategy simulations for 3 days. See text for further discussion.

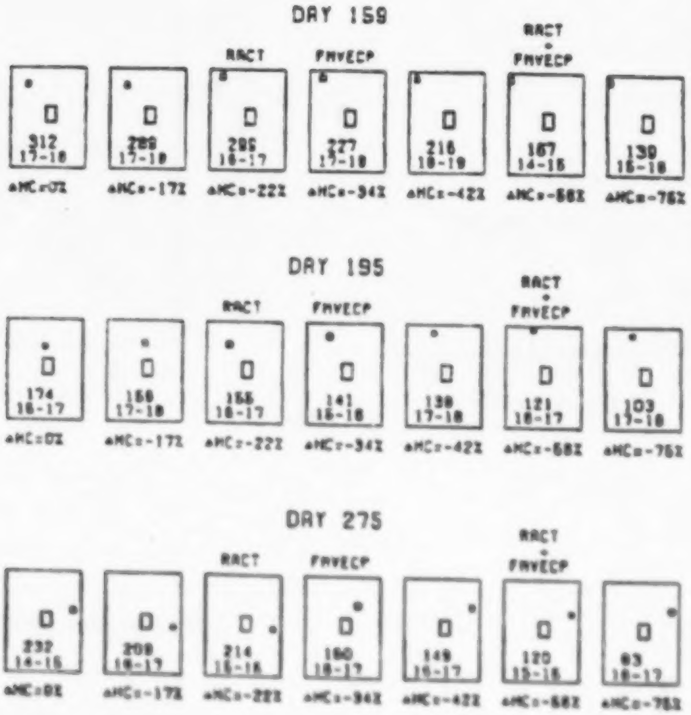

□ = Urban area.

■ = Location of predicted peak ozone.
(Concentration in ppb and time of
peak shown on each diagram.)

Figure 40. Summary of Airshed Control Strategy Simulations.

Table 1

[illegible]

[illegible] AREA SOURCE EMISSIONS INVENTORY

ANNUAL COUNTY SUMMARY FOR 1976 (EMISSIONS IN TONS)

*** AQCR 70 ***

SOURCE	PART	SOX	NOX	HC	CO	FUG DST
RIVER VESSELS	197.91	961.31	3378.69	693.12	1329.14	
FUGITIVE DUST						
UNPAVED ROADS	458605.11	.00	.00	.00	.00	
AGRI TILLING	80299.22	.00	.00	.00	.00	
WIND EROSION	324503.76	.00	.00	.00	.00	
CONSTRUCTION	138155.60	.00	.00	.00	.00	
AGGREGATE STORAGE	937.42	.00	.00	.00	.00	
UNPAVED AIRSTRIPS	409.03	.00	.00	.00	.00	
VEHICLES						
AREA SOURCES	990.99	424.74	9000.57	16685.92	139480.75	8802.70
LINE SOURCES	8910.85	2560.37	79797.36	100220.72	712249.52	58307.74
RAILROADS	877.80	2001.39	11960.34	4229.43	4359.57	
STN SRC F COMB						
RESID FUEL OIL	546.52	1572.61	655.13	162.83	273.41	
RESID NATURAL GAS	431.96	25.20	3453.36	345.06	862.97	
RESID LPG	305.95	1.66	1622.69	162.78	405.90	
RESID COAL	2079.13	9873.34	311.05	2079.13	9354.64	
COMM FUEL OIL	894.80	6676.13	2999.97	149.32	198.78	
COMM NATURAL GAS	218.11	11.90	2612.40	173.66	435.32	
COMM LPG	.00	.00	.00	.00	.00	
COMM COAL	1608.41	8497.15	528.47	114.85	413.61	
EVAP HC-SURF COATING	.00	.00	.00	9020.71	.00	
EVAP HC-AUTO. TANKS	.00	.00	.00	13246.47	.00	
EVAP HC-DRY CLEANING	.00	.00	.00	2925.34	.00	
STRUCTURAL FIRES	300.03	17.82	114.38	873.51	1825.27	
SOLID WASTE DISPOSAL	127.01	13.92	23.58	102.40	205.96	
PRINTING	.00	.00	.00	7993.58	.00	
DEGREASING	.00	.00	.00	5773.40	.00	
MISCELLANEOUS HC	.00	.00	.00	54258.25	.00	
OFF HIGHWAY MOBILE						
MOTORCYCLES	2.99	.43	1.82	220.62	423.08	
LAWN & GARDEN EQUIP	30.50	73.04	116.95	1438.33	11477.80	
FARM EQUIPMENT	390.41	276.68	3287.29	1951.32	23147.76	
CONSTRUCTION EQUIP	964.36	983.32	12651.56	1892.73	19508.18	
INDUSTRIAL EQUIP	733.99	678.49	8764.53	3056.10	66085.19	
OUTBOARD MOTORS	.00	44.83	45.64	7799.38	23475.40	
OTH INDUSTRIAL SOURCES	132.03	38.07	149.06	105.85	19.61	
AIRPORTS	57.39	46.88	341.89	1480.38	2902.97	
TOTAL	1267499.55	31199.16	142017.18	236856.05	1018234.74	

Table 2

```
01976AQCR76

               *********************************************************
               * NAPS POINT SOURCE SUMMARY EMISSIONS REPORT  07-13-82 *
               *********************************************************

                        AQCR(070):METROPOLITAN ST. LOUIS (ILL-MO)

                            EMISSIONS IN TONS/YEAR FOR 1976

                                   PART          SOX           NOX            HC            CO
                               ==========    ==========    ==========    ==========    ==========
FUEL COMBUSTION
**** **********
   EXTCOMB BOILER
      ELECTRIC GENERATN
         BITUMINOUS COAL        8357.20     853431.95     285523.83       2378.42       8017.95
         RESIDUAL OIL             28.95       4271.87       1320.65         12.58         62.89
         DISTILLATE OIL           10.70        547.68        297.64          9.24         45.37
         NATURAL GAS              10.72           .83        687.63          1.39         19.34
         TOTAL(ELECTRIC GENER)  8407.57     858252.31     287829.75       2401.62       8145.55

      INDUSTRIAL
         BITUMINOUS COAL        1617.50      24339.62       4230.93        162.95        382.79
         RESIDUAL OIL             54.50       1484.14        426.52          7.11         35.54
         DISTILLATE OIL            1.18         32.09         12.98           .59          2.95
         NATURAL GAS              72.33        171.31       3914.41         17.92        151.93
         PROCESS GAS                .00        116.81           .00           .00           .00
         OTHER/NOT CLASIFD        63.00       2254.00       1856.00           .00           .00
         TOTAL(INDUSTRIAL    )  1808.50      28398.18      10440.88        188.57        573.22

      COMMERCL-INSTUTNL
         BITUMINOUS COAL        1542.77       1592.04        199.02         13.27         26.54
         RESIDUAL OIL             24.12        348.39        129.39          2.18         10.78
         DISTILLATE OIL             .11          6.94          2.65           .12           .60
         NATURAL GAS               5.01           .57        123.82          1.77         10.34
         TOTAL(COMMERCL-INSTU)  1572.02       1947.94        454.89         17.32         48.26
      TOTAL(EXTCOMB BOILER)    11788.10     888598.38     298725.46       2607.51       8767.03

   INTERNLCOMBUSTION
      ELECTRIC GENERATN
         DIST.OIL/DIESEL            .29          1.60          3.86           .32           .88
         NATURAL GAS               1.48           .07        228.52         85.96         32.89
         TOTAL(ELECTRIC GENER)     1.77          1.67        232.38         86.28         33.76
      TOTAL(INTERNLCOMBUST)        1.77          1.67        232.38         86.28         33.76

   INTERNLCOMBUSTION
      ELECTRIC GENERATN
         DIESEL                     .04           .59          8.91           .71          1.94
         DIESEL FUEL               1.72           .58         15.71          1.26          3.42
         TOTAL(INDUSTRIAL    )     1.76          1.17         24.62          1.97          5.35
      TOTAL(INTERNLCOMBUST)        1.76          1.17         24.62          1.97          5.35
   TOTAL(FUEL COMBUSTION)      11791.63     888601.20     298982.46       2695.76       8806.15

INDUSTRIAL PROCESS
********** *******


      MISCELLANEOUS               16.72   [illegible]   [illegible]   [illegible]   [illegible]
      GRAIN ELEVATORS             34.04           .00           .00           .00           .00
      LEAD SMELTING             2871.41   [illegible]   [illegible]   [illegible]   [illegible]
      IRON/STEEL FOUNDY         3752.68        970.20         25.96           .00       2410.31
      UNSPECIFIED ORE          12197.91      19188.78   [illegible]           .00           .00
      MISCELLANEOUS             1997.10      40614.89       5512.92       6606.16      71004.60
      INPROCESS FUEL               3.12           .00   [illegible]          1.29          9.39
      DEGREASING                    .00           .00           .00         20.40           .00
      SURFACE COATING               .00           .00           .00   [illegible]           .00
      MISCELLANEOUS                 .00           .00           .00      14615.03           .00
      MARINE VESSELS                .00           .00           .00   [illegible]           .00
      MISCELLANEOUS                 .00           .00           .00          6.00           .00
      [illegible]           [illegible]   [illegible]   [illegible]   [illegible]   [illegible]

SOLID WASTE DISPOSAL
***** ***** ********
      GOVERNMENT
         MUNICIPAL INCIN    [illegible]   [illegible]   [illegible]   [illegible]   [illegible]
         TOTAL(GOVERNMENT    )  [illegible]   [illegible]   [illegible]   [illegible]   [illegible]
      TOTAL(SOLID WASTE DI)  [illegible]   [illegible]   [illegible]   [illegible]   [illegible]

GRAND TOTAL             [illegible]   [illegible]   [illegible]   [illegible]   [illegible]

                              **** E N D ****
```

Table 3

A Summary of Meteorological Conditions and Ozone Maxima for the 20 Days Examined[1]

Date	Day (Julian)	WS (m/s)	WD (deg)	Temp (°C)	Solar (ly/min)	Max MH (m)	Max O_3 observed 4-meters (ppb)	O_3 aloft (ppb)
5/22/75	142	1.1	224	29	1.12	1504	195	61
6/27/75	178	0.4	245	29	0.96	1822	202	76
7/01/75	182	1.4	70	29	0.99	2606	142[2]	122
7/02/75	183	1.4	15	30	0.92	2488	171[3]	120
7/03/75	184	1.8	324	30	0.85	1875	184	118
7/26/75	207	1.0	139	26	0.98	1477	185	74
7/28/75	209	2.0	18	30	0.98	1909	209	80
8/09/75	221	0.4	88	26	0.98	1195	166	79
8/18/75	230	1.6	167	27	0.96	1488	193	63
8/19/75	231	1.3	168	28	0.95	1052	233	58
9/08/75	251	1.8	181	25	0.89	1797	179[4]	57
6/07/76	159	1.0	129	25	1.06	1972	172[4]	114
6/08/76	160	1.3	284	27	1.01	1772	221	107
7/13/76	195	2.3	145	28	1.02	1853	223	78
7/29/76	211	0.3	251	26	0.53	1706	155	49
7/30/76	212	1.7	205	30	0.82	1304	170	108
8/12/76	225	2.3	253	29	0.70	730	166	69
8/13/76	226	1.1	273	30	0.86	1427	225	86
8/24/76	237	1.3	110	28	0.82	2124	176	105
10/01/76	275	0.6	222	22	0.78	527	244	63

Notes:

[1] Meteorological variables (except MH) are network averages over the period 0700-1359 CST.

[2] Higher maximum recorded at station 125, located west of the modeling region.

[3] Higher maximum recorded at station 124, located south of the modeling region.

[4] Higher maximum recorded at station 122, located north of the modeling region.

Table 4

DESCRIPTION OF THE INPUT FILES TO THE AIRSHED MODEL

DIFFBREAK	This file contains the mixing height for each column of cells at the beginning and end of each hour of the simulation.
REGIONTOP	This file contains the height of each column of cells at the beginning and end of each hour of the simulation. If this height is greater than the mixing height, the cell or cells above the mixing height are assumed to be within an inversion.
WIND	This file contains the x and y components of the wind velocity for every grid cell for each hour of the simulation. Also the maximum wind speed for the entire grid and average wind speeds at each boundary for each hour are included on this file.
METSCALARS	This file contains the hourly values of the meteorological parameters that do not vary spatially. These scalars are the NO_2 photolysis rate constant, the concentration of water vapor, the temperature gradient above and below the inversion base, the atmospheric pressure, and the exposure class.
AIRQUALITY	This file contains the initial concentrations of each species for each grid cell at the start of the simulation.
BOUNDARY	This file contains the location of the modeling region boundaries. This file also contains the concentration of each species that is used as the boundary condition along each boundary segment at each vertical level.
TOPCONC	This file contains the concentration of each species for the area above the modeling region. These concentrations are the boundary conditions for vertical integration.
TEMPERATUR	This file contains the hourly temperature for each surface layer grid cell.
EMISSIONS	This file contains the ground level emissions of NO, NO_2, five carbon bond categories, and CO for each grid square for each hour of the simulation.
PTSOURCE	This file contains the point source information, including the stack height, temperature and flow rate, the plume rise, the grid cell into which the emissions are emitted, and the emissions rates for NO, NO_2, five carbon bond categories, and CO for each point source for each hour.
TERRAIN	This file contains the value of the surface roughness and deposition factor for each grid square.

Table 5

Example of an array of predicted and observed concentrations from which performance measures are calculated*

DAY 226

HR/STN		101	102	103	104	105	106	107	108	109	110	111	112	113	114	115	116	117	118	119	120	121	MAX	
5	OB	4	3	3	3	3	-8	3	3	3	6	-8	-8	5	-8	-8	3	3	15	-8	-8	21	21	
	PR	2	2	2	3	4	3	4	2	5	9	9	7	6	3	6	5	12	19	15	7	15	19	
6	OB	3	3	3	4	3	-8	4	3	5	12	-8	-8	3	-8	-8	4	3	11	-8	-8	23	23	
	PR	10	11	10	16	20	19	16	17	19	33	32	24	17	20	34	31	36	43	32	20	30	43	
7	OB	9	21	-8	20	4	-8	17	21	19	15	-8	-8	21	-8	-8	14	-8	15	-8	-8	46	46	
	PR	22	25	22	29	30	20	29	31	30	43	30	29	31	36	47	43	46	50	31	22	36	50	
8	OB	41	48	-8	25	17	-8	42	74	38	23	-8	-8	50	-8	-8	51	-8	34	-8	-8	59	74	
	PR	28	33	30	35	34	31	33	40	40	46	30	33	34	43	54	55	54	40	35	33	39	55	
9	OB	69	83	-8	59	65	-8	73	107	89	56	-8	-8	85	-8	-8	90	-8	64	-8	-8	82	107	
	PR	34	43	38	38	38	39	42	48	44	46	44	40	43	48	66	66	62	49	40	37	46	66	
10	OB	-8	106	117	89	94	-8	98	116	141	125	-8	-8	106	-8	-8	136	-8	105	-8	-8	98	141	
	PR	43	51	50	44	43	42	48	68	53	53	47	44	48	55	68	84	67	51	48	59	50	84	
11	OB	-8	122	134	117	121	-8	102	121	180	144	-8	-8	126	-8	-8	147	-8	129	-8	-8	87	180	
	PR	47	55	52	46	46	45	54	58	63	58	53	53	53	59	71	86	79	51	71	76	66	86	
12	OB	-8	122	122	125	130	-8	103	128	196	-8	-8	-8	142	-8	-8	158	-8	-8	123	-8	-8	196	
	PR	54	70	56	51	52	56	68	65	69	58	72	74	72	68	67	92	94	62	92	85	82	92	
13	OB	-8	129	178	131	136	-8	99	129	225	178	-8	-8	142	-8	-8	142	-8	139	125	-8	91	225	F2
	PR	61	90	60	57	57	66	84	76	77 F1	75	90	86	90	71	65	101	104	85	100	89	90	101	A1
14	OB	-8	133	-8	140	109	-8	116	124	-8	-8	-8	-8	139	-8	-8	180	-8	-8	120	-8	-8	180	
	PR	75	104	84	78	68	70	103	83	97	80	96	96	99	74	67	98	112	99	109	96	94	109	
15	OB	-8	149	-8	182	180	-8	120	132	-8	-8	-8	-8	124	-8	-8	170	-8	-8	125	-8	-8	180	
	PR	81	111	102	98	77	79	111	89	114	96	92	108	102	64	71	87	112	106	117	107	98	117	
16	OB	-8	146	150	134	143	-8	132	155	146	137	-8	-8	101	-8	-8	139	-8	121	153	-8	80	155	
	PR	69	104	112	108	94	79	91	100	109	112	101	105	101	78	73	60	80	97	119	117	83	119	
17	OB	-8	121	116	88	108	-8	104	124	118	107	-8	-8	136	-8	-8	111	-8	116	-8	-8	69	136	
	PR	105	98	111	111	118	97	86	103	64	111	104	84	88	95	68	88	36	82	100	111	72	111	
18	OB	66	86	89	87	78	-8	72	92	83	86	-8	-8	87	-8	-8	83	-8	80	-8	-8	83	92	
	PR	79	83	69	90	80	86	90	86	21	80	79	87	81	84	18	12	16	50	65	80	83	90	
19	OB	86	88	61	58	96	-8	40	50	65	67	-8	-8	89	-8	-8	87	-8	72	-8	-8	71	72	
	PR	27	42	19	25	32	30	43	12	12	21	29	34	83	48	12	3	13	10	10	48	69	69	
20	OB	31	27	41	32	88	-8	17	37	80	40	-8	-8	25	-8	-8	80	-8	43	-8	-8	43	88	
	PR	1	4	1		1	1	5	6	7	1		1	11	17	10	9	3		1	20	38	38	
MAX	OB	89	149	178	182	180		132	155	225	178			142			180	3	139	153		91	225	F4
	PR	79	111	112	111	118		111	103	114 F3	112			102			101	36	97	119		90	119	

A2

*The F and A measures are defined in Table 6. Missing values are denoted by the value -8.

Table 6a

Measures Calculated for Each Day Separately

Measure Pairing Method	Residual* (d)	Number of Residuals Per Day	Bias ($\bar{d}$)	Standard Deviation of S	95% Confidence Intervals on Bias
F1 (Totally Paired)	✓	1	NA	NA	NA
F2 (Paired in Time)	✓	1			
F3 (Paired in Space	✓	1			
F4 (Unpaired)	✓	1			
A1 (Paired in Time)	✓	N hrs	$\bar{d} = \Sigma d/N$	S_d✓	✓
A2 (Paired in Space)	✓	M sites	$\bar{d} = \Sigma d/M$	S_d✓	✓
A4 (Unpaired,** highest 25)		25 obs. 25 pred.	$\bar{d} = \bar{O}-\bar{P}$	S_o✓ S_p✓	✓

---

*All residuals (d) are based on O-P (Observed minus predicted concentrations) thus positive residual or bias is underprediction.

**A4 is an unpaired bias calculated as follows

$$\bar{d} = (\bar{O})_{25} - (\bar{P})_{25}$$

where $(\bar{O})_{25}$ is the average of the highest 25 observed values for the day and $(\bar{P})_{25}$ is the average of the highest 25 predicted values for the day.

Table 6b.

Measures for 20-Day Data Set

Pairing Method \ Measure	20 Day Bias Estimate	Standard Deviation of Bias, 95% Confidence Intervals	Scatter Diagrams and Correlation Coefficients of Predicted vs. Observed Concentrations
F1 (Totally paired)	$\bar{d} = \frac{\Sigma d}{20}$	S_d	(O vs. P) Diagrams and r values obtained with the 4 different pairings. Each diagram contains 20 points, 1 per day
F2 (Paired in Time			
F3 (Paired in Space)			
F4 (Unpaired)	See (a)	See (a)	
A1 (Paired in Time)	$d = \frac{\Sigma \bar{d}}{20}$	$S_{\bar{d}}$	($\bar{O}$ vs. $\bar{P}$) Diagram and r values obtained with the 3 different pairings of average observed and predicted concentrations
A2 (Paired in Space)		$S_{\bar{d}}$	
A4 (Unpaired, highest 25)	See (b)	$S_{\bar{o}}, S_{\bar{p}}$ See (c)	

a. For the F measures, the 20-day bias is the average of single residuals (d, Table 6a). $S^2_d = \Sigma(d_i - \bar{d})^2/(20-1)$ i = day

b. For the A measures, the 20-day bias is the average of average residuals ($\bar{d}$, Table 6a).

The average standard deviations for the 20 days are obtained as follows:

$$S^2_{\bar{d}} = \sum^{20}(\bar{d}_i - \bar{\bar{d}})^2/(20-1) \quad i = \text{day}$$

$$S^2_{\bar{o}} = \sum^{20}(\bar{o}_i - \bar{\bar{o}})^2/(20-1) \quad i = \text{day}$$

$$S^2_{\bar{p}} = \sum^{20}(\bar{p}_i - \bar{\bar{p}})^2/(20-1) \quad i = \text{day}$$

c. 95% confidence intervals are constructed as follows:

$\bar{d} \pm t_{.025}\, S/\sqrt{N}$ where N = number of days

S = appropriate standard deviation (S_d for paired analysis and $\sqrt{S^2_o + S^2_p}$ for F4 and A4, unpaired measures).

Table 7

Procedures to Assess Overall Accuracy and Precision*

Attribute	Accuracy			Precision		
Measure Pairing/ Stratification	Frequency Distribution (O vs. P)	Bias ($\bar{d}$)	Avge. Absolute Error $\lvert\bar{d}\rvert$	Standard Deviation S	95% Confidence Intervals	Other
Paired Analysis						For all pairs:
1. All pairs		✓	✓	S_d ✓	✓	Scatter diagrams of observed vs. predicted concentration.
2. ≥ 80 ppb**		✓	✓	S_d ✓	✓	
3. ≥ 120 ppb***		✓	✓	S_d ✓	✓	Analysis of spatial and temporal distribution of errors.
Unpaired Analysis	✓	✓		S_o ✓ S_p ✓	✓	

Formulae **Paired** **Unpaired**

Paired:

$\bar{d} = \frac{1}{N}\sum^{N} d_i$ and $d_i = O_i - P_i$

$S^2_d = \frac{1}{N-1}\Sigma(d_i - \bar{d})$

95% intervals: $\bar{d} \pm t_{.025}\, S_d/\sqrt{N}$

(ith pair, N = number of pairs)

Unpaired:

$\bar{d} = \bar{O} - \bar{P}$

$S^2_o = \frac{1}{N-1}\Sigma(O_i - \bar{O})$

95% intervals: $\bar{d} \pm t_{.025}\left(\frac{S^2_o}{N} + \frac{S^2_p}{N}\right)^{1/2}$

N observations and predictions)

---

*Statistics were calculated separately for each day.

**Pairs with observed or predicted values ≥ 80 ppb.

***Pairs with observed or predicted values ≥ 120 ppb.

Table 8

Procedures to Assess the Model's Ability to Replicate Spatial and Temporal Patterns

I. Spatial Patterns

A. Visual comparison of spatial plots of observed and predicted ozone concentrations for the hour of maximum observed ozone concentration. Comparison of exceedance zones.

B. Spatial Correlation Coefficients (for each day)

r_{s_m}	is the spatial correlation coefficient for the hour of the maximum observed concentration.
$\overline{r}_s$	is the average spatial correlation coefficient (averaged over all hours).

where

$$r_{sm} = \frac{\sum^{I} (O_{im} - \overline{O}_m)(P_{im} - \overline{P}_m)}{\left[\sum^{I} (O_{im} - \overline{O}_m)^2 \sum^{I} (P_{im} - \overline{P}_m)^2\right]^{1/2}}$$

where

O_{im}	is the observed ozone for station i at the hour of the maximum observed ozone
P_{im}	is the predicted ozone for station i at the hour of the maximum observed ozone.
$\overline{O}_m$	is the mean observed ozone at the time of the observed maximum averaged over all sites.
$\overline{P}_m$	is the mean predicted ozone at the time of the observed maximum averaged over all sites.
I	is the number of sites;

and

$$\overline{r}_s = \frac{1}{T} \sum^{T} r_{s_t}$$

where T is the number of hours and r_{st} is the spatial correlation coefficient for hour t.

Table 8 continued

II. Temporal Patterns

A. Visual comparison of time series for observed and predicted ozone for each day.
  1. for the station of the maximum observed ozone.
  2. averaged over all stations.

B. Temporal Correlation Coefficients (for each day)

r_{t_m} is the temporal correlation coefficient for the station of the observed maximum concentration.

$\overline{r}_t$ is the average temporal correlation coefficient (averaged over all stations).

where

$$r_{t_m} = \frac{\sum^{T} (O_{tm} - \overline{O}_m)\ (P_{tm} - \overline{P}_m)}{[\sum^{T} (O_{tm} - \overline{O}_m)^2 \sum^{T} (P_{tm} - \overline{P}_m)^2]^{1/2}}$$

where

O_{tm} is the observed ozone for hour t at the site of the maximum observed ozone;

P_{tm} is the predicted ozone for hour t at the site of the maximum observed ozone.

$\overline{O}_m$ is the mean observed concentration at the site of the maximum observed ozone, averaged over all hours;

$\overline{P}_m$ is the mean predicted ozone concentration at the site of the maximum observed ozone averaged over all hours;

T is the number of hours,

and

$$\overline{r}_t = \frac{1}{I} \sum^{I} r_{t_i}$$

where I is the number of sites and r_{t_i} is the temporal correlation coefficient for site i.

Table 8 continued

III. Overall Correlation

r = overall correlation coefficient for each day

$$r = \frac{\overset{TI}{\Sigma\Sigma} (O_{ti} - \overline{O}) (P_{ti} - \overline{P})}{[\overset{TI}{\Sigma\Sigma} (O_{ti} - \overline{O})^2 \overset{TI}{\Sigma\Sigma} (P_{ti} - \overline{P})^2]}$$

where

T = number of hours

I = number of sites

O_{ti} = observation at hour t, site i

$\overline{O}$ = daily mean concentration averaged over all sites and hours

P_{ti} = prediction at hour t, site i

$\overline{P}$ = daily mean concentration averaged over all sites and hours.

Table 9a

"A" and "F" Residuals of Peak Accuracy for each of 20 Days*

								A-1			A-2				A-4		
DAY	MAX OBS	OBS SPA AVG (42)	F1	F2	F3	F4	AVG RESID	LOW CL	UPP CL	AVG RESID	LOW CL	UPP CL	O-BAR	P-BAR	D-BAR	LO-CL	UP-CL
142	195	142	79	36	46	3	-6.7	-24	11	-20.5	-38	-3	141.8	170.6	-28.8	-39.1	-18.5
178	202	168	46	-1	46	-34	-12.1	-36	11	2.4	-17	21	175.4	194.5	-19.1	-27.0	-11.2
182	142	104	59	24	39	17	5.1	-5	15	3.9	-3	11	122.6	110.9	11.7	7.3	16.2
183	171	132	17	17	17	17	11.9	1	23	11.2	1	22	142.2	126.2	16.1	10.6	21.6
184	184	109	52	52	51	34	14.0	-4	32	5.6	-10	21	141.6	124.1	17.6	9.6	25.5
207	185	141	44	44	44	28	15.1	1	29	32.0	18	46	157.4	156.6	.8	-14.9	16.6
209	210	117	82	82	82	82	26.6	4	49	23.7	9	38	140.0	100.0	40.0	27.7	52.3
221	166	122	48	48	22	22	20.1	11	29	34.5	19	50	142.8	101.2	41.6	33.6	49.6
230	193	89	98	95	75	75	4.8	-18	27	-8.1	-29	13	111.7	100.5	11.2	-1.7	24.0
231	233	102	100	100	72	72	22.8	3	43	12.7	-2	27	128.2	104.0	24.2	9.0	39.4
251	179	99	33	33	33	33	13.0	2	24	12.9	-1	27	110.0	93.3	16.7	6.9	26.4
159	172	129	30	-37	9	-88	-28.1	-46	-10	-24.5	-42	-7	150.5	180.4	-29.9	-42.4	-17.5
160	221	168	100	54	54	37	14.7	3	26	25.9	17	35	185.7	157.8	28.0	20.9	35.0
195	223	151	63	63	55	55	19.6	3	36	25.8	13	38	161.1	141.1	20.0	9.1	30.9
211	155	92	12	12	12	12	2.5	-8	13	-9.9	-19	-1	116.7	115.7	1.0	-7.3	9.3
212	170	121	42	42	42	19	10.6	-4	25	17.4	6	29	138.8	125.6	13.1	4.9	21.3
225	166	116	116	98	107	97	43.1	25	61	57.7	41	75	127.5	63.4	64.1	57.4	70.7
226	225	143	148	124	116	106	39.4	13	66	42.9	20	66	160.4	110.2	50.2	41.8	58.6
237	176	120	57	57	23	23	24.1	6	42	38.6	24	54	141.2	109.7	31.5	23.4	39.5
275	244	173	24	24	7	4	-.9	-13	11	-4.3	-33	24	204.2	205.4	-1.2	-11.4	9.0

---

[*] Concentrations and residuals in ppb.

Table 9b

"A" and "F" Residuals of Peak Accuracy: 20-Day Average

Residuals and 95% Confidence Intervals*

Measure	Residual	Low CL	UP CL	Std. Dev.	Source
F1	63	47	79	36	AMS
F2	48	31	65	38	AMS
F3	48	34	62	31	AMS
F4**	31	11	51	45	AMS
A1	12	5	19	16	Cox
A2	14	4	24	22	Cox
A4**	16	-4	35	44	Cox

*Residuals, deviations in ppb.

**Confidence intervals for unpaired measures based on $S = \sqrt{S^2_o + S^2_p}$

Table 10a

Bias and Confidence Limits (Paired)

	All Pairs						$O_3 \geq 80$ ppb*			$O_3 \geq 120$ ppb**		
Day	N	$\overline{O-P}$	95% Conf. Intervals	S^2_o	S^2_p	S^2_o/S^2_p F_{calc}	N	$\overline{O-P}$	95% Conf. Limits	N	$\overline{O-P}$	95% Conf. Intervals
142	233	-10.6	± 3.4	2098	2631	0.78	105	-15.8	± 6.8	56	-27.1	± 10.3
178	235	3.5	3.9	3136	3238	0.97	137	7.0	6.2	90	4.3	8.9
182	304	- 5.4	2.9	1218	557	2.18§	184	3.3	2.2	15	20.7	10.6
183	241	- 5.6	3.2	1989	992	2.00§	160	2.0	3.9	51	14.4	5.8
184	276	0.9	3.6	1918	824	2.32§	193	9.8	4.2	41	14.5	11.5
207	249	10.6	2.9	2070	961	2.15§	125	23.7	3.8	47	38.0	5.0
209	263	5.5	3.1	1391	773	1.80§	127	13.4	5.6	17	64.0	16.0
221	291	17.5	2.9	1722	790	2.18§	102	36.3	5.2	34	54.3	9.9
230	236	-12.3	2.8	1162	847	1.37§	56	- 5.6	8.9	9	55.5	18.1
231	299	- 4.0	2.6	1339	790	1.70§	54	17.9	8.4	10	47.8	15.4
251	281	4.2	2.5	1274	676	1.88§	104	24.5	6.1	5	37.1	21.1
159	279	-12.3	3.1	2304	2116	1.08	202	- 9.0	3.8	113	-10.0	5.8
160	282	11.5	3.3	3124	1475	2.12§	193	21.5	3.7	130	30.0	3.6
195	224	5.9	2.6	1953	1176	1.66§	118	12.3	4.4	50	28.0	5.2
211	258	-10.1	2.5	1281	1075	1.19§	88	- 8.4	5.8	11	11.2	15.7
212	243	1.1	2.5	1918	992	1.93§	106	14.8	3.1	24	26.7	8.0
225	247	26.6	3.2	1183	342	3.46§	69	55.8	5.1	14	87.6	9.1
226	191	28.6	5.0	2798	1102	2.53§	104	47.6	6.2	59	60.9	7.6
237	277	29.8	4.0	2209	1017	2.17§	160	48.5	4.7	55	57.3	7.5
275	300	-23.9	5.9	4502	4651	0.97	178	-35.7	9.5	134	-35.3	11.9

*Pairs for which observed or predicted values ≥ 80.

**Pairs for which observed or predicted values ≥ 120.

§In these cases the calculated ratio exceeds the critical tabular F of 1.3. There is less than a .05 probability that a calculated F of this size is due to chance alone.

Table 10b

Bias and Confidence Limits (Unpaired)

Day	N	$\overline{O}-\overline{P}$	95% Confidence Limits
142	233	-10.6	± 9.0
178	235	3.5	10.4
182	304	- 5.4	4.8
183	241	- 5.6	7.0
184	276	0.9	6.3
207	249	10.6	6.9
209	263	5.5	5.7
221	291	17.5	5.9
230	236	-12.3	5.8
231	299	4.0	5.3
251	281	4.2	5.3
159	279	-12.3	8.0
160	282	11.5	8.1
195	224	5.9	8.1
211	258	-10.1	6.1
212	243	1.1	7.01
225	247	26.6	5.0
226	191	28.6	9.0
237	277	29.8	6.8
275	300	-23.9	11

Table 11

Correlation Coefficients Between Predicted and Observed O_3

Day	r	r_{s_p}	$\bar{r}_s$	r_{t_p}	$\bar{r}_t$
142-75	.86	.26	.27	.87	.90
178-75	.85	.58	.47	.93	.90
182-75	.83	.56	.46	.65	.86
183-75	.84	.47	.38	.83	.86
184-75	.73	.83	.38	.88	.70
207-75	.88	.70	.36	.96	.92
209-75	.72	.46	.29	.89	.75
221-75	.80	.80	.36	.91	.82
230-75	.77	.15	.27	.86	.84
231-75	.79	.90	.32	.94	.83
251-75	.81	.74	.37	.97	.86
159-76	.85	.52	.35	.93	.90
160-76	.89	.54	.56	.78	.90
195-76	.90	.73	.39	.98	.92
211-76	.84	.81	.42	.94	.74
212-76	.91	.78	.59	.96	.92
225-76	.69	-.38	.44	.75	.74
226-76	.76	-.29	.10	.78	.76
237-76	.69	.46	.32	.90	.76
275-76	.70	.12	.23	.83	.78
Avg.	.81	.49	.37	.88	.83

$r \sim$ the overall correlation coefficient for each day, obtained by using all paired data sets.

$r_{s_p} \sim$ the spatial correlation coefficient for the hour of the maximum observed concentration.

$\bar{r}_s \sim$ the average spatial correlation coefficient (averaged over all hours).

$r_{t_p} \sim$ the temporal correlation coefficient for the station of the observed maximum concentration.

$\bar{r}_t \sim$ the average temporal correlation coefficient (averaged over all stations).

Table 12

Correlation of F4 Residuals vs. Input Parameters for 20-Day Test Set

Variable	Correl. coeff, r	Sig. at 95% lev.
Wind speed	.53	Yes
Average temp.	.37	Marginal
Solar rad.	-.21	No
Max. mix ht.	-.29	No
Ozone aloft	-.28	No

Table 13

CARBON-BOND FRACTIONS (AS CARBON) OF TOTAL REACTIVE HYDROCARBON EMISSIONS IN ST. LOUIS, TULSA, PHILADELPHIA, AND LOS ANGELES.

	AVG. CARBON FRACTION OF RHC			
	ST. LOUIS	TULSA	PHIL	LA
PAR	74.5	80.0	74.0	70.5
OLE	4.8	4.2	2.8	4.9
ETH	4.3	4.2	4.1	9.0
ARO	14.9	8.0	13.2	15.4
CARB	1.5	3.6	5.9	4.6

Table 14

Change in Peak Predicted Ozone Concentration in Response to Uniform Changes in Hydrocarbon Emissions and Initial Conditions

Simulation Description	Day 159		Day 195		Day 275	
	Peak O_3 (ppb)	% Change	Peak O_3 (ppb)	% Change	Peak O_3 (ppb)	% Change
Base Case	312	-	174	-	232	-
Increase HC Emissions by 67%	325	+4.2	211	+21.3	331	+42.7
Increase HC Emissions by 17%	318	+1.9	187	+ 7.5	267	+15.1
Decrease HC Emissions by 5%	308	-1.3	169	- 2.9	225	- 3.0
Decrease HC Emissions by 17%	289	-7.4	159	- 8.6	209	- 9.9
Decrease HC Emissions by 42%	216	-30.8	139	-20.1	149	-35.8
Decrease HC Emissions by 75%	139	-55.4	103	-40.8	83	-64.2

Table 15

Statistical Analysis of Uniform Hydrocarbon Emission Changes

Sensitivity Test Description	Mean Normalized Residual	Mean Absolute Normalized Residual	Spatial Correlation Coefficient
+67% HC, D159	-0.084	0.087	0.974
+67% HC, D195	-0.086	0.086	0.971
-42% HC, D159	0.069	0.070	0.959
-42% HC, D195	0.063	0.063	0.963
-75% HC, D159	0.122	0.124	0.743
-75% HC, D195	0.109	0.110	0.792

Table 16

Effect of Uniform Hydrocarbon Emission Changes on Overall Normalized Areal Exceedance (ONAE)

Sensitivity Test Description	ONAE[1] %
+67% HC, D159	-31.0
+67% HC, D195	-81.1
-42% HC, D159	+34.3
-42% HC, D195	+80.6
-75% HC, D159	+89.7
-75% HC, D195	+100.0

---

[1] $$\text{ONAE} = \frac{\text{NGE}_b - \text{NGE}_s}{\text{NGE}_b} \times 100\%$$

where NGE = number of grid cells exceeding the NAAQS for ozone during simulation

and b = base case

s = sensitivity case

Table 17

Change in peak predicted ozone concentration in response to uniform changes in oxides of nitrogen emissions and initial conditions

Simulation Description	Day 159		Day 195		Day 275	
	Peak O_3 (ppb)	% Change	Peak O_3 (ppb)	% Change	Peak O_3 (ppb)	% Change
Decrease HC Emissions by 42%	216	-	139	-	149	-
Decrease HC Emissions by 42%, Increase NO_x Emissions by 40%	-	-	-	-	123	-17.5
Decrease HC Emissions by 42%, Increase NO_x Emissions by 20%	187	-13.4	131	-5.8	134	-10.1
Decrease HC Emissions by 42%, Decrease NO_x Emissions by 20%	242	+12.0	142	+2.2	170	+14.1
Decrease HC Emissions by 42%, Decrease NO_x Emissions by 40%	-	-	-	-	176	+18.1

Table 18

Fraction of total reactive carbon in each carbon-bond category used for uniform reactivity sensitivity tests

Simulation Description	Carbon Fraction				
	PAR	OLE	ETH	ARO	CARB
St. Louis Uniform Reactivity	0.745	0.048	0.043	0.149	0.015
Philadelphia Uniform Reactivity	0.740	0.028	0.041	0.132	0.059
Tulsa Uniform Reactivity	0.800	0.042	0.042	0.080	0.036
BOM Uniform Reactivity	0.639	0.054	0.054	0.203	0.050

Table 19

Change in peak predicted ozone concentration in response to uniform changes in hydrocarbon reactivity

Simulation Description	Day 195		Day 275	
	Peak O_3 (ppb)	% Change	Peak O_3 (ppb)	% Change
St. Louis Uniform Reactivity (Base Case)	172	-	216	-
Philadelphia Uniform Reactivity	180	+4.7	241	+11.6
Tulsa Uniform Reactivity	170	-1.2	215	- 0.5
BOM Uniform Reactivity	187	+8.7	280	+29.6

Table 20

Effect of hydrocarbon reactivity on the change in peak predicted ozone concentration in response to uniform changes in hydrocarbon emissions and initial conditions

Simulation Description	Day 195		Day 275	
	Peak O_3 (ppb)	% Change	Peak O_3 (ppb)	% Change
Base Case	174	-	232	-
Decrease HC Emissions by 42%	139	-20.1	149	-35.8
BOM Uniform Reactivity	187	-	280	-
BOM Uniform Reactivity, Decrease HC Emissions by 42%	149	-20.3	174	-37.9

Table 21

Change in peak predicted ozone concentration in response to other sensitivity tests

Simulation Description	Day 195		Day 275	
	Peak O_3 (ppb)	% Change	Peak O_3 (ppb)	% Change
Base Case	174	-	232	-
Uniform Spatial Distribution	141	-18.9	189	-18.5
St. Louis Uniform Reactivity	172	- 1.1	216	- 6.9
Temporal Redistribution	184	+ 5.7	281	+21.1
Increase Mixing Height by 25%	176	+ 1.1	236	+ 1.7
Decrease Mixing Height by 25%	177	+ 1.7	310	+33.6
Increase Photolysis Rates by 10%	187	+ 7.5	254	+ 9.5
Decrease Photolysis Rates by 10%	160	- 8.0	214	- 7.8

Table 22

St. Louis Control Strategy Simulation Descriptions

Simulation Number	Description
1,2,3	Reduce stationary source HC emissions by application of (RACT) to appropriate point and area sources. Reduce HC initial conditions proportionally. Days 159, 195 and 275.
4,5,6	Reduce mobile source HC emissions by the application of the Federal Motor Vehicle Control Program (FMVECP). Apply these reductions uniformly over the modeling region and in the initial conditions. Days 159, 195 and 275.
7	Reduce mobile and HC and NO_x emissions by the application of the Federal Motor Vehicle Control Program (FMVECP). Apply these reductions uniformly over the modeling region and in the initial conditions. Day 195.
8,9,10	Reduce mobile and stationary source HC emissions by the combined application of RACT and FMVECP. Reduce initial conditions proportionally. Days 159, 195 and 275.
11	Reduce mobile and stationary source HC emissions by the combined application of RACT, FMVECP and I/M (inspection and maintenance). Reduce initial conditions proportionally. Day 195.
12,13,14	Reduce mobile and stationary source HC emissions by the combined application of RACT and FMVECP. Reduce initial and boundary conditions proportionally. Days 159, 195 and 275.
15	Reduce mobile and stationary source HC emissions by the combined application of RACT, FMVECP and I/M. Reduce initial and boundary conditions proportionally. Day 195.
16	Reduce mobile and stationary source emissions by the combined application of RACT (HC), FMVECP (HC and NO_x) and I/M (HC). Reduce initial and boundary conditions proportionally. Day 195.

Table 23

St. Louis Control Strategy and Evaluation

Control Strategy	Day 159		Day 195		Day 275	
	Peak O_3 ppb	% Change	Peak O_3 ppb	% Change	Peak O_3 ppb	% Change
Base Case	312	-	174	-	232	-
RACT	285	- 8.7%	155	-10.9%	214	- 7.8%
FMVECP (HC)	227	-27.2%	141	-19.0%	160	-31.0%
FMVECP (HC and NO_x)			150	-13.8%		
RACT + FMVECP (HC)	167	-46.5%	121	-30.5%	120	-48.3%
RACT + FMVECP (HC) + BOUNDARY	154	-50.6%	111	-36.2%	118	-49.1%
RACT + FMVECP (HC) + I/M			115	-33.9%		
RACT + FMVECP (HC) + I/M + BOUNDARY			104	-40.2%		
RACT + FMVECP (HC and NO_x) + I/M + BOUNDARY			116	-33.3%		

RACT	Reasonably Available Control Technology
FMVECP	Federal Motor Vehicle Control Program
I/M	Inspection and Maintenance